

POLITECNICO DI TORINO

Master of Science in Mechanical Engineering

Master's Degree Thesis

**Thermal-Structural FEM Analyses
of Upgraded Components in an
Industrial Gas Turbine**



Academic Supervisors:

Prof. Daniela Anna MISUL

Prof. Mirko BARATTA

Graduate:

Antonino RIGGIO

Academic Year: 2018-2019

Summary

1 Introduction.....	2
1.1 Energy Outlook.....	2
1.2 Gas Turbine.....	4
2 Base theory.....	8
2.1 FEM Analysis.....	8
2.1 Thermal-Structural Analysis.....	12
3 Case study: TG20 B7/8.....	14
3.1 Standard engine.....	14
3.2 Analysis Setting.....	15
3.3 Heat Transfer Coefficients.....	19
3.4 TG20 B7/8: Turbine stage 1.....	22
3.4.1 Thermal analysis.....	22
3.4.2 Thermo-structural analysis.....	26
3.5 TG20 B7/8: Turbine stage 2.....	34
3.5.1 Thermal analysis.....	34
3.5.2 Thermo-structural analysis.....	38
3.6 TG20 B7/8: Turbine stage 3.....	45
3.6.1 Thermal analysis.....	45
3.6.2 Thermo-structural analysis.....	48
3.7 Creep and cyclic life (LCF).....	55
3.7.1 First stage analysis.....	59
3.7.2 Second stage analysis.....	62
3.7.3 Third stage analysis.....	66
4 Case study: TG20 B7/8 UG3.....	69
4.1 The engine.....	69
4.2 TG20 B7/8 UG3: Turbine stage 1.....	70
4.2.1 Thermal analysis.....	70
4.2.2 Thermo-structural analysis.....	74
4.3 TG20 B7/8: Turbine stage 2.....	80
4.3.1 Thermal analysis.....	81
4.3.2 Thermo-structural analysis.....	84
4.4 TG20 B7/8: Turbine stage 3.....	89
4.4.1 Thermal analysis.....	89
4.4.2 Thermo-structural analysis.....	91
4.5 Creep and cyclic life (LCF).....	94

4.5.1 First stage analysis.....	94
4.5.2 Second stage analysis.....	97
4.5.3 Third stage analysis	100
4.6 First stage disk examination.....	103
5 Conclusions	105
References	107
Acknowledgement.....	109

Alla pazienza delle persone a me più care
per il tempo che questo lavoro ha loro sottratto

Abstract

This thesis is a result of a partnership between *Politecnico di Torino* and *Ethos Energy Group*. The main project is based on the improvement of TG20 B7/8 (gas turbine produced by *Ethos Energy Group*) to a new upgrade called “TG20 B7/8 UG3”. The aims of this improvement are to increase efficiency and the net produced power and furthermore to decrease the NO_x emission. This work is one of the parts of the entire project and it is regarding the analyses of the thermal and structural loads that are applied in the turbine. This is done to ensure that innovations applied to the engine do not endanger the gas turbine’s life. Initially, analyses are done for the standard version of the gas turbine, to create a base of comparison for the upgraded version. This evaluation is computed in three phases: thermal analysis, structural and thermal analysis and the creep and Low cycle fatigue (LCF) analyses. These three parts are done separately for each of the stage of the turbine. The combined load and the life analysis are computed for the disks.

After that, the study moves to the improved design of the turbine (UG3), by considering all the modifications, a new analysis is done, and an evaluation of the results is made to understand the feasibility of the modifications. For all these analyses, a computation of the different heat transfer coefficients is needed, also because they are different from the first studied configurations. Finally, the LCF and the creep life are studied to verify that the new turbine reaches the targets imposed by the company in terms of life and to understand if a modification is needed.

1 Introduction

1.1 Energy Outlook

Electric energy is practically used in each field and it is fundamental for human life. Nowadays, each human activity requires electric energy, indeed the world request of electric energy is huge (23400 TWh, in 2018) and constantly growing year by year (*Figure 1.1*). This request is also connected to the GDP, in fact 2009 experienced a small decreases due to the financial crisis.

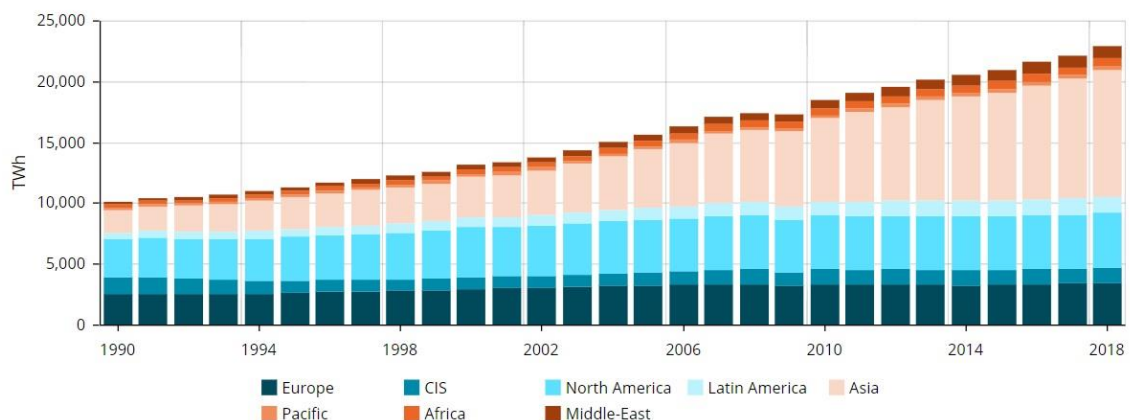


Figure 1.1: world electric energy request over the years.

In the 2018 the electric energy demand rose up of 4% equal to 900 TWh, followed by the rise of CO₂ emission by 1,7%. This type of energy is so important because it is easy to convert in other forms of energy and easily to carry.

The production of electric energy is the process in which primary energy sources are used to obtain an electric power, that will be sorted to the users. The primary energy sources from which this electric energy is obtained are different:

- Oil
- Nuclear
- Gas
- Coal
- Renewables: wind, solar, geothermic
- Hydraulic

In accordance with IEA (International Energy Agency) [1], the installed power capacity of gas and renewable power plants will increase in the next years, so electric energy production will be more dependent on the natural gas. As is possible to see in *figure 1.2*, forecasts (“New

Policies Scenario”, NPS) for the future point out a sharp increase in the installed power generation capacity of the natural gas, that will also overtake the coal’s one.

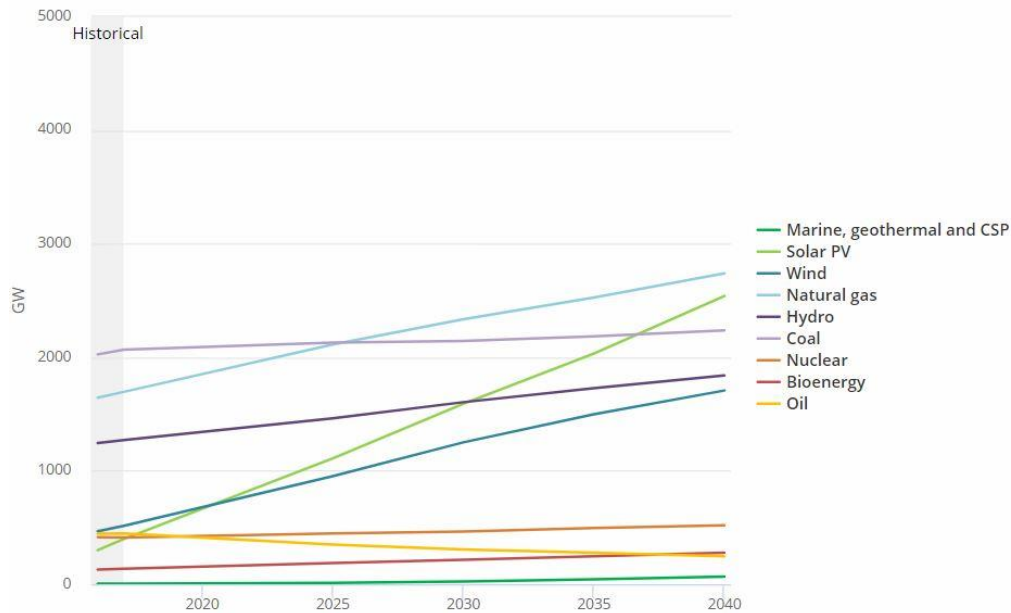


Figure 1.2: forecast for installed power generation capacity for different sources (NPS).

According to this, it is expected that business interests regard the world of the gas turbine is going to grow up in next years, but according to specialists in the field (Turbomachinery) the sales increase will start only in the 2020 (figure 1.3). This fact is due to the development of large combined cycle facilities in industrialized nations and to the modernization of older facilities to meet efficiency and pollutant standards.

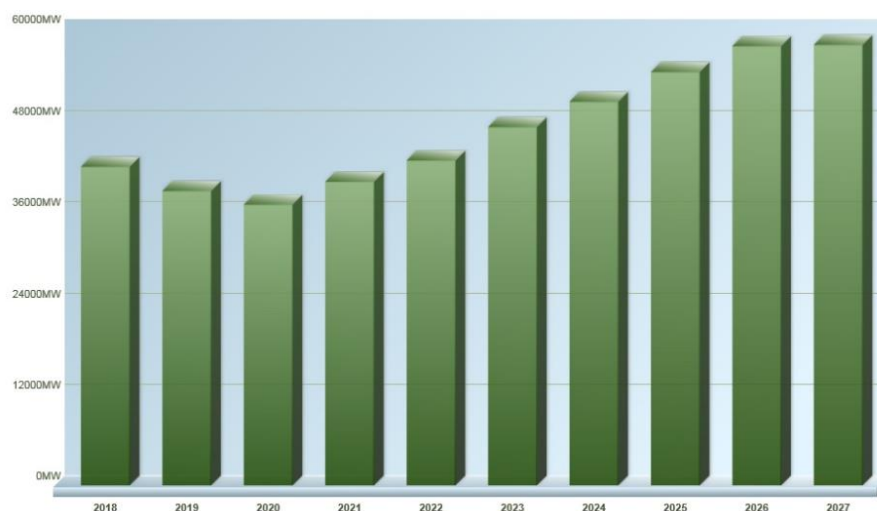


Figure 1.3: forecast of gas turbine electrical power generation over the years.

1.2 Gas Turbine

A gas turbine is a turbomachinery used to produce power by means of a working fluid (usually it is air) and natural gas as fuel. This power is available to the rotor and it could be used to produce electric energy as well as to power certain vehicles likes airplanes. Working principle of gas turbine is based on Bryton-Joule cycle (*Figure 1.4*) and it is made by three principal phases: compression of the working fluid (1-2 ideal cycle, 1-2' real one), combustion of gas and compressed air mixed (2-3 ideal, 2'-3' real) and expansion of the mixture (3-4 ideal, 3'-4' real); this cycle is open, it means that transition from point 4 (or 4') to 1 does not really happen for the mixture that has expanded into the turbine. To obtain this process, three main components are always present in a gas turbine:

- An upstream compressor
- A combustor
- A downstream turbine on the same compressor's shaft

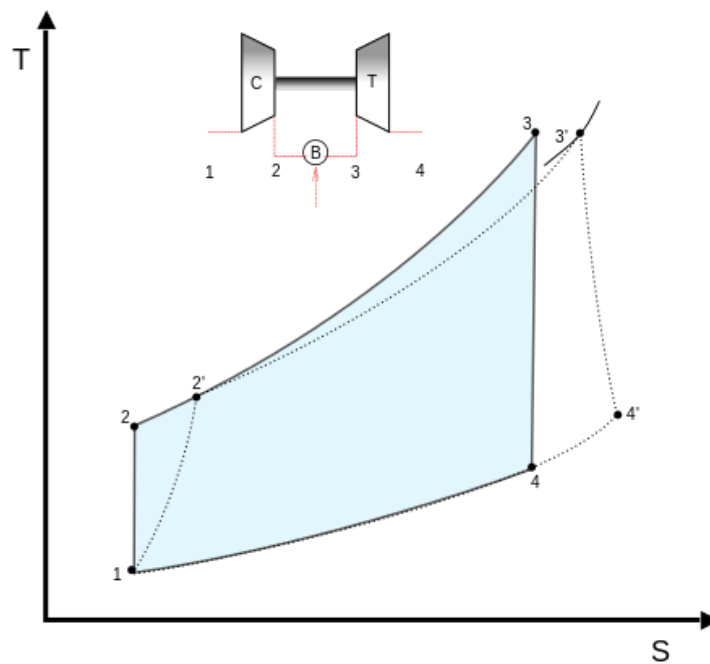


Figure 1.4: Bryton-Joule cycles, ideal (continuous line) and real one (dashed line).

At first, the chemical energy of the natural gas is converted into thermal energy that is converted into mechanical energy through the turbine part. Finally, in a gas turbine used for production of electric energy, the mechanical energy is converted into electrical one by a generator.

The entire process starts when the compressor sucks air from the environment in ambient condition (P_1 and T_1) and compress it with compression ratio β_c that is the ratio between outlet and inlet pressures; for an axial compressor, compressor needs many stages because a single

stage can achieve a small compression ratio. Therefore, compressed air (P_2 and T_2) arrives into the combustor; here, after it was mixed with the natural gas, the combustion takes place. So, the hot mixture (P_3 and T_3) enters on the turbine part, where mixture expands with (this is the phase in which the mechanical power is produced) and finally gases are exhausted in the environment (P_4 and T_4).

As is possible to see in the *Figure 1.4*, the real cycle is different from the ideal one due to some irreversibility; them entail for the real cycle a lower efficiency ($\eta_{real} < \eta_{ideal}$). Obviously, the real efficiency depends on compressor, turbine and combustion efficiencies, that in ideal case are equal to 1, so compression and expansion ratios are equal in this case ($\beta_{c,id} = \beta_{e,id}$).

In the ideal cycle we have a certain value of the efficiency (η_{id}):

$$\eta_{id} = 1 - \frac{1}{\beta^{\frac{k-1}{k}}}$$

Ideal efficiency is function of:

- Compression ratio $\beta = \frac{P_2}{P_1}$
- Heat capacity ratio $k = \frac{c_p}{c_v} = \frac{\text{heat capacity at constant pressure}}{\text{heat capacity at constant volume}}$

In the real cycle the expression of the global efficiency changes, since different losses as pressure and viscous losses are considered. The new global efficiency η_g is equal to:

$$\eta_g = \eta_m \eta_b \frac{\eta_{mt} \eta_t \left[\frac{T_3}{T_1} \cdot \frac{1}{\beta^{\frac{k-1}{k}}} \cdot \frac{\left(\beta^{\frac{k-1}{k}} - 1 \right)}{\left(\frac{\beta}{\eta_{\pi b}} \right)^{\frac{k-1}{k}} - 1} - \frac{1}{\eta_{mc} \eta_{mt} \eta_t \eta_c} \right]}{\frac{T_3}{T_1} - \left(\frac{\beta}{\eta_{\pi b}} \right)^{\frac{k-1}{k}} - \frac{1 - \eta_c}{\left(\frac{\beta}{\eta_{\pi b}} \right)^{\frac{k-1}{k}} - 1}}$$

Where:

- η_m , η_b , η_{mt} , η_t , η_{mc} , η_c , $\eta_{\pi b}$ are all efficiencies, they are mechanical, burner, turbine, compressor and burner pneumatic.
- T_3 is the turbine inlet temperature
- T_1 is the ambient temperature at compressor inlet
- β and k are the same of the ideal efficiency.

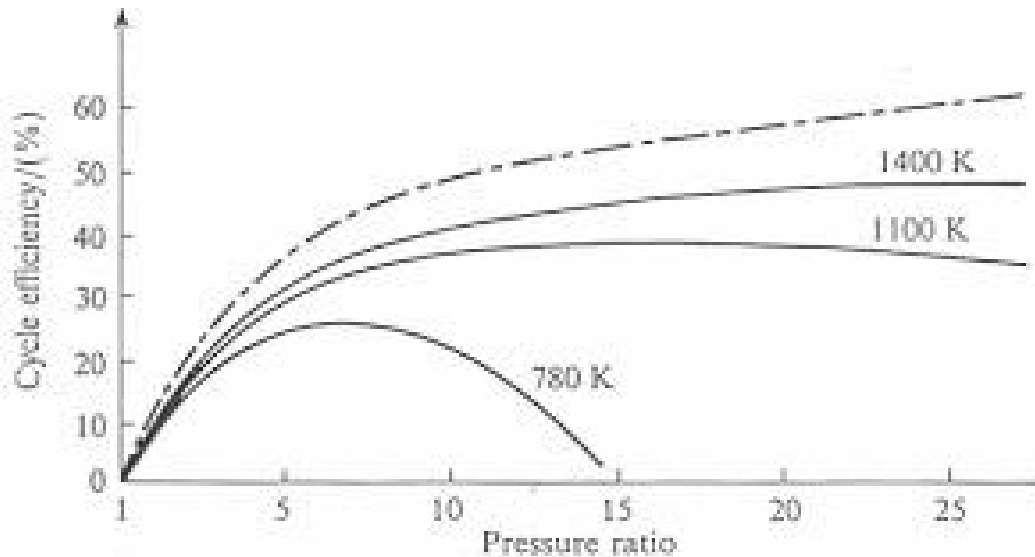


Figure 1.5: efficiency trend with temperature e pressure drop variations.

As is possible to see from *figure 1.5*, if the inlet turbine temperature rises, the entire system behaviour moves close to the ideal case (dashed line). In this case, temperature is the limiting factor due to technological thresholds fixed by materials sensibility to the creep phenomenon. The other important factor is the pressure drop that influence the quantity of work that it is possible to extrapolate from the gas turbine (*Figure 1.6*) and the dimension of the machine (linked to stages number).

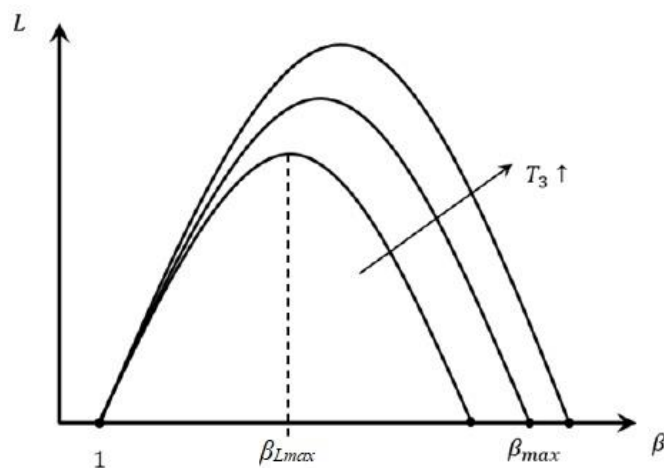


Figure 1.6: Trend of the work produced as function of the pressure ratio.

β_{Lmax} is the compression ratio that gives the maximum work possible for a given T_3 .

$$L_u = \frac{1 + \alpha}{\alpha} L_t - L_c = \frac{1 + \alpha}{\alpha} \eta_t c_p' T_3 \left[1 - \frac{1}{(\eta_{\pi b} \beta_c)^{\frac{R}{c_p}}} \right] - \frac{1}{\eta_c} c_p T_1 (\beta_c^{\frac{R}{c_p}} - 1)$$

- α is the ratio between air mass flow and fuel mass flow.
- η_t and η_c are the turbine and compressor efficiencies.
- c_p and c_p' are specific heat capacities at constant pressure. The first one is for the air instead the second one is for the mixture of air and gas.
- β_c is the compression ratio of the compressor.
- R is the universal gas constant.

The net power produced is given by the power generated with the turbine part less the power absorbed by the compressor part to work on the air.

Nowadays, principal interests during the develop of gas turbine are to increase efficiency and to reduce the pollutants at the exhaust of the turbine part.

2 Base theory

2.1 FEM Analysis

The Finite Element Method is a numerical method used to solve partial differential equations (PDE) that describe a problem with some approximations: change PDE system into an algebraic one. It means that to solve the problem the geometry under investigation is divided into small parts with defined form called “Elements”, the sum of all of them is the “mesh”. Elements are modelled with simple equations: when all these equations are summed, a very large system that describe the whole problem is assembled. Each element is identified by its vertices that in FEM are known as “Nodes”. A value of the field of interest is associated to each node (for mechanical elements the field of interest is the displacement, it means that each node is associated to a displacement).

FEM is the method used for the FEA: Finite Element Analysis; usually, it is applied when the analysed system has a complex geometry (the main advantage) and when the domain is variable.

Nowadays, Finite element analysis (FEA) is used in engineering environment as a computerized method for predicting how a product reacts to real-world forces, structural loads, vibrations, thermal loads, fluid flow, and other physical effects.

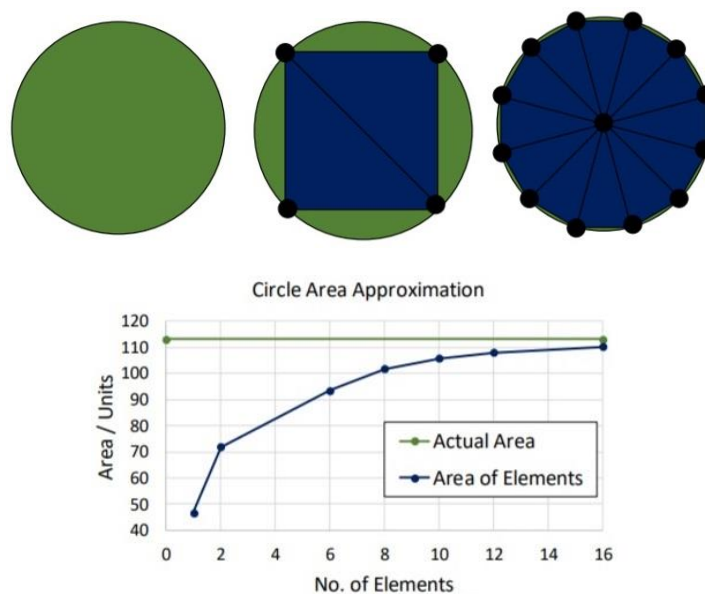


Figure 2.1: Basic idea of finite elements, increasing number of elements (blue) leads to a better approximation of real body (green).

Thanks to this type of analysis used during the development process, it is possible to predict what happens to the product when it is in its working condition. FEA is especially useful for analysing large structures, for complex loads and complex constraints.

The partial differential equations (PDEs) are complicated equations that need to be solved in order to compute relevant quantities of a structure (like stresses ($\epsilon\epsilon$), strains ($\epsilon\epsilon$), etc.) in order to estimate a certain behaviour of the investigated component under a given load.

FEM is characterized by a variational formulation (as Galerkin method that convert continuous problem with infinite degrees of freedom into a discretized one with a finite number of degrees of freedom), a discretization strategy (creation of meshes, definition of basic functions of elements named shape functions and the mapping of reference elements), one or more solution algorithms (direct solver for small and medium problems or iterative solver for large problems) and post-processing procedures (extrapolation of solution data and estimation of the error). The coefficients of the linear combination of shape functions are the degrees of freedom (DOFs) of the system and they are the unknown of the problem.

The general expression of the discretized mechanical system that comes from the polynomial expression is:

$$[K]\{u\} = \{f\}$$

Where:

- $[K]$: is the stiffness matrix
- $\{u\}$: is the vector in which are included the DOFs
- $\{f\}$: is the vector of the external forces

This formulation is the simplification of the discrete variational formulation of the elastic string problem (in mechanical it is known as “*Principle of virtual work*”):

$$\left\{ \int_0^L \mu \frac{du_h}{dx} \frac{dv_h}{dx} dx = \int_0^L f v_h dx \right. \quad \begin{array}{l} u_h \in V_h \text{ and satisfies} \\ \text{for all } v_h \in V_h \end{array}$$

Where:

- “ μ ” is the elastic coefficient.
- “ f ” is the concentrated weight.
- “ V_h ” is a space vector made by the linear combination of a finite number of independent admissible displacements. V_h is finite-dimensional.
- “ v_h ” is the discrete displacement. It is determined by its values $v_j = v_h(x_j)$ at the internal nodes $j=1, \dots, N$. A displacement is associated to each node and it changes with position of the node x_j .

- “ u_h ” is the approximate solution coming from the discretization.

The stiffness matrix \mathbf{K} must satisfy three conditions to be considered valid:

- The matrix \mathbf{K} is symmetric and positive definite
- The matrix \mathbf{K} has not to be ill-conditioned, so: $\left\{ \text{cond}_2(\mathbf{K}) = \frac{\lambda_{h,\max}}{\lambda_{h,\min}} \sim ch^{-2} \right\}$, where: “ c ” is $\frac{4L^2}{\pi^2}$ and “ h ” is the step.
- The maximum error between exact solution (u) and discretised one (u_h) is:

$$\max_{x \in [0,L]} |u(x) - u_h(x)| \leq Ch^2 \max_{x \in [0,L]} \left| \frac{d^2 u}{dx^2} \right|$$

Where “ C ” is a constant and “ L ” is the total length of the string.

To discretize a polygon $\tilde{\Omega} = \Omega \cup \partial\Omega$ (Ω is the area and $\partial\Omega$ is the boundary), the discrete variational formulation change:

$$\left\{ \begin{array}{l} u_h \in V_h(g) \text{ and satisfies} \\ \int_{\Omega} \mu \nabla u_h \cdot \nabla v_h \, dx = \int_{\Omega} f v_h \, dx \quad \text{for each } v_h \in V_h(0) \end{array} \right.$$

Where $V_h(g)$ is the set of discrete admissible displacements.

During the Finite Element Analysis, one of the most important steps is the one regarding the boundary conditions (*Figure 2.2*), that define the environment in which the system under investigation is located. The boundary conditions are the specified values of the field variables (or related variables such as derivatives) on the boundaries of the body. These are usually divided into three categories:

- Dirichlet boundary condition: it prescribes the values associated to the solution on the boundary of the domain. For an ordinary differential equation (ODE):

$$-\frac{d}{dx} \left(\mu \frac{du}{dx} \right) = f \text{ in } (0, L), \text{ Dirichlet boundary conditions are like } u(0)=g_0 \text{ and } u(L)=g_L.$$

If the value is equal to zero, it is homogeneous. Furthermore, for a partial differential equation (PDE) in a domain Ω : $-\nabla \cdot (\mu \nabla u) = f$ in Ω , the Dirichlet boundary condition becomes $u = g$ in $\partial\Omega_D$ (that is the border with Dirichlet boundary condition applied).

- Neumann Boundary Condition: it specifies the values that derivative must take on the boundary of the domain. For an ODE: $\mu \frac{du}{dx}(0) = \psi_0$ and $\mu \frac{du}{dx}(L) = \psi_L$. Here, the domain is $[0,L]$ and ψ_0 and ψ_L are known numbers. It could be written also for PDE: on domain Ω , $\mu \frac{\partial u}{\partial n} = \psi$ on $\partial\Omega_N$, where “ $\partial\Omega_N$ ” is the boundary with Neumann condition applied and “ n ” indicates the vector normal to the boundary.

- Robin Boundary Condition: it is a more general version of the Neumann boundary condition combined to the Dirichlet's one. It imposes along the boundary of the domain a linear combination of value of a function and the value of its derivative. For a 2D domain, Robin boundary condition is written as: $\mu \frac{\partial u}{\partial n} + \alpha u = \psi$ on $\partial\Omega_R$, where " $\partial\Omega_R$ " is the boundary with Robin boundary condition applied and α is a given coefficient. It is often applied in heat transfer problems, to impose a convective flux.

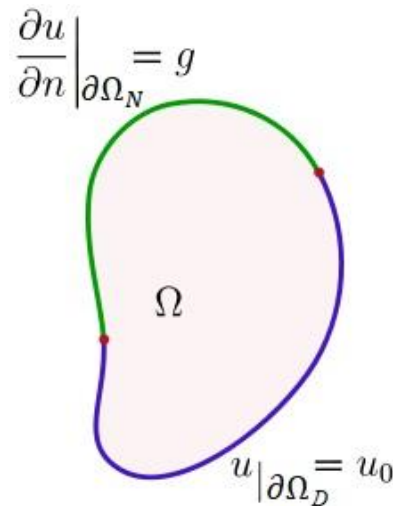


Figure 2.2: two different boundary conditions applied in a polygon, Dirichlet (blue border) and Neumann (green border).

FEA is applicable for modelling several mechanical exercises. One of the most powerful aspect of this analysis is the application to coupled problems like thermo-mechanical, fluid-structure interaction or thermo-chemical. For each field studied, data analysed are totally different, as it is possible to see in the following *Table 2.1* for structural and thermal cases.

STRUCTURAL ANALYSIS	THERMAL ANALYSIS
Displacement	Temperature
Stress	Heat flux
Load	Heat
Stiffness	Conductivity

Table 2.1

2.1 Thermal-Structural Analysis

Coupled-field analyses are useful for solving problems where the coupled interaction of phenomena from various disciplines of physical science is significant. Several examples of this analysis include: an electric field interacting with a magnetic field, a magnetic field producing structural forces, a temperature field influencing fluid flow, a temperature field giving rise to thermal strains and the usual influence of temperature dependent material properties. The latter two examples regard the combined analysis that is applied to a high temperature turbine, as the case study of this thesis work.

There are two type of coupling method differentiated by the finite element techniques used to elaborate the matrix equation: strong coupling and weak coupling. They are both used for the thermal-structural analysis. The solution chain follows the same methodology of standard finite element. Convergence is achieved when changes in all unknowns (degrees of freedom) and knowns, regardless of units, are less than the values specified. The coupling analysed here is one way: temperature affects the displacement field of the body through the thermal strain, instead the displacement usually does not influence the temperature.

The strong coupling provides for a coupled response in the solution after one iteration, thanks to the fact that the coupling effect is considered by the presence of the off-diagonal submatrices.

The matrix formulation for the strong coupling of the thermal-structural analysis is:

$$\begin{bmatrix} [M] & [0] \\ [0] & [0] \end{bmatrix} \begin{Bmatrix} \{\ddot{u}\} \\ \{\dot{T}\} \end{Bmatrix} + \begin{bmatrix} [C] & [0] \\ [C^{tu}] & [C^t] \end{bmatrix} \begin{Bmatrix} \{\dot{u}\} \\ \{\dot{T}\} \end{Bmatrix} + \begin{bmatrix} [K] & [K^{ut}] \\ [0] & [K^t] \end{bmatrix} \begin{Bmatrix} \{u\} \\ \{T\} \end{Bmatrix} = \begin{Bmatrix} \{F\} \\ \{Q\} \end{Bmatrix}$$

Where:

- $[K^t] = [K^{tb}] + [K^{tc}]$
- $\{F\} = \{F^{nd}\} + \{F^{pr}\} + \{F^{ac}\}$
- $\{Q\} = \{Q^{nd}\} + \{Q^g\} + \{Q^c\}$

The weak coupling needs at least two iterations to obtain a coupling response; this happens because the coupling effect is taken into account in the dependency of the “stiffness” matrix and external force vector of the first field on the dof of the second field and vice versa. So, in this case the off-diagonal submatrices are all zero matrices. The matrix formulation for the weak coupling of the thermal-structural analysis is:

$$\begin{bmatrix} [M] & [0] \\ [0] & [0] \end{bmatrix} \begin{Bmatrix} \{\ddot{u}\} \\ \{\dot{T}\} \end{Bmatrix} + \begin{bmatrix} [C] & [0] \\ [0] & [C^t] \end{bmatrix} \begin{Bmatrix} \{\dot{u}\} \\ \{\dot{T}\} \end{Bmatrix} + \begin{bmatrix} [K] & [0] \\ [0] & [K^t] \end{bmatrix} \begin{Bmatrix} \{u\} \\ \{T\} \end{Bmatrix} = \begin{Bmatrix} \{F\} + \{F^{th}\} \\ \{Q\} + \{Q^{ted}\} \end{Bmatrix}$$

The different components of the two matrices equations are:

- $[M]$: structural mass matrix
- $[C]$: structural damping matrix
- $[C^t]$: thermal specific heat matrix
- $[C^{tu}]$: thermoelastic damping matrix
- $[K]$: structural stiffness matrix
- $[K^t]$: thermal conductivity matrix
- $[K^{ut}]$: thermoelastic stiffness matrix
- $[K^{tb}]$: thermal conductivity matrix of material
-
- $[K^{tc}]$: thermal conductivity matrix of convection surface
- $\{u\}$: displacement vector
- $\{T\}$: thermal potential (temperature) vector
- $\{F\}$: sum of the element nodal force and element pressure vectors
- $\{F^{nd}\}$: applied nodal force vector
- $\{F^{pr}\}$: pressure load vector
- $\{F^{ac}\}$: force vector due to acceleration effects
- $\{F^{th}\}$: thermal strain force vector
- $\{Q\}$: sum of the element heat generation load and element convection surface heat flow vectors
- $\{Q^{nd}\}$: applied nodal heat flow rate vector
- $\{Q^g\}$: heat generation rate vector for causes other than Joule heating
- $\{Q^c\}$: convection surface vector
- $\{Q^{ted}\}$: heat generation rate vector for thermoelastic damping

3 Case study: TG20 B7/8

3.1 Standard engine

The TG20 B7/8 is a gas turbine produced by *Ethos Energy Group* with a maximum power equal to 47 MW (*Figure 3.1*). It was born in the 70's, as a project of *Westinghouse*. Initially under the name of CW251WB8, this machine has the following rating (*Table 3.1*):

DATA	VALUE	UNIT
Nominal power	39,41	MW
Maximum power	47	MW
Efficiency (no generator)	30,7	-
Specific consumption	11,740	MJ/kWh
Rotational speed	4918	rpm
Exhaust temperature	520	°C
Compression ratio	11,9	-

Table 3.1

This model was sold all around the world and nowadays there are some TG20B7/8 that are still working. This gas turbine is made by 18 compressor stages composed by disks shrunk on compressor shaft. The burner is composed by 8 combustors arranged in a ring, where the air flow is sent after the compressor.

The last step is composed by the turbine that has 3 expansion stages, connected each other by the curvic clutches (integrated in each disk face) and by the use of tie rods. Moreover, the turbine is connected to the compressor through the main flange, connected with these two parts by bolts. The cooling system is critical in the turbine part, due to the sensibility of the material to the high temperature reached at the turbine inlet. As a matter of fact, the cooling configuration has been changed over the years; a lot of modifications has been done to improve step by step the machine's life.

The analysed arrangement (called "Standard configuration") is the one with a cooling system just in the first rotating stage to cool down the temperature of the blades when engine is working. It is necessary for the high temperature reached in this stage. The vane precedes the blade in each stage, it is a stator blades arranged to deflect fluid with a certain angle to enhance the working condition of the rotating part. All the vane rings have a dedicated cooling system, to avoid high temperature on the rotating blades. The cooling scheme of the vanes was also

subjected to some improvements because this part of the turbine is a critical one. This system used to cool down the machine is fed with air that is bled from the delivery of the compressor.

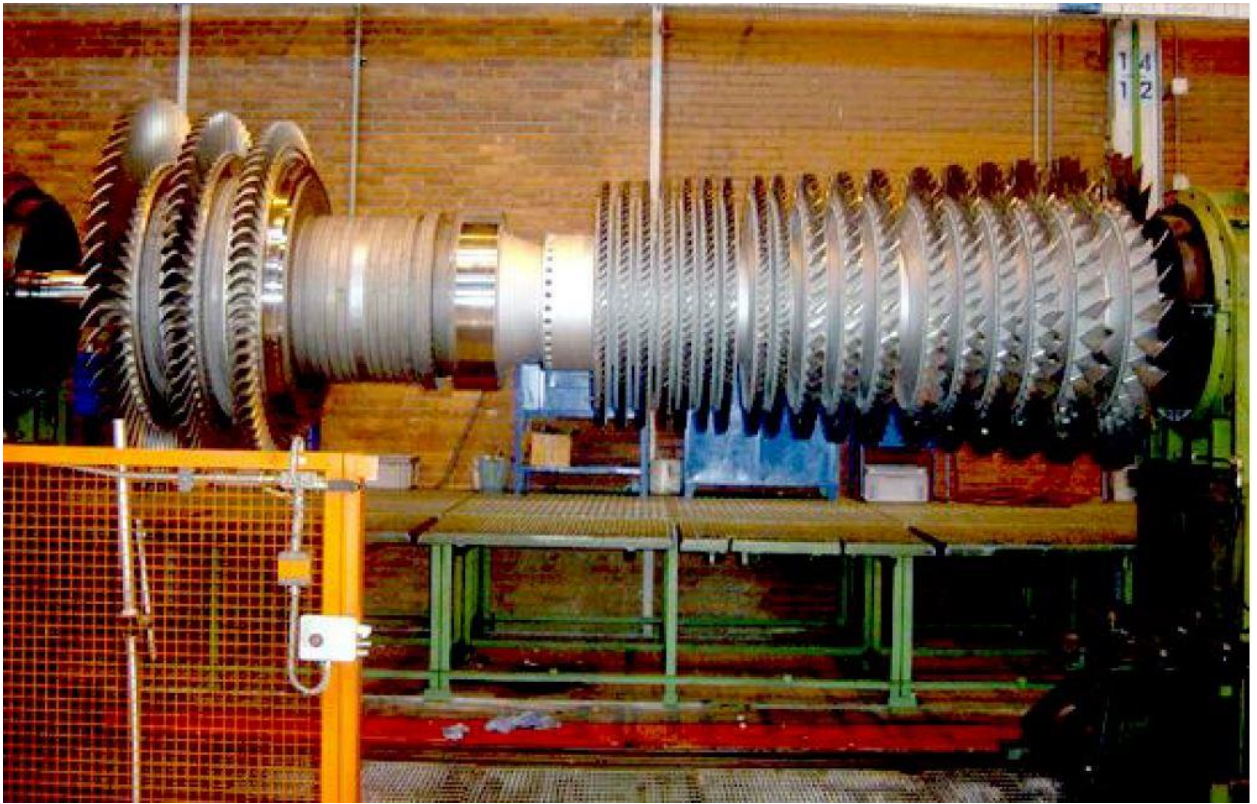


Figure 3.1: TG20 B7/8 compressor and turbine rotor during a rotor overhaul.

3.2 Analysis Setting

All the Finite Element Analyses (FEA) are done by the software *Ansys Mechanical 19.2*, that analyse the different geometries of the gas turbine. Obviously, each time the object under investigation has to be defined in every possible aspect. In this way it is possible to improve the simulation; if the degree of detail is higher, the simulation will be closer to the real object. To set up the analysis, Ansys requires information (*Figure 3.2*) about the system in many respects:

- Geometry under examination
- Materials
- Coordinate systems (the universal one is set automatically)
- Symmetry condition (if it is present in the analysed system)
- Connections (if the analysis consist of more than one part)
- Mesh
- All the different loads and constraints applied

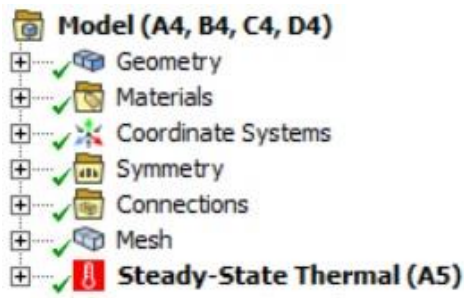


Figure 3.2: General settings menu of Ansys Mechanical 19.2 for a Steady-State Thermal analysis.

The geometry is fundamental, because it is the graphic representation of the object of the study. Usually, this geometry is drawn by means of a CAD software. For the geometries used in this thesis two CAD parametric software: *Creo parametric 3D PTC* and *Catia 3D by Dassault Systèmes*. They are used to draw all the 3D geometries used in all the analyses done during this thesis work.

The following passage is to assign a material to each body, in this way the system has physical properties and the characteristics of each element in the FEM are given for every possible type of load that could affect the system. All the materials known by the software are listed in the “Engineering Data”, where we can find the default materials, we can load an existing material, or we can characterize a material in all its aspect into this digital library directly.

The coordinate systems are important to define accurately different elements of the simulation like loads or constraints. It is possible to add many coordinate systems in order to simplify the following steps as the symmetry condition. This passage allows to study only a part of a body by considering the fact that it is symmetric, the results will be equal for these parts. Obviously, this condition is useful only in certain analyses, like those on turbine disks. In this thesis work, all the analyses are done with a symmetry condition imposed, in particular the one called “*Cyclic region*” that is suitable for the case of a turbine disk, where a slice only is analysed, instead of the entire disk. In this way the two opposite faces of the 3D slice are uniform. In the following pages, every time that we will talk about disk analysis, the connected figure will show only a slice of the disk, but the results are valid for the entire one (*Figure 3.3*).

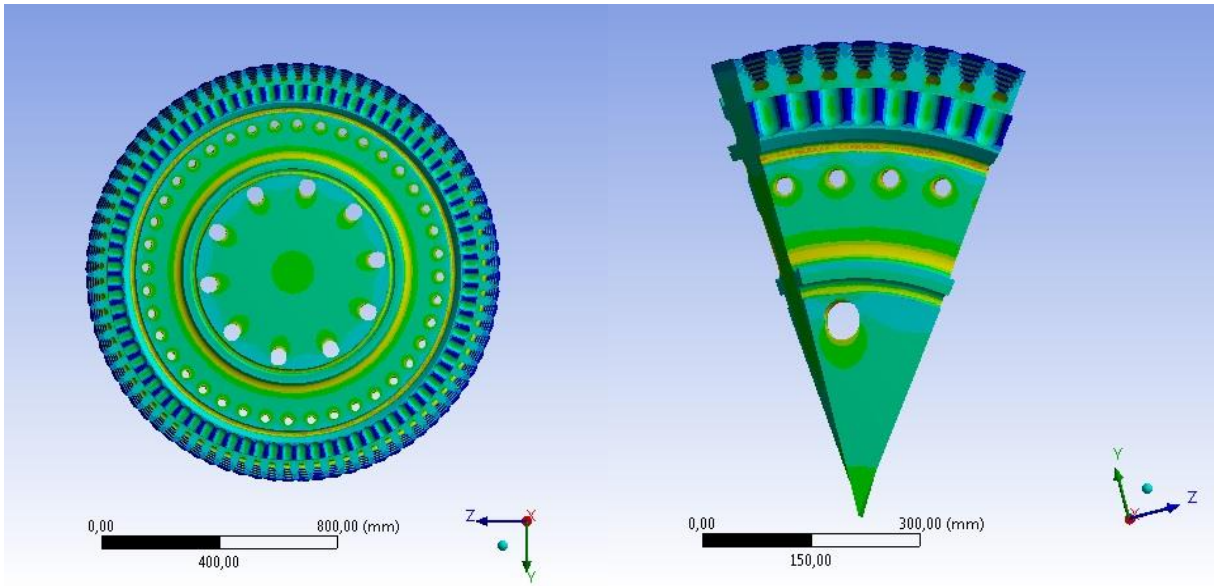


Figure 3.3: the entire disk analysed (left) and the slice used to do the analysis (right), the result is exactly the same.

This expedient is helpful to reduce the computational time of the software, due to a strong reduction in the number of elements have to be analysed.

The connections are imposed when more than one object is present on the analysis. Indeed, it is relevant to define which are the contact surfaces between the bodies and which type of contact is established here (Bonded, No separation, Frictionless, Rough, Frictional). Obviously, each type of contact is not an exact representation of the reality, so deciding which to choose is not so trivial. For some analysis, many attempts were done to find the most suitable type of contact.

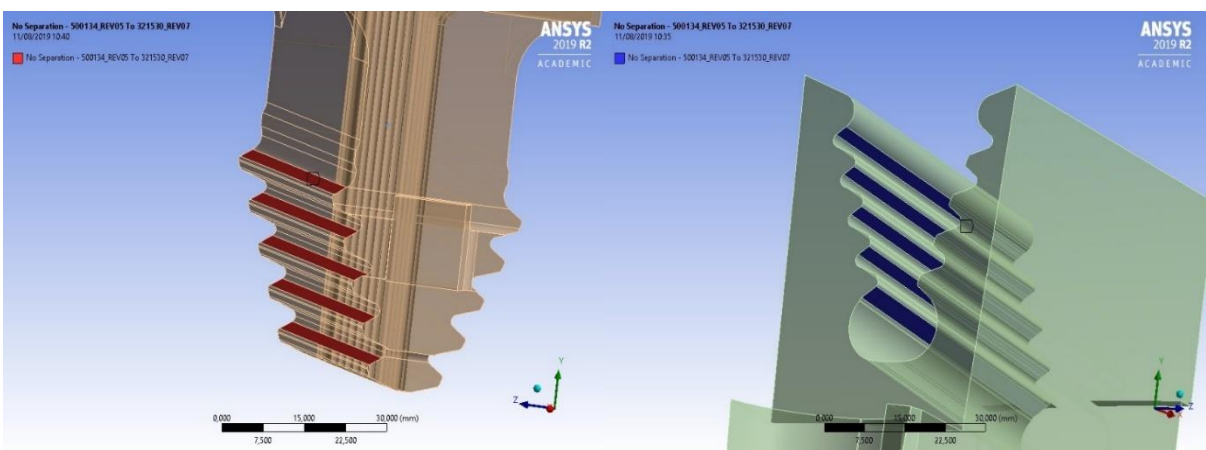


Figure 3.4: Active surfaces are highlighted in red for the fir tree root of the blade and in blue for the grooves of the disk.

For what concern the thesis work, connections are important in the thermal analysis, where are present both the blade and the disk (they are both rotating), as in *Figure 3.4*. Surface that are in contact are called “active surfaces”.

The mesh step is the discretization of the structure under evaluation. It is the base of the Finite Element Method as mentioned above. The mesh influences the accuracy, convergence and speed of the solution. Ansys allows an automatic meshing but it could also be strongly customised.

As input data, we give to Ansys the physics preference (mechanical, CFD, Hydrodynamics, etc), that in the examination of turbine disks is still “mechanical”. By setting the preference, the software adapts to more logical defaults in the meshing process to obtain a higher solution accuracy. This software also provides the flexibility to produce meshes that range in complexity from pure hex to highly detailed hybrid. For 3D models, ANSYS meshing method provide well-shaped quadratic tetrahedral meshing, that is the one used in all the analyses in this thesis work (*Figure 3.5*). It also possible to impose different mesh condition in different areas of the same body.



Figure 3.5: meshes of a single slide of the disk and the blade of a first stage, standard version.

The last step is the one that characterize the analysis. Until now, all the passages were done to characterize the model, but a load is necessary to understand what happen to it. So, Ansys allows many different types of loads linked to different type of analyses, like *Static Structural*, *Steady-State Thermal*, *Transient Structural*, *Transient Thermal* and many others. If, for example, we want to implement a Steady-State Thermal analysis, we will give different load to the system, as a fixed temperature on a surface (It is a Dirichlet boundary condition), a

convection on an external surface (Robin boundary condition), a heat flux and others. In this step, it is possible to set loads, constraints and boundary condition of the system. The different analyses could be also summarised among them, as it is done in this thesis work to evaluate the thermo-mechanical loads.

The entire procedure follows during a FEA on Ansys (for a structure) could be schematized into:

- *Pre-processing*: meshing of the structure, select elements and properties, choose the material of the elements and apply loads and boundary conditions.
- *Solution*: choose the solver, calculate for each element the stiffness matrix and assemble the global stiffness matrix. Then it is possible to solve for strain, stresses, etc.
- *Post-processing*: display solution of strain, stresses and the others and calculate user defined parameters from the results.

3.3 Heat Transfer Coefficients

To compute the temperature reaches by each blade and each disk, it is fundamental understand how the flow behaves when it is in contact with the different parts of the system under investigation. During the thermal analysis of a turbine stage, there are two typologies of flow: the hot mixture air-gas that is expanding in turbine and the cooling fluid that ensures a higher life of the engine. To compute the temperatures distribution on the bodies, we must know the temperature and the heat transfer coefficient of each flow that affects a surface. It means that many different coefficients have to be computed to solve the thermal analysis and it is not trivial. Experiments are needed to compute the exact values of these coefficients, but it is not feasible. Therefore, a theoretical method is adopted to evaluate these coefficients; since the geometries are not simple, there are not exact formulations that allow to compute the coefficients. *Ethos Energy* adopts a comparison method in these cases: They compare the evaluated machine (for which the heat transfer coefficient is unknown) with a machine for which these coefficients are known; it is done by using the DuPont formulation (*Fiat-Westinghouse* design criterion):

$$h_1 = h_2 \cdot \frac{k_1}{k_2} \cdot \frac{D_{eq2}}{D_{eq1}} \cdot \left(\frac{Re_1}{Re_2} \right)^{0,8}$$

Where:

- 1 is the subscript for the investigated engine and 2 is the one for the reference engine.

- h : convective heat transfer coefficient $\left[\frac{W}{K \cdot m^2} \right]$
- k : thermal conductivity of the fluid $\left[\frac{W}{K \cdot m} \right]$
- D_{eq} : equivalent diameter; it is the diameter referred to the cross-sectional area.
- Re : Reynolds number

This analogy is applied for each surface of the stage turbine where there is a fluid that influences the temperature of the structure. The known heat transfer coefficients are the ones of the TG50C, a machine bigger than TG20 B7/8 and for which these coefficients were computed exactly and therefore it becomes the basis of comparison.

Data needed to compute these coefficients were extrapolated from the *PH4165* and through an *Excel* file, time after time, each heat transfer coefficient was calculated.

To validate these computations, two studies were also done on the first stage for the values found for the blades: a sensitivity analysis and another computational way to compute them. The sensitivity analysis gives an idea about the error on the output (in this case, the maximum temperature on the disk), with a certain error imposed on the heat transfer coefficients computed for the blades.

The other way to compute the coefficients is one coming from experimental on a NACA airfoil and this result is used to validate the result of the comparison.

The sensitivity analysis done on the blade of the first stage was done by considering an error of +100% (duplicate the heat transfer coefficients that affect the blade) and -50% (half of the values computed with DuPont formulation). The disk is the body under control (*Figure 3.6*), because it is the one with the most dangerous maximum temperature, even if the blades experience a higher temperature, they are made with Inconel that is much more resistant than the customised structural steel used for the disks and so they are safe. For this, the results are compared for the three cases.

As is possible to see from the *Figure 3.6*, the resulting error on the maximum temperature computed on the disk is $\pm 1^\circ C$, that is a negligible error. To support this test, an alternative method is used to compute an average heat transfer coefficient on the blade and compare it with the one obtained before to verify that the order of magnitude is correct.

The computation is based on the evaluation of the average Nusselt number, that depends on Reynolds and Prandtl numbers and on m and c coefficients; from Nu , the average heat transfer coefficient h is computed by considering the chord of airfoil l and the thermal conductivity of the air k_{air} :

$$Nu = c \cdot Re^m \cdot Pr^{\frac{1}{3}} \qquad h = \frac{Nu \cdot k_{air}}{l}$$

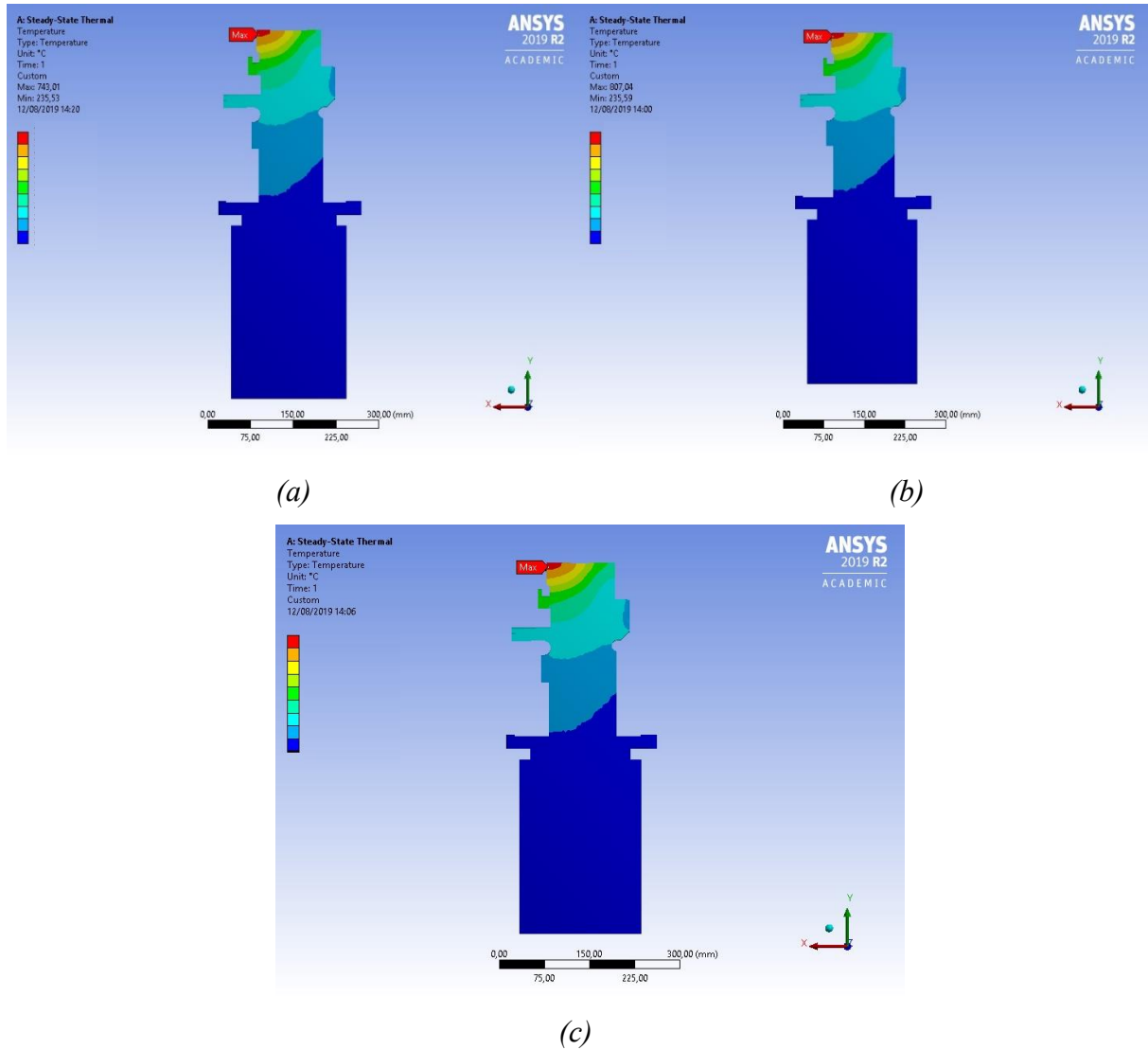


Figure 3.6: The results of the sensitivity analysis for the 3 cases: (a) blade's coefficients computed, (b) simulation with +100% and (c) simulation with -50% of the coefficients value.

Thanks to the chart in Figure 3.7, from the computation of Re (~ 350000), it is possible to extrapolate from the chart a Nu that is almost 330 and consequently an h equal to $275 \frac{W}{m^2 \cdot K}$.

The weighted average of heat transfer coefficients computed with DuPont formulation is equal to 607; this is not equal to the heat transfer coefficient computed with these experimental data, due to different shape of the blade profile, different temperature scenario (the experiments are isothermal) and also some approximations done in the two computations.

Since the grade of magnitude is the same and the result obtained is similar to the reduction of -50% did for the sensitivity analysis, we can consider acceptable results coming from the DuPont formulation.

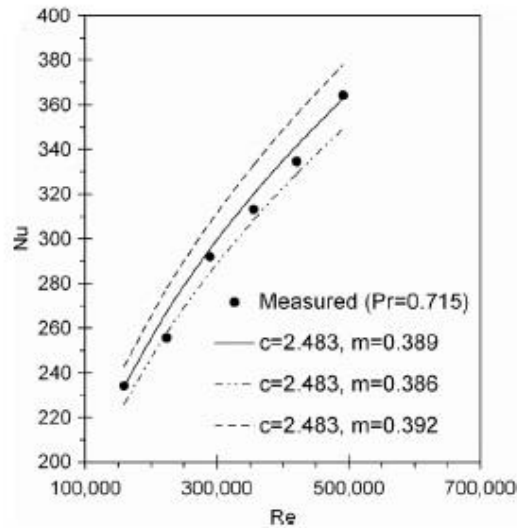


Figure 3.7: The chart used to compute Nu from Re .

3.4 TG20 B7/8: Turbine stage 1

3.4.1 Thermal analysis

The first stage in the standard version is the only one with a dedicated cooling system, also the blades have 15 channels each one to allow the transition of the cooling air inside the blades to decrease the temperature. It is necessary for the high temperature of the mixture air-gas that touch the blades, due to the high Turbine Inlet Temperature (TIT). This stage is composed by 80 blades, so the slice of disk used for the thermal analysis is one eightieth of the total (*Figure 3.8*); in the two faces the condition of cyclic symmetry is imposed.

The disk is made with a customised structural steel, a particular alloy used by *Ethos Energy Group* for each turbine stage of this machine. Instead, the blades are made with an Inconel alloy: an austenitic nickel-chromium-based superalloy. This material ensures high resistance at high temperature and for this reason it is used for all the blades of the turbine part. Active surfaces are the one described in *Figure 3.4*; they are the ones through the heat is exchanged between the two bodies. The contact is defined as “no separation”, it represents a condition with no gap between the body (this is ensured by the rotational speed of the machine, or better from the centrifugal force) and allowed sliding due to a friction coefficient μ considered null. For what concern the mesh, it is depicted in *Figure 3.5* and it is different for the two components: the maximum element size is 2 mm for the blade and 6 mm for the disk. This is due to the

presence of many details in the blade (as cooling channels), for which a better accuracy is needed.

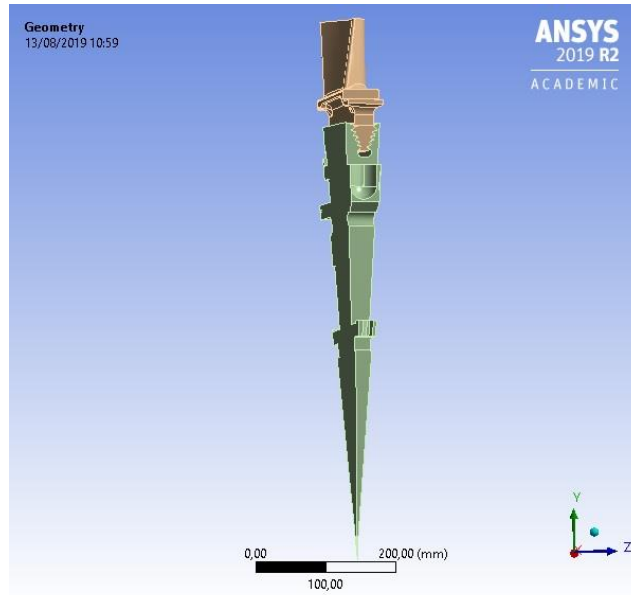


Figure 3.8: analysed slice of the first stage of the turbine

The cooling system is described by the Figure 3.9 and it does not include only the part regard the blades (right part of the scheme), but it also depicts all the flows that are in contact with the disk. This scheme depicted below is used together with the software *PH4165*, it is an internal software property of *Ethos Energy* used to compute all the data about the cooling arrangement as pressure and flows.

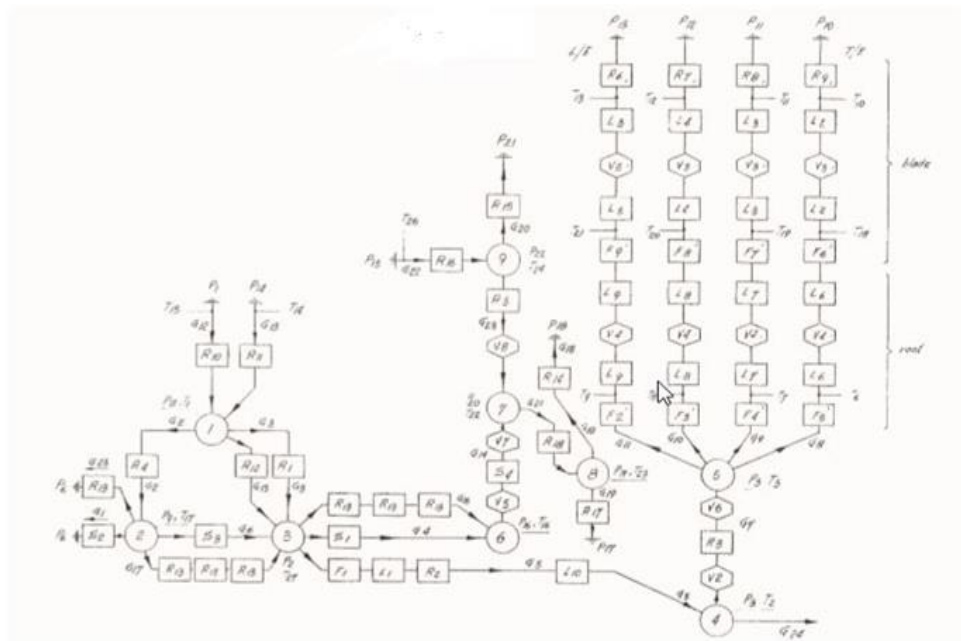


Figure 3.9: The cooling scheme of the whole first stage of the turbine.

The information on this scheme are used to compute the different heat transfer coefficients that affect the convection on the different surfaces and to set up the different temperature of the fluids that are in touch with the two bodies assembled.

To compute these heat transfer coefficients, with DuPont formulation, the disk is divided in many surfaces, since the different condition of the flow and the different restriction areas cause a variation of the heat transfer coefficient region by region. These are listed in the *Table 3.2*.

Region	Heat transfer coeff.	Max air temperature	Min air temperature
BLADE	$\frac{W}{m^2 \cdot K}$	°C	°C
Inlet surface	1270	1065	940
Outlet surface	300	860	760
Pressure surface	540	880	770
Suction surface	635	880	770
Shank	150	320	330
Channel group 1	Max 4039 Min 2182	463	257
Channel group 2	Max 3436 Min 2148	610	257
Channel group 3	Max 4601 Min 2610	606	449
Channel group 4	Max 3472 Min 2549	605	449
Channel group 5	Max 4739 Min 2490	613	449
DISK			
Root input surface	460	330	330
Root output surface	100	330	330
Inlet surface	180	200	200
Outlet upper surface	100	330	330
Outlet middle	30	240	240
Outlet lower surface	20	220	220
Grooves surface	400	230	230

Table 3.2

The coefficients of the blades for example are computed for two different heights and then the average is used; this is done because the temperature profile on the inlet of the blade is parabolic. For the inlet and outlet parts, the total temperature of the fluid is taken into account to compute the coefficients and as temperatures of the fluid for the convection, because these two regions are stagnation points. Instead of, the pressure and suction surfaces of the blades are affected by static temperatures since there the fluid is moving. The heat transfer coefficients

and temperatures on cooling channels are taken from a previous thesis work regarding exactly this argument and they are divided into 5 groups (three channels in each group). For each group there are a temperature variation and also a heat transfer coefficient variation. All the temperatures that affect the external part of the blade are coming from the software *AxSTREAM*, it is a turbomachinery design software used for conceptual design of compressors and turbines and also for thermodynamic calculations of existing machines (also for off-design operation).this software use a 1D/2D solver for the calculation and optimization. In this case it is used to define the flow path of the TG20 B7/8 for 7 sections distributed from the root to the tip of the blade. The input data are geometries of the blades, mass flow rate, turbine inlet temperature and other feature regarding the turbine. In this way a parabolic temperature profile is depicted both for inlet and outlet part of each stage and therefore a temperature map of the blade is drawn.

One of the most important issue is regarding the division between the hot gases that expand in contact with the blades and the other part of the machine. It is fundamental to avoid an abrupt brake that the direction of the flows is from the colder fluids to the hotter. The gas ingestion is prevented by use of seals that are kept in position with a pressure inside higher than the one of the fluids in contact with the blades. This expedient ensures that the maximum temperature of the disk is mainly dependent on the blade's root temperature and no direct contacts occur between disk and hot gases that expand in the chamber.

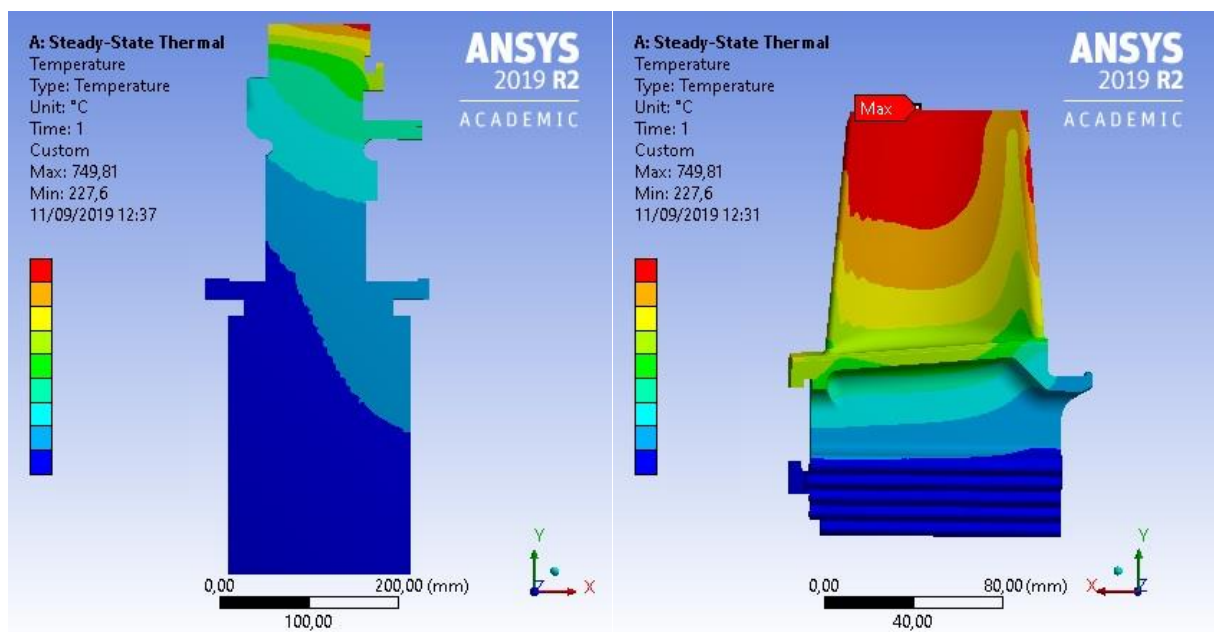


Figure 3.10: Temperature scenarios for the disk and the blade of the first rotating stage of TG20 B7/8.

The combined analysis is focused on the disk, since historically it has a shorter life than the blade. The resulting maximum temperature on the blade is located in the tip and it is equal to 749,81 °C, instead of the maximum value of the disk that is 296,34 °C, is located in the upper outlet part of the groove. The temperature solutions for the two parts are reported in *Figure 3.10*.

3.4.2 Thermo-structural analysis

Once the thermal analysis is completed, the following step is to set up the structural analysis; here we also take into account the thermal load. Now, only the disk is examined and the CAD model that represent the geometry is different: the slice is bigger (one tenth of the total) than thermal analysis, now it includes 8 grooves. This is done to integrate holes and other details that are not present before because they are not influent for the thermal analysis, but they are present in the real body and they are influent for the structural analysis; the smaller holes are used to tighten bolts that fix the front ring for the cooling air direction, meanwhile the larger ones are used for the tie rod that joints all the turbine disks. Material, coordinate system and symmetry conditions are the same applied for the first analysis; connections are not described since only one body is present on the system. The mesh is differentiated within the same component: in the upper part the maximum dimension of the element is 2 mm, instead of the rest of the body for which it is 4 mm (*Figure 3.11*). This distinction is due to a more precision needed in the area where the blade is mounted.

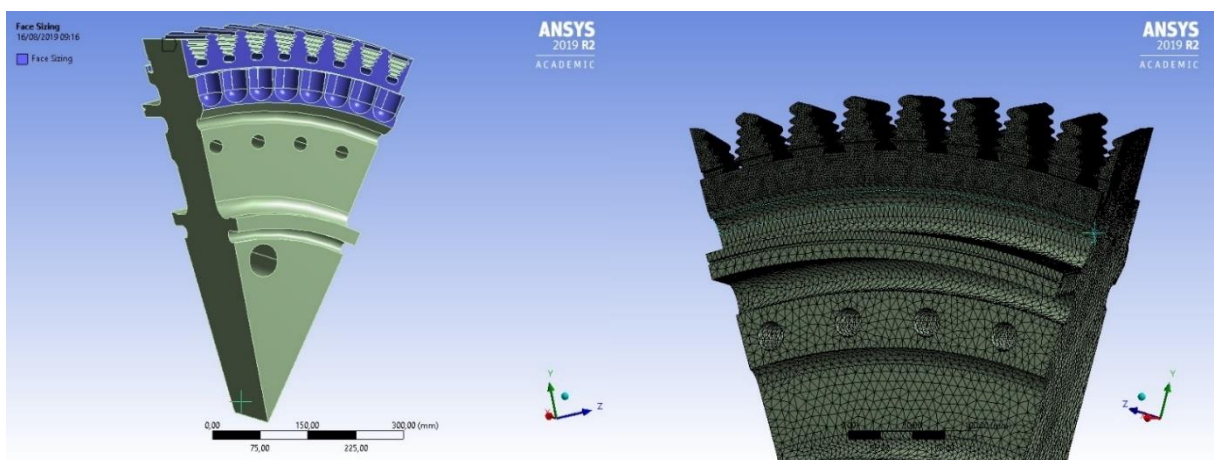


Figure 3.11: the analysed slice with refined part highlighted in violet (on the left) and final result of the mesh (on the right).

The thermal load that is present is made by two parts: the convection conditions on the disk (the same used before) and the temperatures of the blade in the active surfaces: it means that for each contact region coming from the first study, many points distributed along the active surface are taken and they create a temperature scenario in the active surface of the disk; this temperature trend is different for each surface. The following passage is to set up the structural loads by considering the fact that the disk is rotating and the presence of the blades in the grooves: the weight of the blade during rotation is converted in load through the centrifugal force (F_c) that it exerts on the active surfaces of the disk:

$$F_c = m \cdot r \cdot \omega^2$$

Where:

- m is the mass of the blade concentrated on the centre of gravity. In this case, $m = 3 \text{ Kg}$
- r is the distance between the centre of the disk and the blade centre of gravity. In this case it is $r = 0,65 \text{ m}$
- ω is theoretically the rotational speed of the engine, that is equal to 4918 rpm; but for compute centrifugal force, this value is increased of 3%, to be safe with the over speed, so $\omega = 5065,5 \text{ rpm}$

The force due to the weight of the blade is applied in the active surfaces, where the blade exchange forces with the disk and it is equal to 620 kN . This force is directed along the radial direction of the disk.

The imposed speed on the disk's slice is 5065,5 rpm instead of 4918 rpm for the same reason explained before.

Before running the Ansys simulation, it is fundamental define the condition of constraint and so the allowable displacements. As said previously, it is hard to understand where the constrain has to be put and many attempts are done to find the simulation that is closest to the real behaviour of the body.

Finally, the best simulation is obtained by blocking the displacement of the yellow surface in *Figure 3.12* along the circumferential and the axial direction (y and z axes in the local coordinate system of the disk, in the picture) and by leaving free to move the body along the radial direction (x axis in the picture).

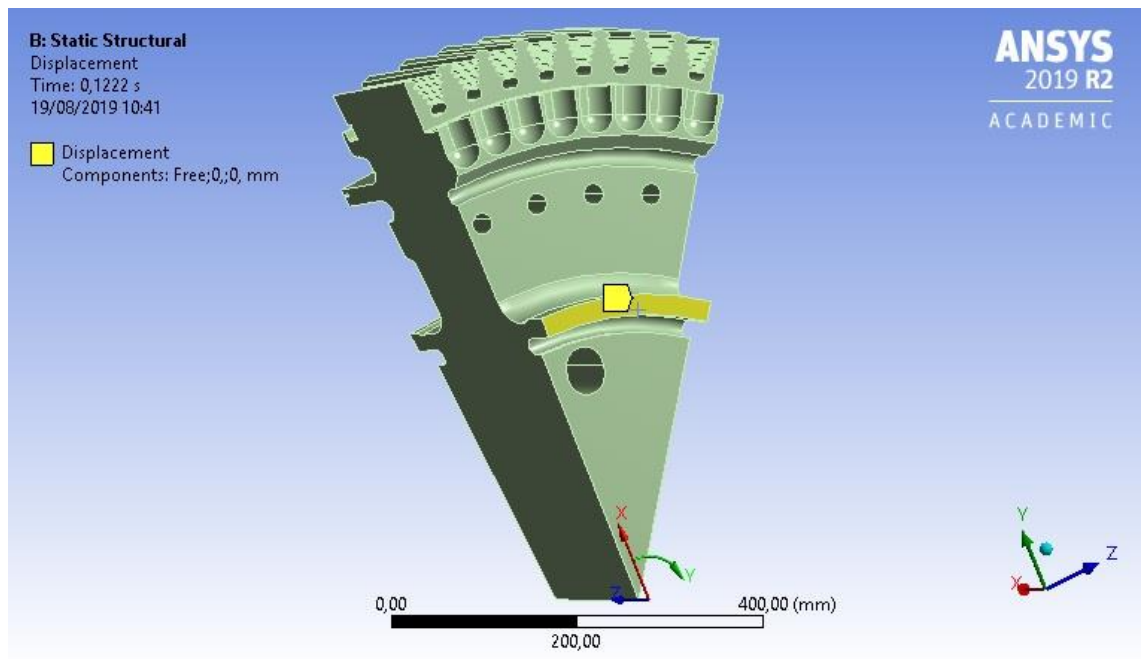


Figure 3.12: constrained surface is highlighted in the slice of the first stage disk (inlet face).

This displacement is chosen because it produces a solution that has reasonable values and distribution of the stress.

The results under examination are three: Maximum principal stress, equivalent stress and total deformation. These are enough to obtain general information about the behaviour of the body. The “Maximum Principal Stress” results provided by *Ansys* corresponds with the principal stress (or normal stress), it is calculated at a certain angle when shear stress is considered as zero (Usually it is described by the Mohr’s circles). The maximum value of normal stress is known as maximum principal stress. Instead, the minimum value of normal stress is known as “Minimum principal stress”, that is provide by *Ansys* through a separate viewer. Obviously, this computation is done for each element of the meshed body. For the turbine first stage, the *Figure 3.13* displays the result for “Maximum Principal Stress”, where the maximum value is 836,07 MPa. This is in the outlet face of the disk, where there is a shrinkage.

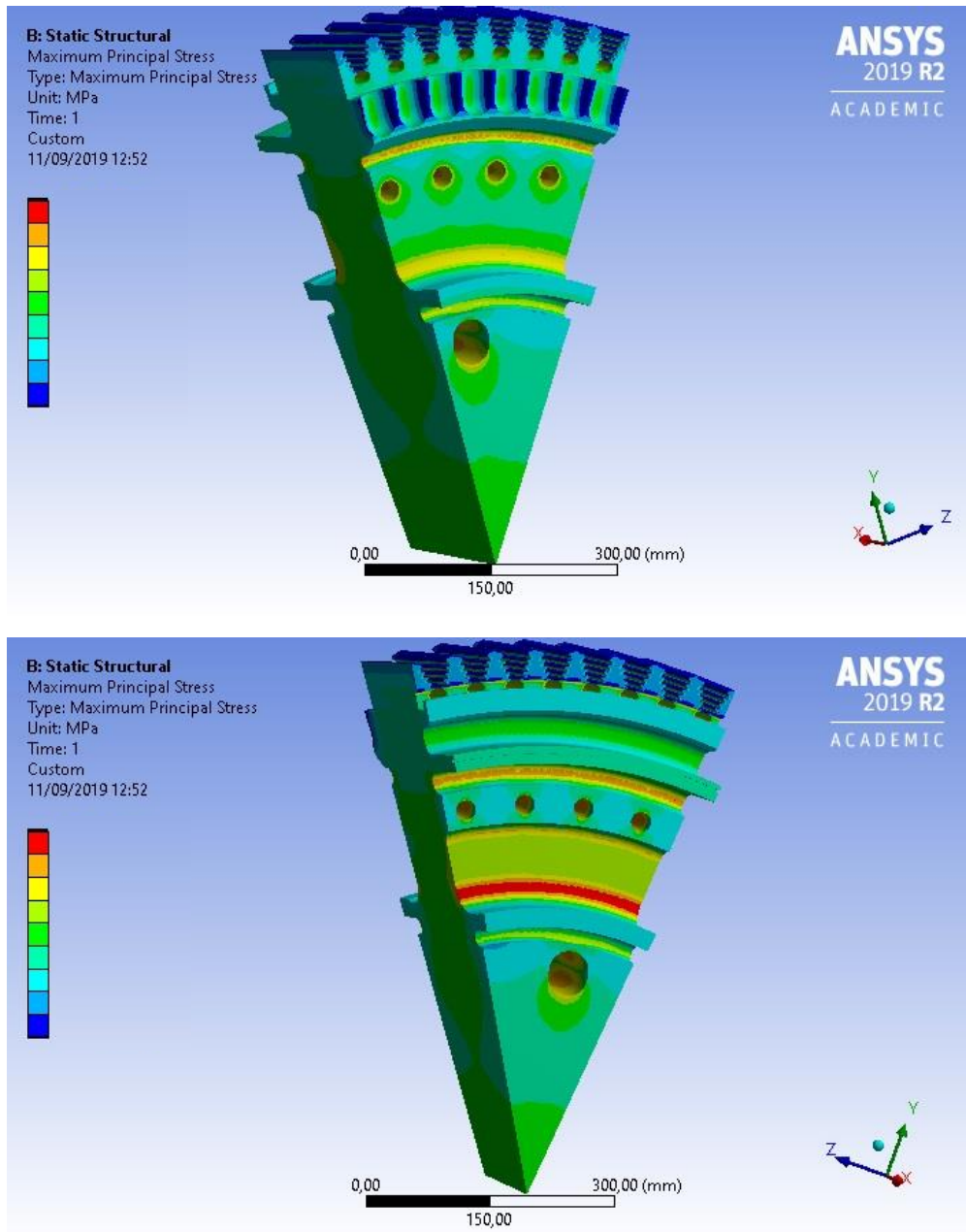


Figure 3.13: the maximum principal stresses in the front side (above) and rear one (below).

The grooves are dangerous areas due to the few material quantities, the load directly applied and the highest temperatures of the disk, here the maximum value of maximum principal stress is almost 684,53 MPa. The most stressed area is the one in red and a zoom of this area with some values are reported in Figure 3.14.

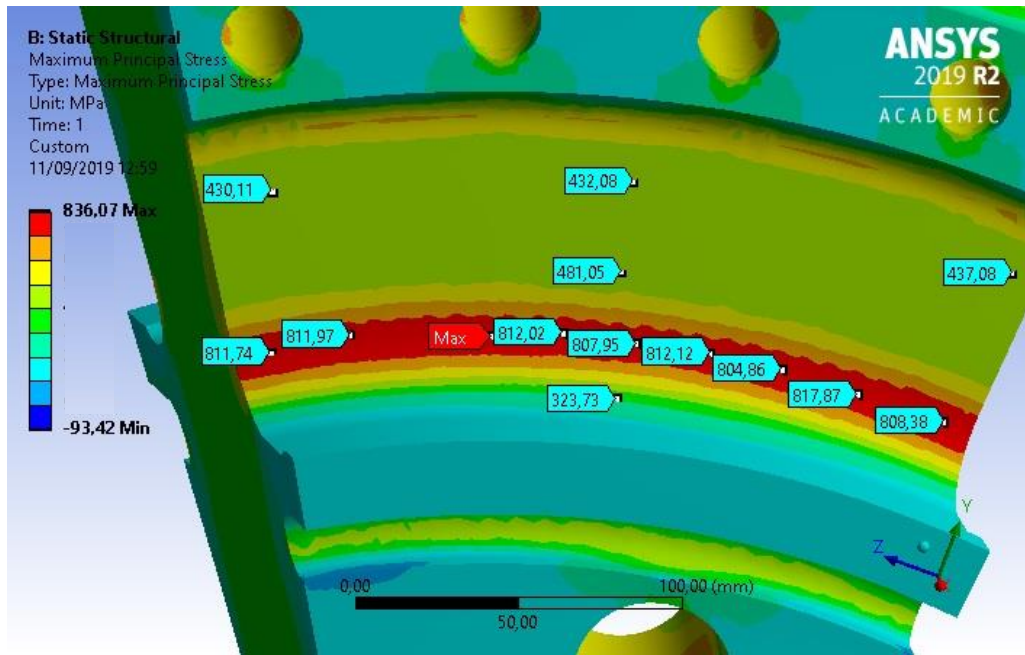


Figure 3.14: most loaded zone with values of maximum principal stress expressed in MPa

Strains may be related to the nodal displacements:

$$\{\varepsilon\} = [B]\{u\}$$

Where:

- $\{\varepsilon\}$ is the elastic strain vector that cause stresses.
- $[B]$ = strain-displacement matrix, based on the element shape function
- $\{u\}$ = nodal displacement vector

In this way, the stresses are calculated through the elastic stiffness matrix:

$$\{\sigma\} = [D]\{\varepsilon\}$$

Where:

- $\{\sigma\}$ is the stress vector.
- $[D]$ is the elastic stiffness matrix. It is function of Poisson's ratio, Young's modulus and shear modulus.
- $\{\varepsilon\}$ is the elastic strain vector that cause stresses.

From the stress components, the principal stresses (σ_1 , σ_2 , σ_3) are computed; they are ordered so that σ_1 is the most positive (tensile) and σ_3 is the most negative (compressive). The equivalent stress σ_e (or Von Mises stress) is calculated with the formula:

$$\sigma_e = \sqrt{\frac{1}{2}[(\sigma_1 - \sigma_2)^2 + (\sigma_2 - \sigma_3)^2 + (\sigma_3 - \sigma_1)^2]}$$

So, this base theory is used by *Ansys* to provide a viewer of the entire “equivalent stress” overview, as it is possible to appreciate in the *Figure 3.15*, for the thermo-structural analysis of the first stage.

The maximum value of the equivalent stress is 737,83 MPa and this time it is detected in the smaller holes, the ones for clamping the front ring that direct the cooling air to the blades (*Figure 3.16*). As is possible to see in *Figure 3.15*, the most stressed area for the maximum principal stresses is still one of the most loaded.

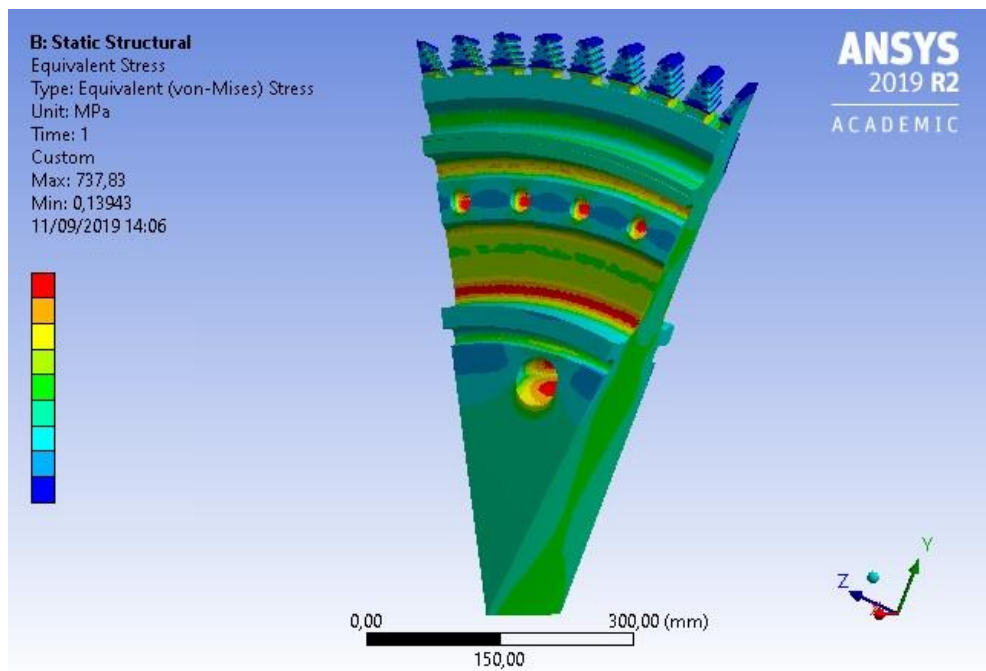


Figure 3.15: equivalent stress of the first turbine stage.

However, it is necessary to interpret the result obtained: under working condition, this body is not alone, but it is assembled with other elements. So, the holes are exposed to the highest equivalent load are not empty, but bolts are tightened there. It means that tensions are not so high, because there is not concentration stress due to lack on material and the deformation in this zone is not so easy due to the presence of another body. For the same reason, the high load on the larger hole is not so dangerous. These high values could be caused also by the sharp edge at the hole inlet or by the mesh that create sharp edge on the discretization of the hole. Therefore, the attention is shifted to the red zone (*Figure 3.16, right picture*), the same examined for the maximum principal stress. The highest value found here is equal to 700 MPa.

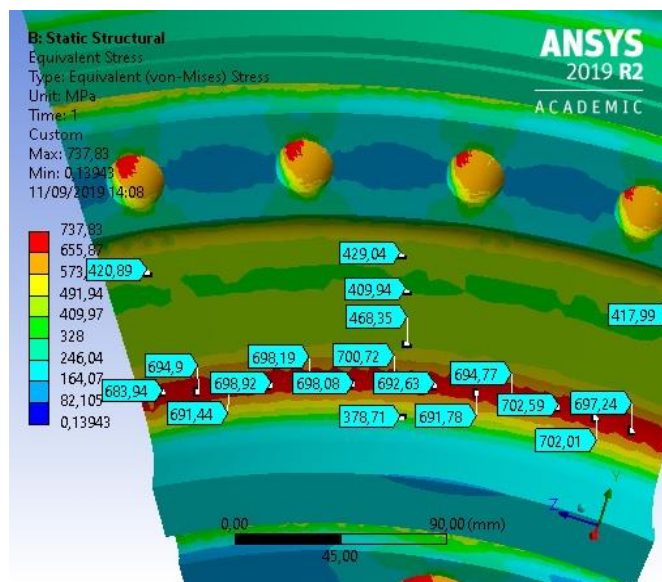
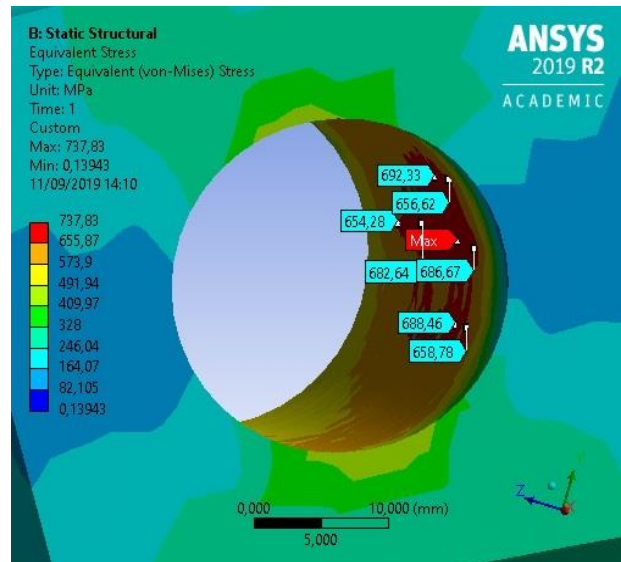
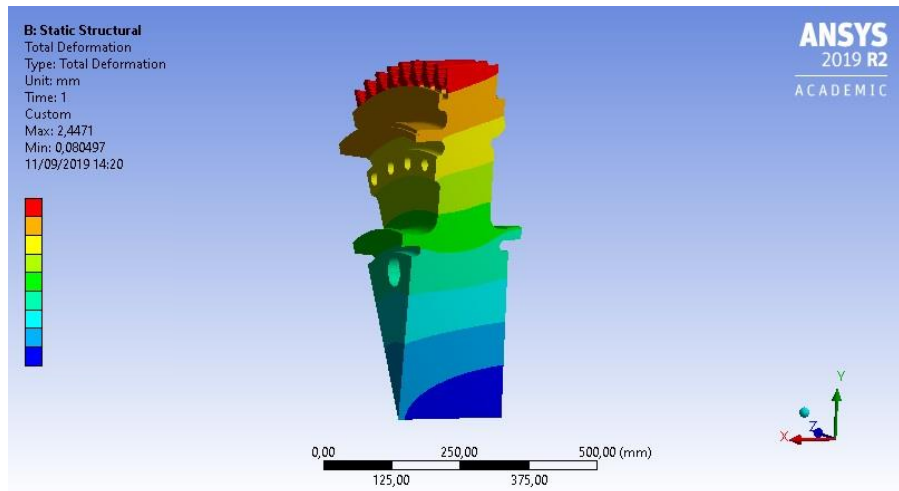
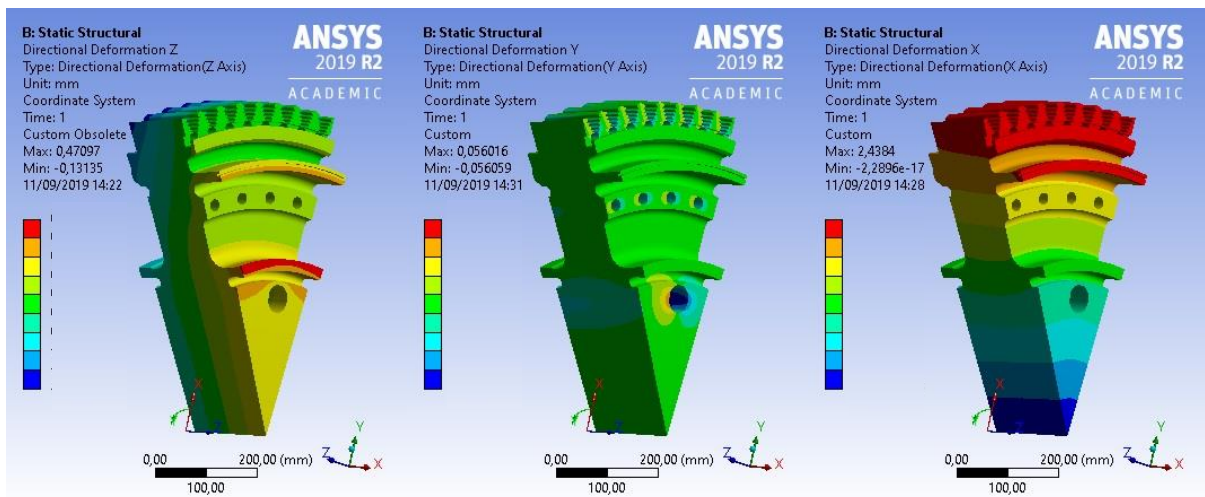


Figure 3.16: details of the smaller hole with the highest equivalent load and equivalent load scenario for the most dangerous area.

The last analysis is the one about the deformation: *Ansys* displays both total and singular direction deformations as it is possible to see in *Figure 3.17*. The deformation is very important also to ensure that blade remains clamped to the disk and also to guarantee that plays are respected and there are not interferences. The highest deformation is equal to 2,5 mm and it is detected in the vertex of the slice, but it is due to the cyclic symmetry, so in all the similar points of each groove the deformation is almost equal. Observing each direction of deformation is not difficult understand that the largest contribution for the total deformation is coming from the radial deformation, that reaches a peak equal to 2,4 mm, whereas the axial deformation reaches a maximum value of 0,5 mm and the circumferential one reaches a 0,1 mm.



(a)



(b)

(c)

(d)

Figure 3.17: total deformation (a) and deformation for (b) axial, (c) circumferential and (d) radial direction (different scales for the colours).

The first rotating stage does not worry the company, because to date it has never experienced a rupture in the operating machines.

In conclusion for the disk of first stage, it is possible to compare the analysis of thermal-structural load (primary plus secondary loads) so far studied with one that considers only the structural load (primary load): the maximum principal stress is compared in the Figure 3.18, instead for the equivalent stress and the total deformation a numerical comparison is done.

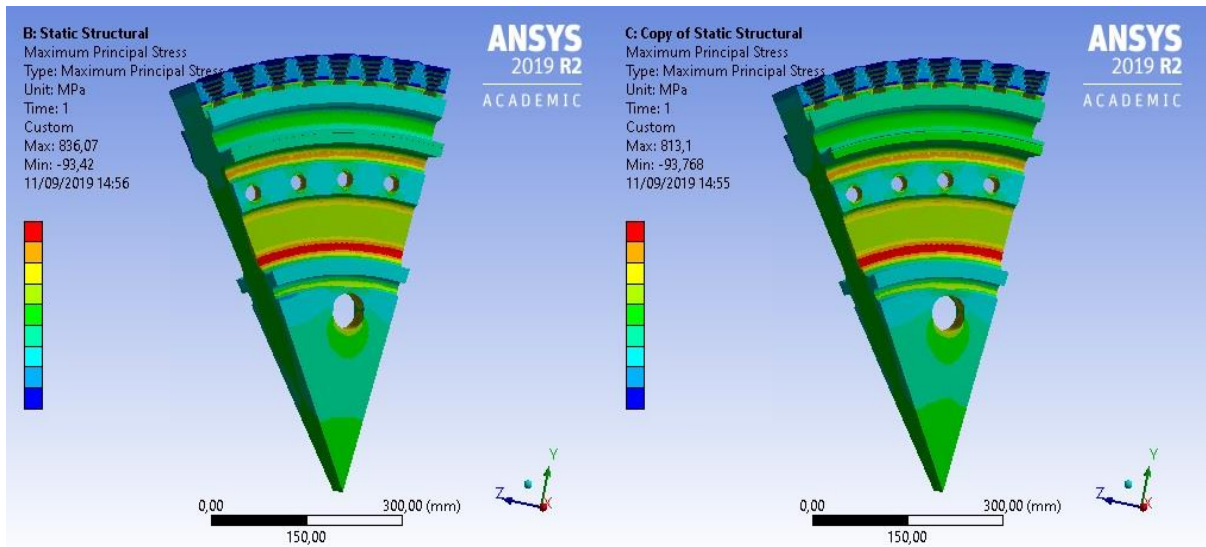


Figure 3.18: comparison of combined load (left) and only structural load (right); the scales are different.

The result only due to blade's force and rotational speed has a maximum value of 810 MPa; it means that the thermal load added to the structural one increases the highest value of the maximum principal stress of 3%. A similar increment is found for the equivalent stress (from 710 MPa to 740 MPa), whereas the deformation is strongly influenced by the thermal load, the total deformation is 0,8 mm for the single load, it moves to 2,5 mm for the combined one. The thermal load is much more effective also regarding the creep and the low cycle fatigue, for which a small increment in the temperatures sharply reduces the life of the component. Since the primary load has lower equivalent stresses and maximum principal stresses than the combined load (in all the critical), for what regard the analysis of the component's life, only the results coming from the thermal-structural load are examined.

3.5 TG20 B7/8: Turbine stage 2

3.5.1 Thermal analysis

The second stage of the turbine part needs an accurate analysis, because during the years it is always been the turbine part with the shortest life, the one most prone to break. This is due to the high loads (the blade is bigger than the one of the first stage) and temperatures without a dedicated cooling system. Now the stage has 70 blades and the same number of grooves; it leads to a CAD model for the thermal study that is one seventieth of the total body under

investigation (*Figure 3.19*). As the first stage, the disk is made with the customised structural steel and the blade of Inconel alloy. The first is always the one with a shorter creep life, due to the fact that construction material decreases strongly its resistance with increasing temperature.

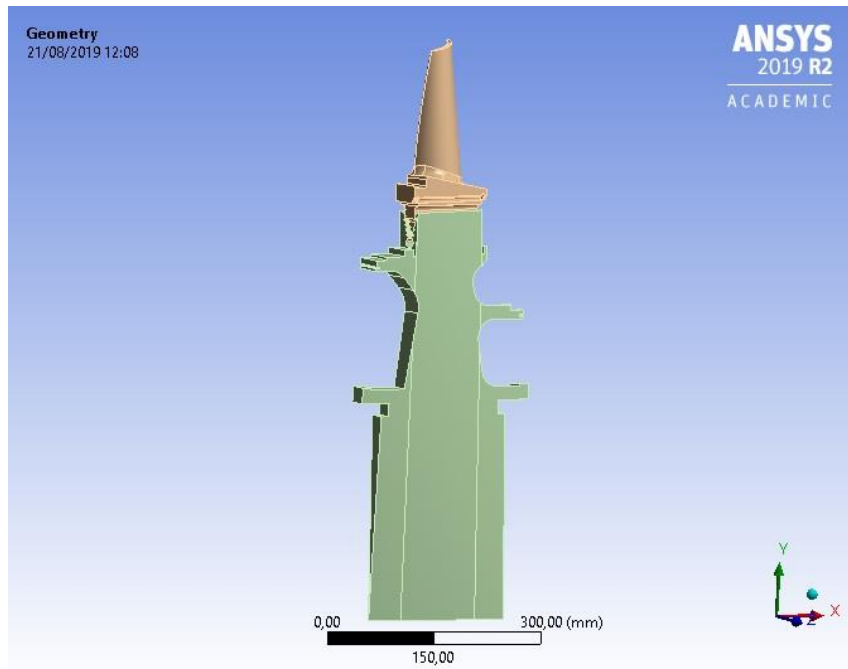


Figure 3.19: analysed slice of the second turbine stage.

The same arrangement used in the first stage is adopted to avoid the hot gases ingestion, based on the pressure difference.

The following step is to define a cyclic symmetry that ensure an examination of the whole stage. Active surfaces are 10 for the disk and 10 for the root of the blade, they are depicted in *Figure 3.20*. The type of contact chosen is “No separation” also in this case; it imposes no gap between selected surfaces and no friction between them. After many trials with different contact typology, this one provides the result closest to the reality. “No separation” is very similar to the reality thanks to centrifugal force acting on the blade that obligate active surfaces to remain in contact.

The mesh adopted is always the same for thermal analysis: maximum element dimension is equal to 6 mm for the disk and 2 mm for the blade and for the active surfaces.

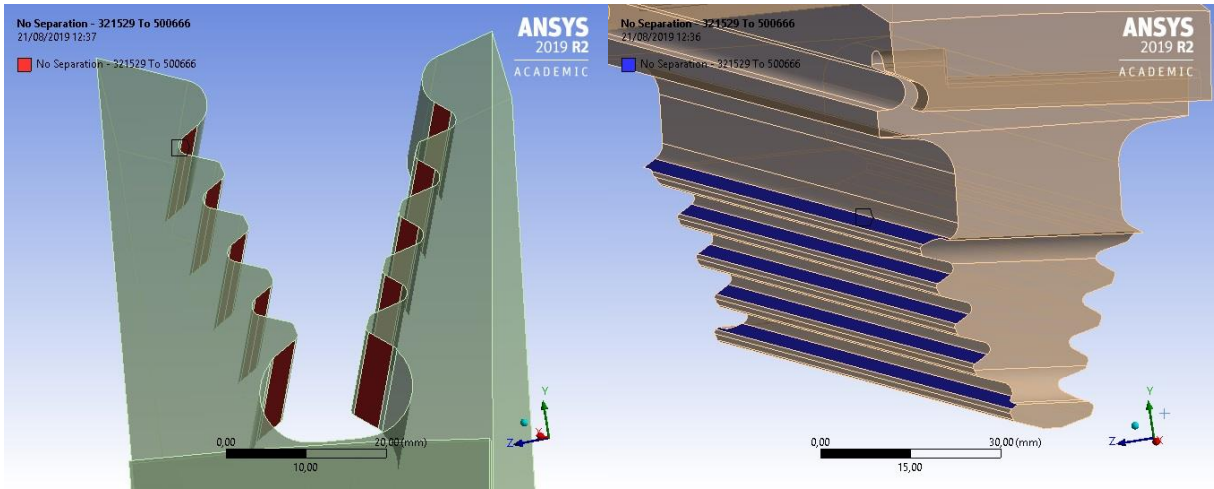


Figure 3.20: active surfaces of disk (red surfaces) and blade's root (blue surfaces).

The second rotating stage does not have a dedicate cooling scheme, but there are some flows coming from the second vane stage (cooled inside) that pass on the surfaces of the disk under examination, especially on the areas where disk and blade are keep in contact (Figure 3.21). These flows cause different heat transfer coefficients (listed in Table 3.3). In this case, the blade has no internal channels, so it is cooled down only by the disk (it is at a lower temperature).

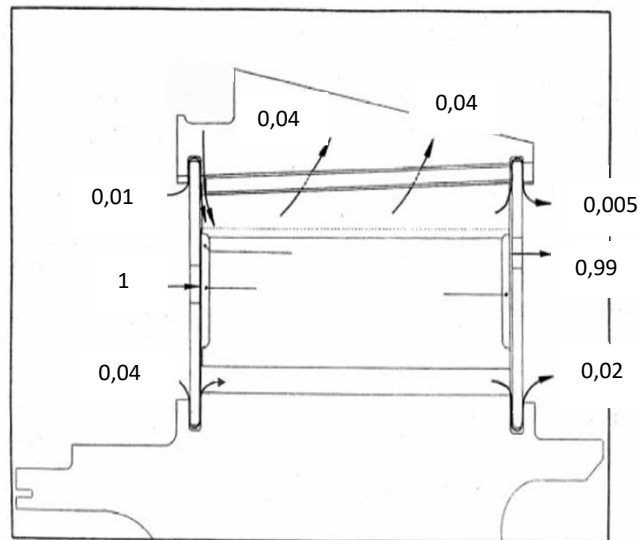


Figure 3.21: flows passing for the groove of the disk (normalised values).

For what regard the heat transfer coefficients on the blades, they are estimated thanks to data about temperature and speed of the fluid obtained by AxSTREAM; as done for the first stage analysed, the temperatures found are one for each section of the blade (it was “cut” in 7 sections). They make a parabolic profile for inlet and outlet, temperature for pressure and

suction surfaces are computed by interpolation. Since temperature, speed and density change along the height of the blade, two heat transfer coefficients are computed (one for the section number 4 and one for the number 7, 50% and 100% of the total blade's height) and then an average between them is calculated. Moreover, in this case the coefficients on the shank of the blades are two, since they diverge for cross section. For the heat transfer coefficients on the disk (and the root of the blade), *PH4165* gives all the data necessary for the computation (using also the cooling schematization, similar *Figure 3.9*) by DuPont formulation. As it was done for the first stage, the disk and the blades are divided into many surfaces, in this way each of them experienced different heat transfer coefficient caused by the different flow conditions and restriction areas. All the computed data are inserted in *Table 3.3*.

In the second stage there are two particular disk's surfaces (they create a chamber if they are seen in the whole disk), called lower inlet and lower outlet, for which the coefficient is not computed but it is approximated, since here the fluid is at 220-200 °C (inlet-outlet) and at a very low speed.

Region	Heat transfer coeff.	Max air temperature	Min air temperature
BLADE	$\frac{W}{m^2 \cdot K}$	°C	°C
Inlet surface	1660	850	750
Outlet surface	165	660	550
Pressure surface	490	690	590
Suction surface	545	690	590
Lower shank surface	50	340	340
Upper shank surface	40	320	320
Inlet/Outlet root	150	343	290
DISK			
Inlet surface	60	290	290
Inlet surface lower	20	220	220
Outlet upper surface	80	340	340
Outlet middle surface	80	240	240
Outlet lower surface	20	200	200
Grooves surface	150	315	315

Table 3.3

Given that this rotating stage is the most prone among the three of the turbine's part, it is preferred analyse blade and disk individually (*Figure 3.22*). For the blade, the maximum temperature resulting from the simulation is 763,07 °C; it is higher than the value found for the blade in the first stage, although the inlet temperatures of the gas are much higher in that case.

Obviously, it is due to the absence of a dedicated cooling system for the second stage. The experience teaches that is the disk of the second rotating stage the weakest link of the turbine part (largely caused by the centrifugal load): the maximum temperature computed is equal to 363,46 °C. This maximum value is discovered in the extreme vertex of the groove's outlet section, as happen for the first stage, for which the temperature peak is equal to 296,34 °C. The higher value found for the second stage is not strange in spite of the temperatures of gas mixture are lower, since this stage has no cooling system and the temperatures of the disk are mainly function of the blade's ones.

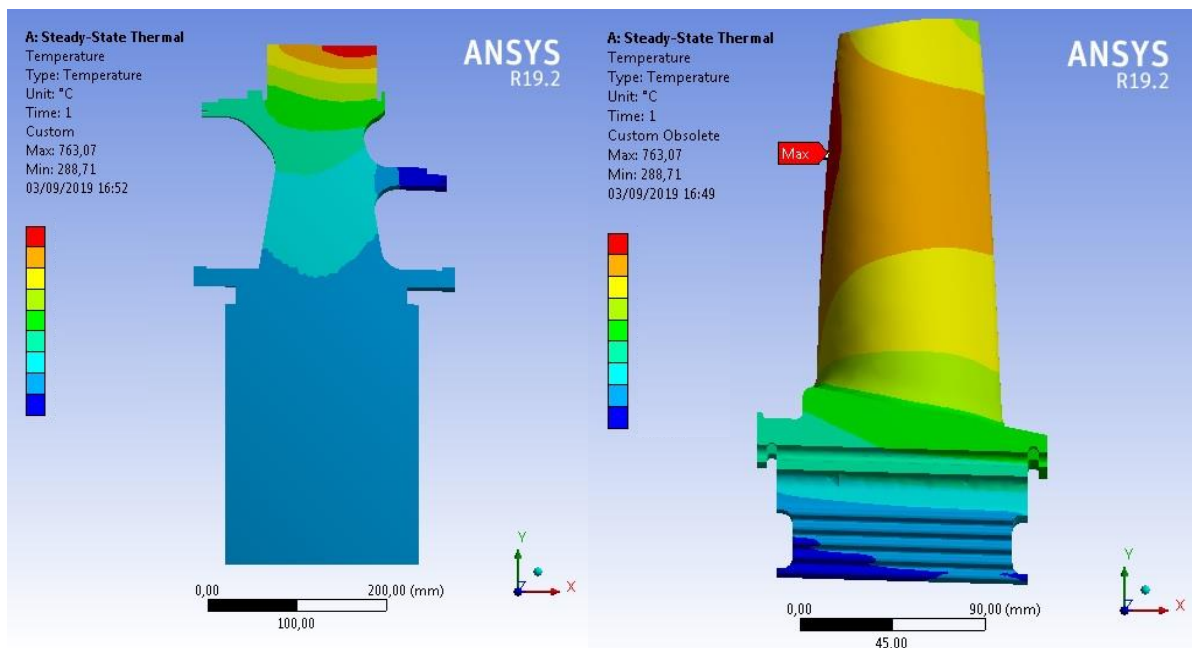


Figure 3.22: temperature scenarios for disk and blade of the second rotating stage (pay attention to the different scales).

The maximum value for the blade is found in the inlet surface, but it is predictable since in this surface the temperature of the fluid is the total one, because the fluid bumps into the inlet surface (stagnation point).

3.5.2 Thermo-structural analysis

Once the thermal analysis is completed, it is possible to move towards the combined analysis. The first step is to choose a new CAD model that include all the details of the real body, in order to obtain a simulation as close as possible to the real behaviour: in this stage, disk has holes for the tie rod (the same that pass through the first disk) and connection radii that could

be points of stress concentration and they influence stress distribution. In this part of the analysis, only the structure of the disk is under examination. Since the grooves are 70 in the second rotating stage, the slide of the disk (*Figure 3.23*) is cut in order to be one tenth of the total: in the simulation there are 7 grooves.

Material, coordinate system and symmetry conditions are applied as it was done for the thermal analysis, whereas the connection are not present for one body study. For what regard the mesh, the same type of discretization used for the first stage thermal-structural analysis is adopted (*Figure 3.23*). The maximum element dimension is set equal to 4 mm with a refined mesh for the upper part where the upper limit for the element dimension is 2 mm, since this part is usually critical; it is shown in the third picture of *Figure 3.23*.

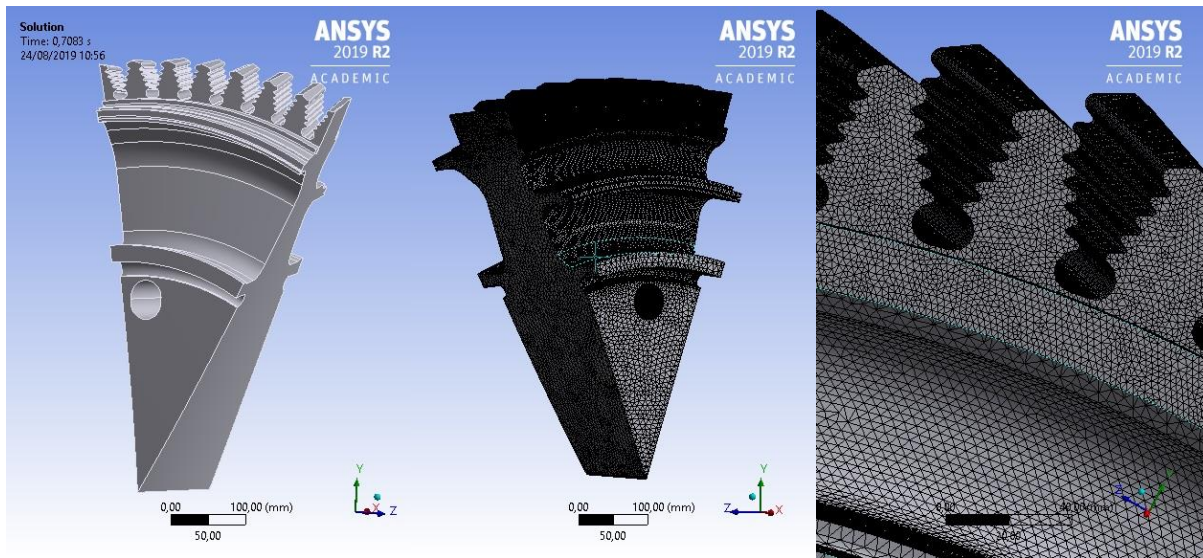


Figure 3.23: front, rear (meshed) and mesh specific views of the CAD model for thermo-structural loads of second stage.

The thermal load is imposed in two different way: convection on the inlet and outlet parts of the disk (as the ones of the previous simulation) and temperatures on the active surfaces (*Figure 3.24*). Along the active surfaces of the disk's grooves, the temperature trend is established from the thermal analysis by take into account many points of these surfaces: the active surfaces are divided in 5 couples, the ones at the same height (symmetric) experienced the same temperatures. In the groove the temperatures are comprised in the range from 310 °C to 360°C. The temperature scenario is almost the same of the previous simulation.

The second part of the analysis setting regards the centrifugal load induced by the blade on the groove of the disk, or better in the active surfaces.

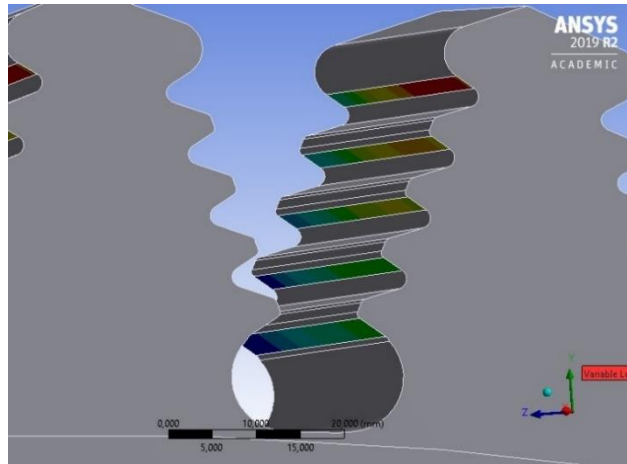


Figure 3.24: active surfaces with temperature variation along the axial direction of the groove.

Ansys evaluates also the rotation of the disk that conditions the final result. For the second rotating stage, the centrifugal force “ $F_c = m \cdot r \cdot \omega^2$ ” reaches a higher value than the first one. This is due to the weight of the blade (m) that now is 5 Kg. The mass is concentrated in the blade’s centre of gravity at a distance (r) from the centre of the disk equal to 0,6 m. Clearly, the considered rotational speed (ω) is the same adopted for the first stage. The resultant force applied in the active surfaces is equal to 850 kN and it is radially directed. Respect the first stage, the force is increased of 37%, therefore the temperatures are higher too: combination of these two factors explain why this stage is the most critical one. The rotational speed is imposed to the disk and it is the overspeed one (+3% respect the nominal one) and it is 5065,5 rpm, as it was imposed for the disk on the analysis of the first stage. In this simulation, constraint must be set to define the allowable displacements for the disk, as it was done for the first one. Many trials are done to find constraint that leads to the most realistic simulation. The chosen one (*Figure 3.25*) is on the inlet surface and here the disk is free to move only in the radial direction, along the other two directions it is blocked.

The analysis is focused on the same three results of the first stage work: maximum principal stress, equivalent stress and total deformation. These are used to have an overview on the studied body and during the work process they are used to understand if all the conditions are set in the right way.

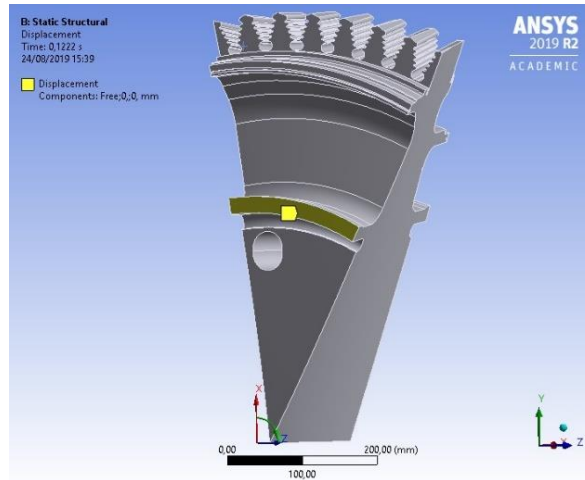
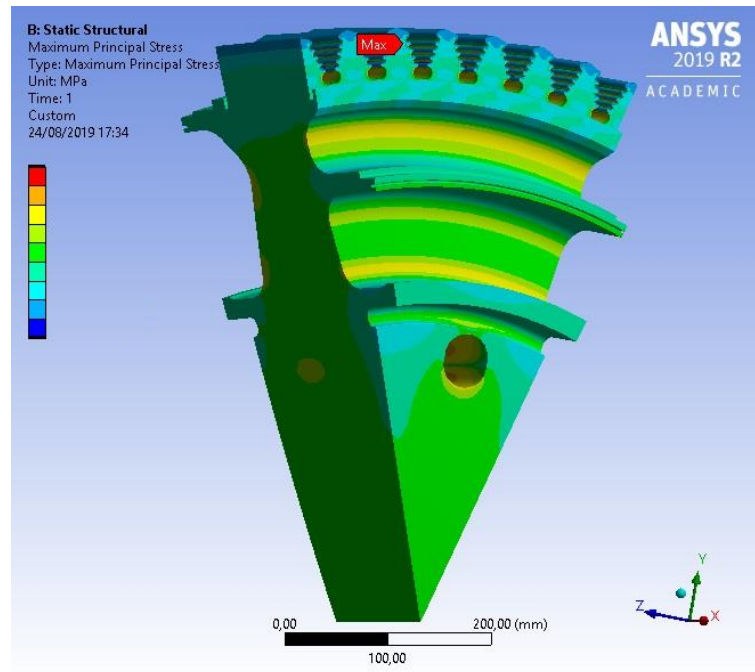


Figure 3.25: constrained surface is highlight in yellow.

The maximum principal stress, one of the results used to understand if the body withstands the thermal and structural load, is reported in the *Figure 3.26*: there are result for the entire disk and an enlargement on the most dangerous area. The peak value is equal to 811,63 MPa; this time it is not detected on the shrinkage of the disk, as happen for the first stage, but it is found in the groove (near the outlet face of the disk). As said previously, the groove is critical due to the high temperature and the geometry, therefore the fact that the maximum principal stress is detected here is a wake-up call.



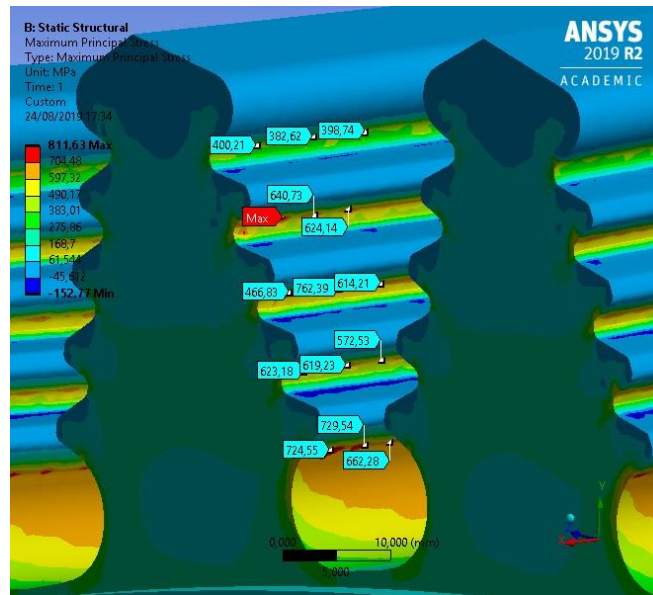


Figure 3.26: max principal stress result, overall and zoom on most loaded zone (results in MPa).

Ansys compute everything during the simulation and so it displays what is requested by the user, as the equivalent stress. During the examination of the second rotating stage, the maximum value of the equivalent stress is equal to 822,20 MPa (Figure 3.27); it is discover in the groove as for the maximum principal stress, but it is not near the outlet surface, but in the middle of the lowest active surface (Figure 3.28).

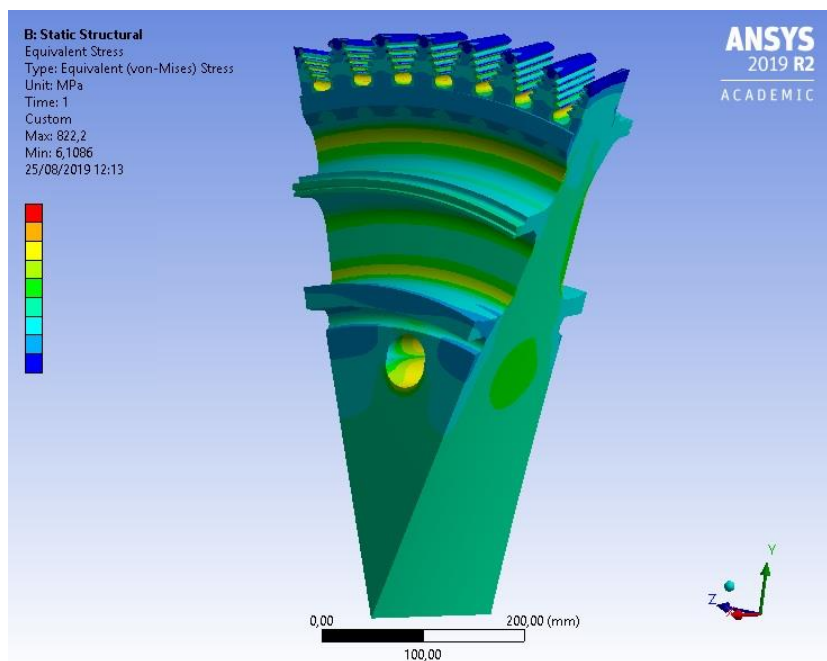


Figure 3.27: overall view of the equivalent stress variation on the disk of the second turbine stage.

This maximum value is much higher than the one computed for the first stage and it is also located in a more critical zone; as it is possible to see from the *Figure 3.28*, the high equivalent stress is not in a large area (as it happened for the equivalent stress in the first stage), but it is detected in a very small area and so it may be not so dangerous as it seems. The shrinkage part of the disk experience a high equivalent stress also in this case due to thickness variation, but differently from the first stage, here it is much lower than valued found in the grooves.

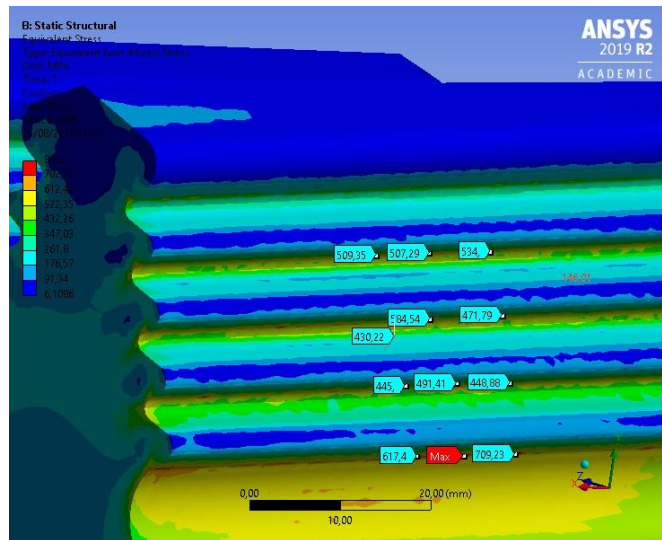
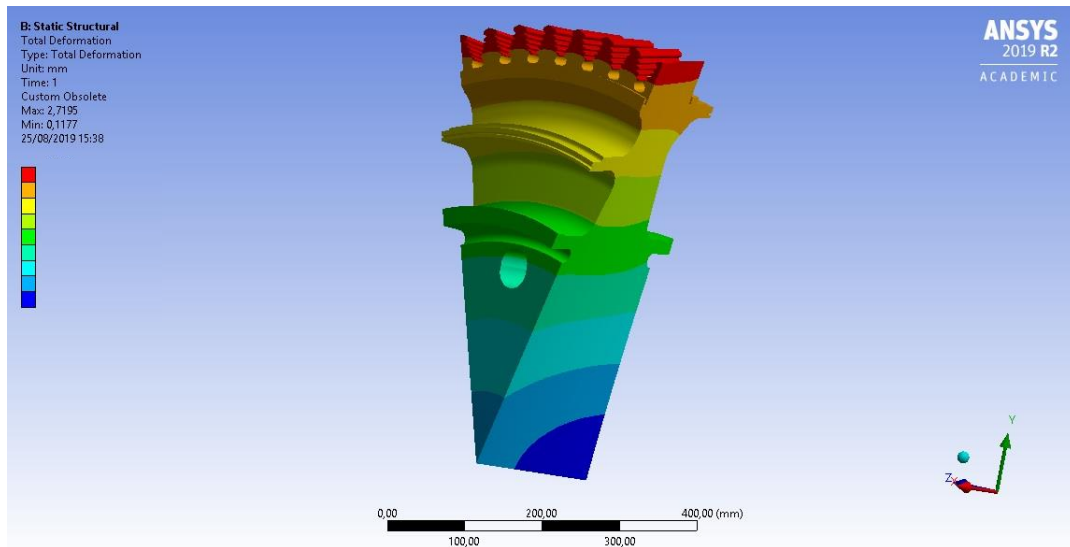
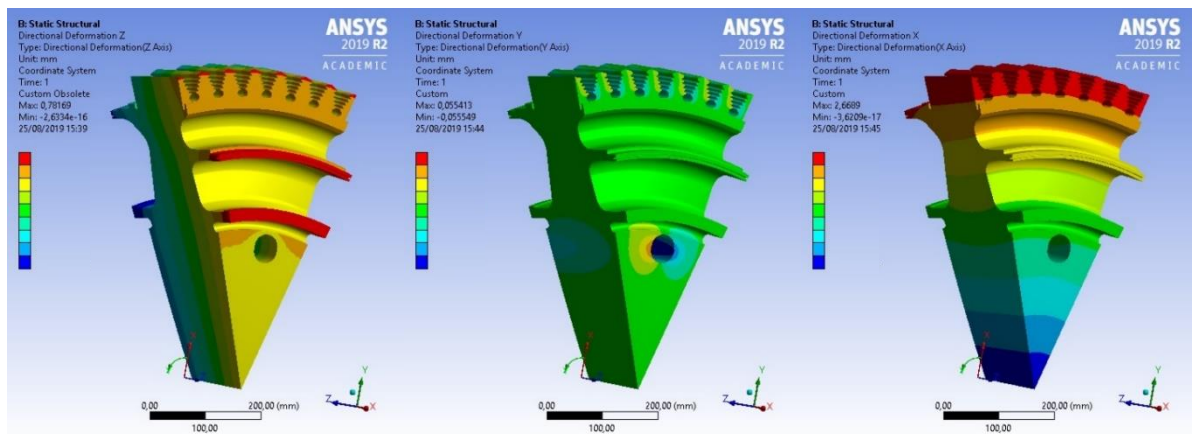


Figure 3.28: zoom in the area where the equivalent stress value is the highest identified.

The next and last step is the examination of the total deformation occurred to the disk. *Ansys* allows to observe each displacement individually and then also the summation of them (*Figure 3.29*). The deformations are the data used by the software to compute all the stresses and they are useful to understand which is the real configuration of the machine when it is working. The highest deformation's value is estimated 2,7 mm, it is lightly higher than the one computed for the first stage. This peak value is found near the outlet face of the disk, in the tip of the groove. As it possible to see from *Figure 3.29*, the trend of the deformation is almost symmetric for the inlet and outlet surfaces of the disk (in the first stage the deformations are higher in the outlet surface). This behaviour finds an explanation when the singular directions are observed (*Figure 3.29*). The radial deformation, the most relevant component, has also a symmetry trend and it influences a lot the final result. The circumferential deformation reaches a peak equal to 0,05 mm, similar to the first stage's one. This contribution is unimportant. The greatest value for the axial deformation is 0,8 mm.



(a)



(b)

(c)

(d)

Figure 3.29: total deformation (a) and deformation for (b) axial, (c) circumferential and (d) radial direction (different scales for the colours).

As last part of the investigation, the results coming from the combination of thermal and structural loads just analysed are compared with ones only due to the structural loads. The maximum principal stress distribution for the two cases is almost the same, instead of the equivalent stress trend that is much lower for the single load case: for the latter, maximal value measured is 731,42 MPa, whereas for the first one it is 822,20 MPa. It indicates a rise of 12% on the peak value caused by the thermal load. The most affected result among the ones examined is the total deformation (it happened for the first stage too) and the comparison between these outcomes is reported in Figure 3.30. the maximum deformation value moves from 0,7 mm to 2,7 mm by adding the thermal load to the simulation.

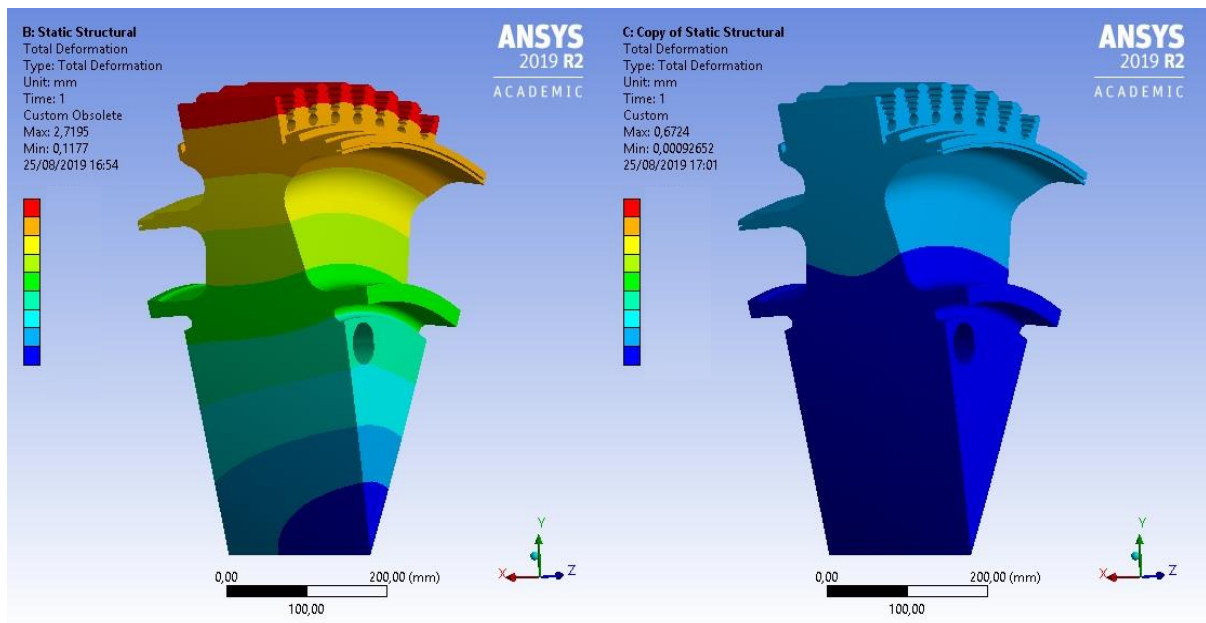


Figure 3.30: comparison of combined load (left) and only structural load (right); the scales are almost similar in this case.

3.6 TG20 B7/8: Turbine stage 3

3.6.1 Thermal analysis

The third and last stage is composed by 65 blades wedged in the grooves of the disk. Here the temperatures are lower than other stages and no dedicated cooling system is planned. The CAD model (*Figure 3.31*) used is one sixty-fifth of the whole disk, thus result is computed for a disk's slice and a blade. The disk is different from the ones in other stages: in the outlet face a kind of shaft is integrated with the disk in order to support an outlet ring for directing of the exhaust gas and to position the bearing that support the entire rotor.

The cyclic symmetry condition is imposed in the two lateral surfaces of the disk, as it was done for the other stages. In the same way, the chosen materials are not changed: customised structural steel for the disk and Inconel alloy for the blade.

Considering that the relative movement of the blade is always the same for the three stages, the connections between active surfaces (still the same selected for the second stage, *Figure 3.20*) is imposed as “No separation”, like it was done in the other two cases. Furthermore, here the blade is heavier and this leads to a higher centrifugal force that mainly confirms this choice for the simulation of connections.

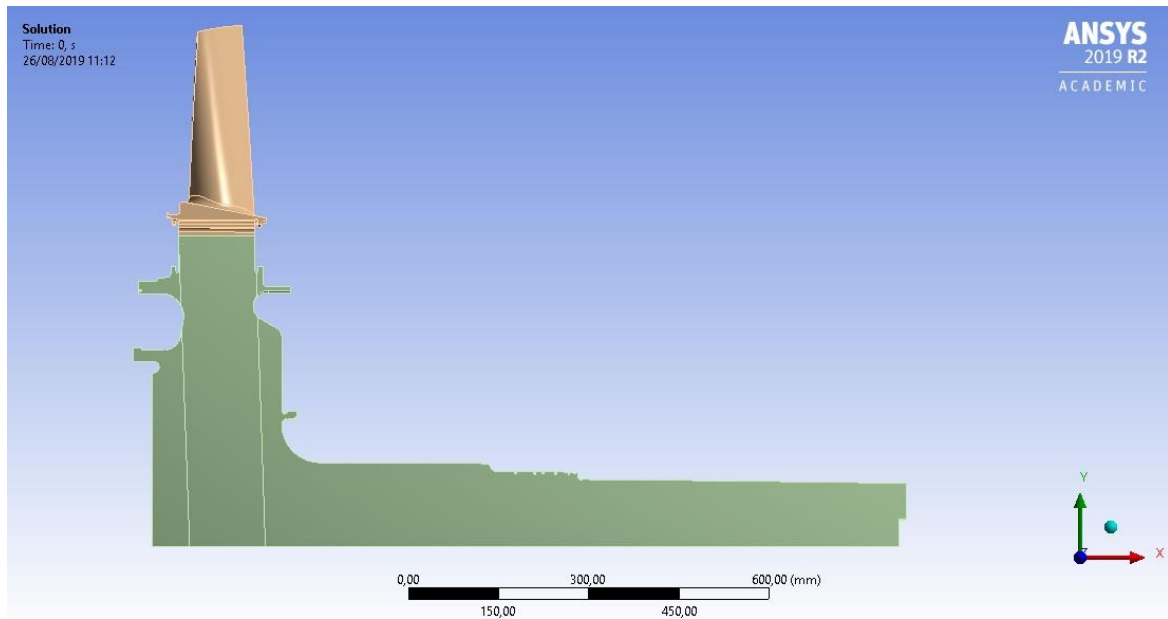


Figure 3.31: analysed slice of the turbine third stage.

The mesh applied is the one already used for the others thermal analyses: the maximum element size for the disk is 6 mm and the one for the blade and for the active surfaces is 2 mm.

For what regard the different thermal loads, in this case the internal software PH4165 cannot give any information on cooling, as this stage is not model here (since the temperatures are lower and no problem has never occurred to this stage). Then, the different heat transfer coefficients for the convection acting on the disk and on the blade's root (listed in *Table 3.4*) are calculated by scaling the second stage's data for different working conditions and temperatures. So, DuPont formulation is used to compute the coefficients but this time the TG50C is no longer the basis of comparison. Now the "known" coefficients are taken from the second stage of the TG20 B7/8, considering that it is very similar to the third one. These air fluxes pass through the disk surfaces and cool down the temperature: they come from the third stage vane, as it happens in the second stage. As for the second stage, there are two disk's surfaces (lower inlet and lower outlet) for which the coefficient is estimated: in this stage it is evaluated by comparison with the previous stage.

To compute the heat transfer coefficients of the blade, *AxSTREAM*'s data are taken from 2 of the 7 section in which it is schematized (half height and tip of the blade); then the average between these two sections is computed and the value of the heat transfer coefficient for the surface is found. This software supplies the temperatures of the gas that expands in the turbine; as in the other stages, the temperatures has a parabolic profile in the inlet and outlet surfaces, but values are lower than other cases.

In this case, the presence of the bearing in contact with the disk cause another thermal load: the temperature reached by the bearing when the engine is at full speed is equal to 80 °C; since bearing is in close contact with the shaft, we can assume this same temperature (due to thermal conduction) imposed in the contact surface between them.

Region	Heat transfer coeff.	Max air temperature	Min air temperature
BLADE	$\frac{W}{m^2 \cdot K}$	°C	°C
Inlet surface	1200	670	560
Outlet surface	150	500	370
Pressure surface	375	500	400
Suction surface	420	500	400
Shank surface	40	290	240
Inlet/Outlet root	80	290	240
DISK			
Inlet surface upper	30	240	240
Inlet surface lower	20	200	200
Outlet surface upper	50	300	300
Outlet surface lower	20	200	200
Grooves surface	80	300	240

Table 3.4

As it was done in the second stage, the two bodies that compose the analysed system are examined separately (*Figure 3.32*). The blade experiences a peak temperature value of 575,95 °C and it is detected in the inlet surface, where the total temperature (due to the stagnation points at the inlet) of the gas mixture reaches its highest value. This value is much lower than the ones found for the other two cases analysed, despite of this stage (as the second one) has no dedicated cooling system. The same situation comes up again for the disk, for which the highest temperature computed by simulation is 300,35 °C. This is discovered in the highest active surface of the groove, near the outlet upper surface of the disk, as it happened for the other disks. This temperature peak is much lower than ones of the other two stages (almost 16% respect the second stage) and this fact ensures a higher life for the stage: this conclusion coming from simulation is confirmed from the real experience.

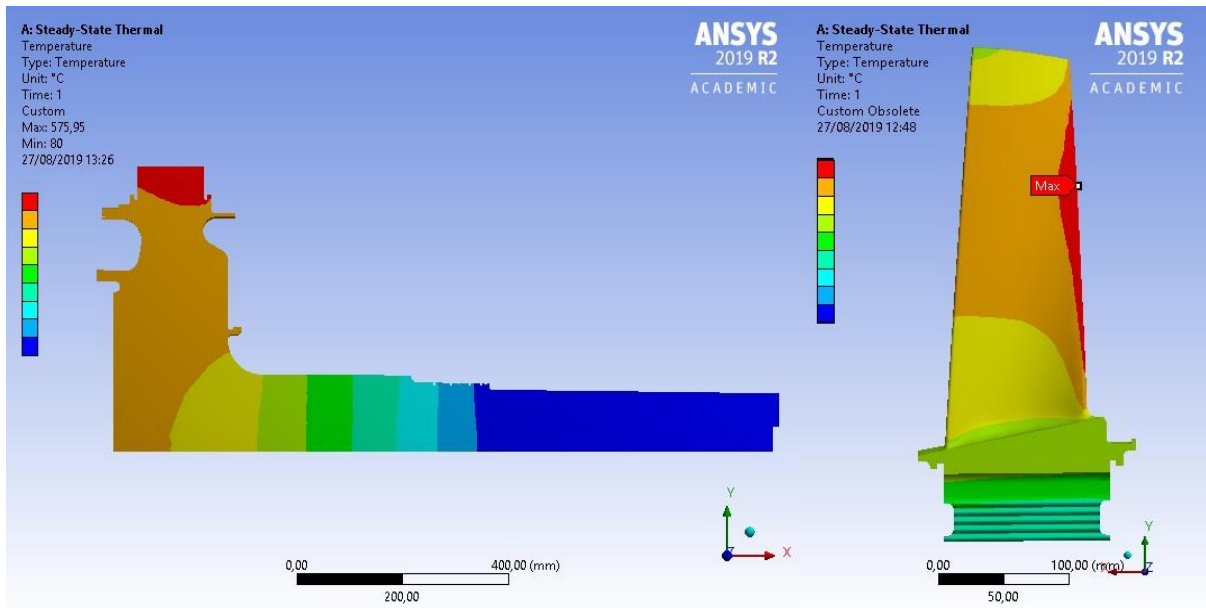


Figure 3.32: temperature scenarios for disk and blade of the third rotating stage (pay attention to the different scales).

3.6.2 Thermo-structural analysis

Once obtained the temperature as final result of the previous analysis, the following passage is to sum this thermal load to the one due to centrifugal forces and in this way simulate the real behaviour of the disk of the third rotating stage. The new CAD model (*Figure 3.33*) includes all the details and the connection radii that are not influent for the thermal load, but they change a lot the stresses' distribution. Obviously, the holes are present here as well, for the passage of the tie rod that keeps closed the turbine pack. The real third stage has 65 grooves, but to avoid problem with the cyclic symmetry, the number of grooves in the CAD model is reduced to 64. In this way, it is possible to obtain a slice that is one eighty of the total and has exactly 8 grooves. Nevertheless, the simulation is close to the real behaviour of the stage.

All the initial data requested by *Ansys* are the same of the other stages: materials, coordinate systems, symmetry regions and the connections (that are not present for one body examination). The mesh has the same characteristics of the ones just made, too: tetrahedron elements with a maximum element size of 4 mm for all the body and 2 mm only for the grooves, where the disk has more details and the centrifugal loads are directly applied; the difference is well visible in the right part of *Figure 3.33*.

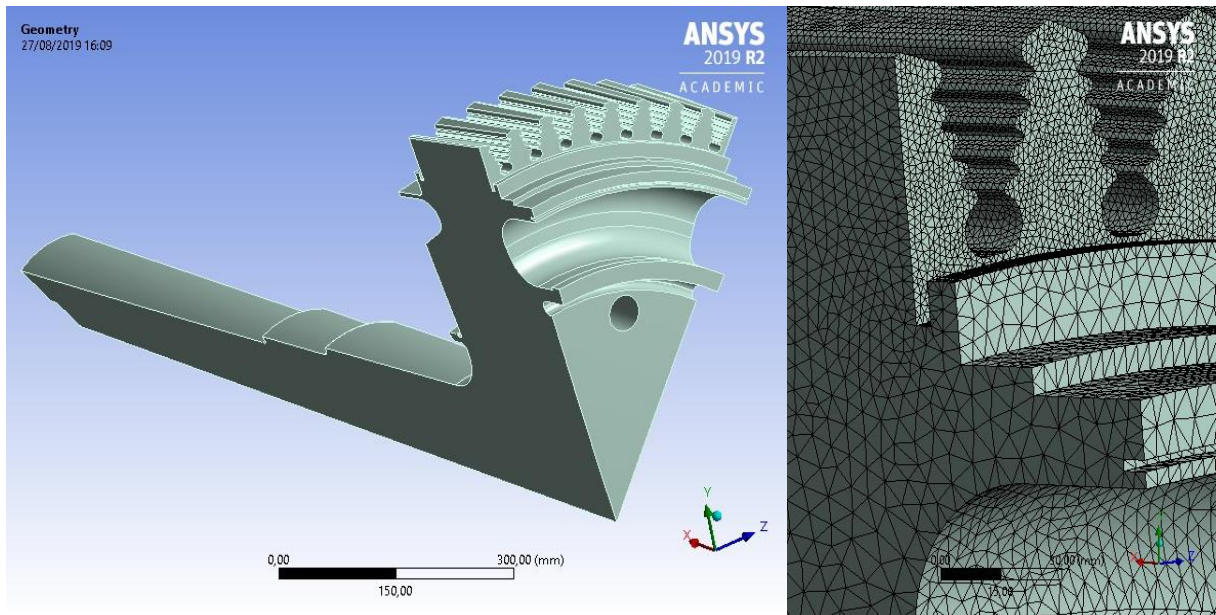


Figure 3.33: CAD model and zoom on mesh's details of the third stage simulation.

The first load imposed is the thermal one: the convection on the disk are imposed surface by surface (the data are listed in *Table 3.4*) for the inlet and outlet faces, instead regarding the temperatures of the whole blade that affect the behaviour of the disk, only the temperatures of the active surfaces in contact with the disk's grooves are imposed as thermal load (*Figure 3.34*) caused by conduction.

These values imposed to the grooves are taken from the thermal analysis, by collecting more than 50 values for each active surface of the blade's root along the axial direction (symmetric surfaces have the same temperatures). The imposed temperatures reach a peak of 302 °C, while the lowest one is equal to 280 °C. The first one is located at the outlet of the highest active surface, whereas the latter is located in the inlet part of the lowest active surface. Another imposed temperature is the one of the bearing (80 °C) on the last part of the disk. It gives a trend to the temperature's scenario.

After that the thermal load is settled, the analysis arouses its interest in the centrifugal load that affects the active surfaces of the disk's groove and the one that considers the disk's rotation. The blades assembled on the third rotating stage are the biggest among the three stages of the turbine part.

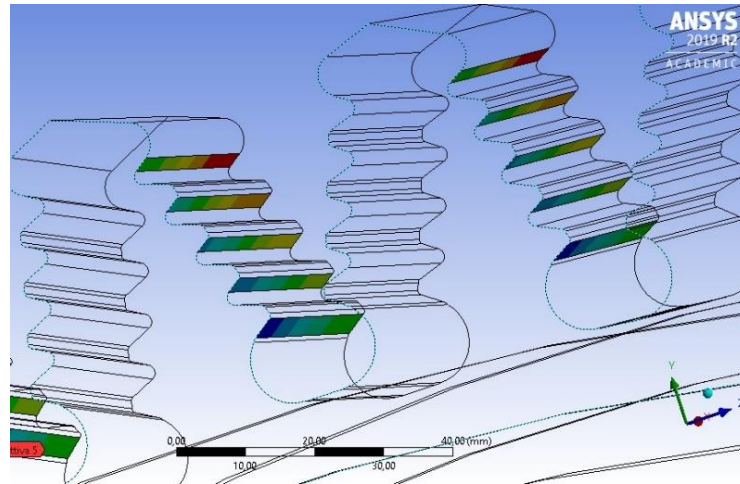


Figure 3.34: temperature trend on the active surfaces represented in the wireframe graphic model.

It means that the centrifugal force “ $F_c = m \cdot r \cdot \omega^2$ ” is the highest one: the mass (m) of the single blade in this case is 6 Kg (heavier than the second stage’s one), while its centre of gravity (r) is at 0,6 m from the disk’s centre (less than the second stage’s case). Since the rotational speed (ω) is still equal to 5065 rpm, due to the tie rod that forces the three disks to rotate in the same way and with the same relative positions. The resultant force applied to simulate the blade’s presence is 1010 kN, radially directed and it is set on each groove where it is divided through all the active surfaces. This force is 18% higher than the one of the second stage and it is almost 65% higher than the one of the first stage.

The rotational imposed to all the body is 5065 rpm, as it was done for the other stages, the overspeed is imposed to be safe.

The constraint imposed is like the one chosen in the second stage: the surface on the inlet face highlighted in the *Figure 3.35*. In this case the axial and circumferential displacements are constrained and the radial displacement is leaved free to move, exactly as for the firsts two stages. This condition leads to the simulation closest to the real behaviour of the stage.

As it was done for the other two stages, three type of results are investigated: maximum principal stress, equivalent stress and total deformation. These allow to make a general idea about the studied component and to compute the number of equivalent hours that the disk can bear without breaking and the number of equivalent cycles that it can stand, or rather the life of the body.

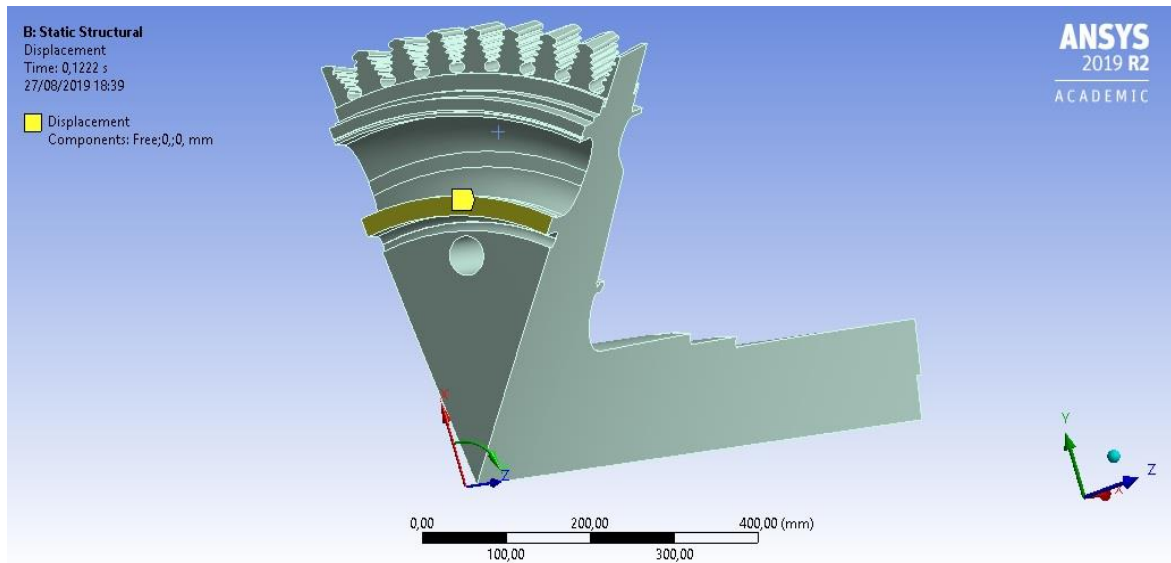
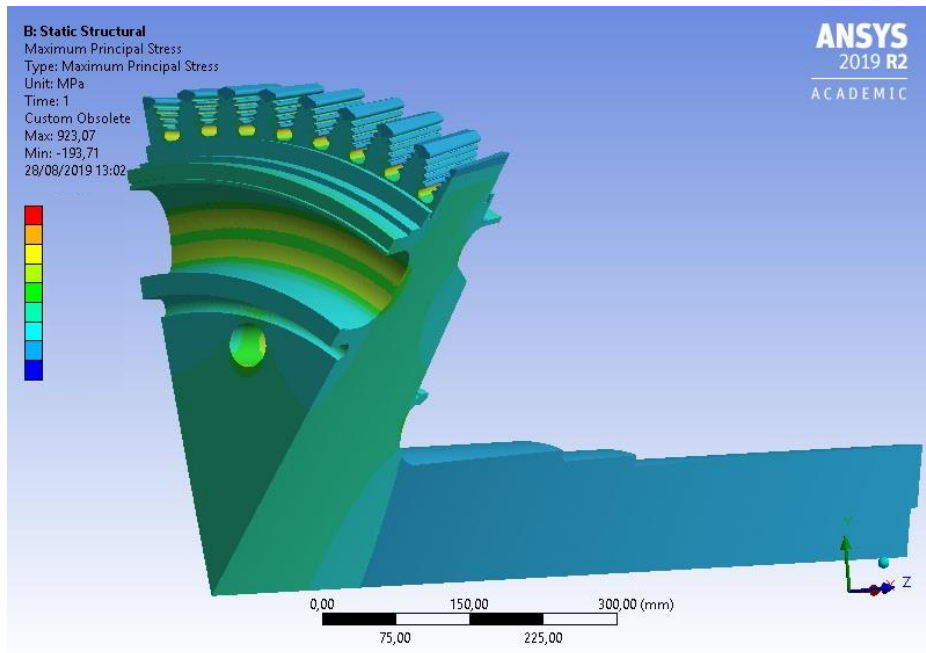
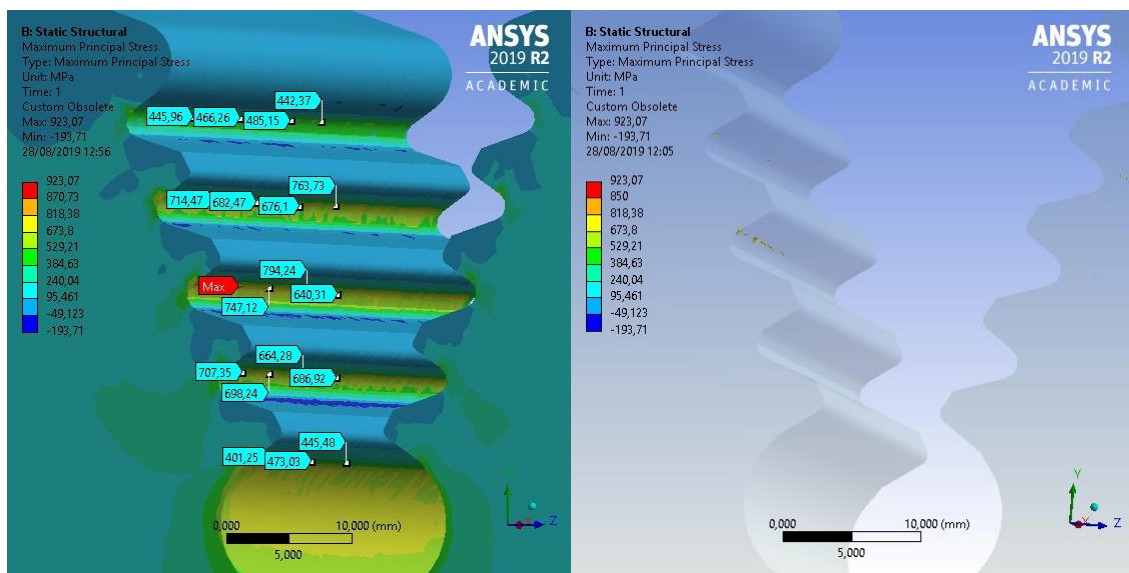


Figure 3.35: constrained surface chosen to simulate the third stage.

The first one analysed is the maximum principal stress (or maximum value of the normal stress), it is shown in the *Figure 3.36*: the highest value is equal to 923 MPa and it is located in the active surface in the middle of the groove. This value repeats for the same active surface on each groove more or less with the same magnitude, but it is only in one node and only in one of the two symmetric surfaces. This high stress is not scattered, so probably it is not a real value, but only an error due to 3D geometry imperfection or to the mesh imperfection, since it could be not totally representative of the real shape of the groove (due to the imposed dimension). This is confirmed by the *Figure 3.36 (c)* where are coloured only the areas for which the maximum principal stress exceeds 800 MPa (the highest values in the second stage is 811 MPa). As is possible to see, very few elements exceed this threshold. So, the maximum value found from the simulation must be contextualised and it could be also not considered for the purpose of disk's life. In the same figure, also the zoom on the most dangerous part are reported. As it is possible to see, the different values measured in this zone are very similar to the ones reported for the second stage (*Figure 3.26*); it is another proof about the not-reliability of the maximum value discovered. As it happened for the first two stages, the shrinkage of the disk and the hole are high stresses zones, due to stress concentration.



(a)



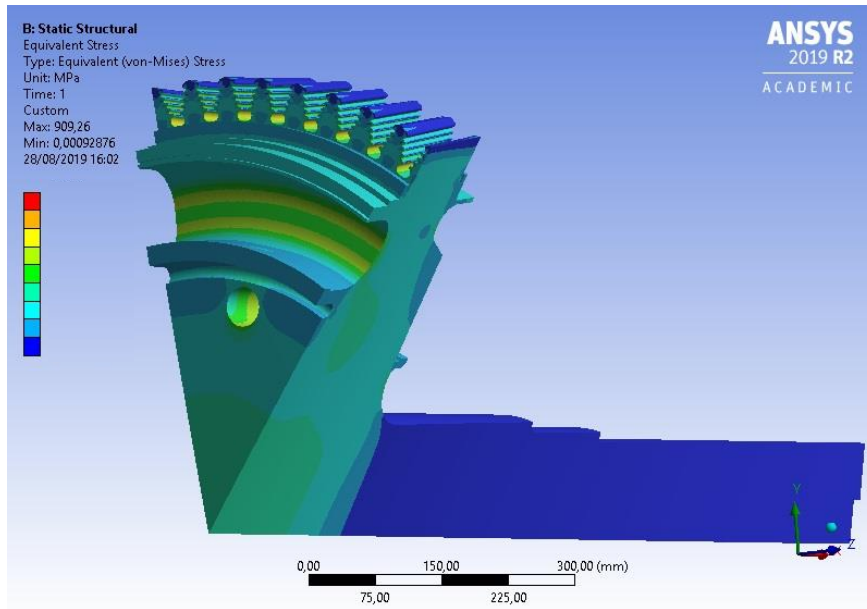
(b)

(c)

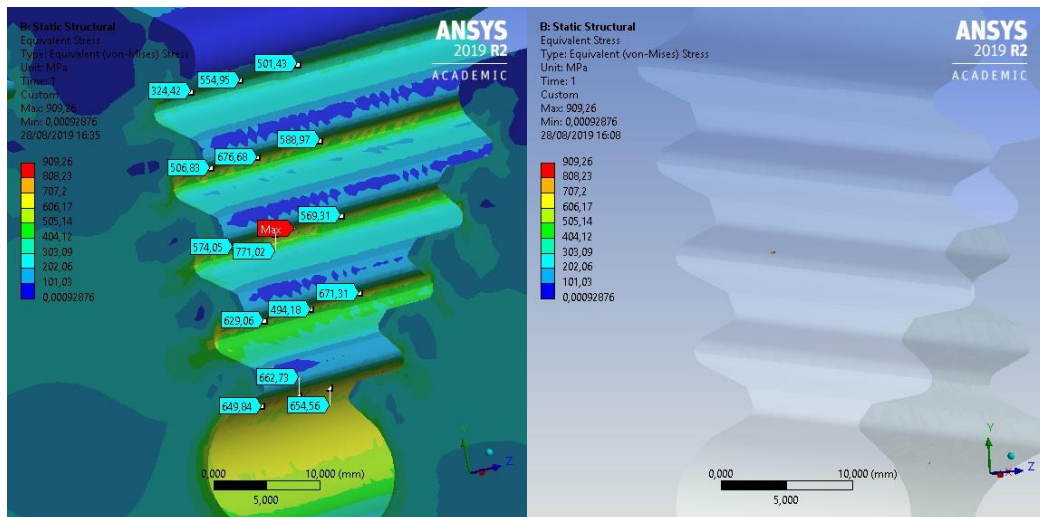
Figure 3.36: maximum principal stress overall result view (a), zoom on the most stressed zone with whole values in MPa (b) and with only values higher than 800 MPa coloured (c).

The second result request to Ansys is the equivalent stress. Obviously, this result is also influenced by the overvaluation done for some nodes. As a matter of fact, the highest value of the equivalent stress is equal to 910 MPa and it is positioned where the greatest value of maximum principal stress is too. As the first result, this is an isolated case, no other area has a similar value and it is easy to understand from the Figure 3.37(c), where only the areas for which the equivalent stress are equal or higher than 800 MPa are coloured, since only the peak

value exceeds the threshold in the entire groove, the coloured area is very small and difficult to be seen. A peak value made by singular point like this cannot be considered dependable. The different results obtained for the groove are than reported in the *Figure 3.37(b)*, where an overview of the different values is given.



(a)



(b)

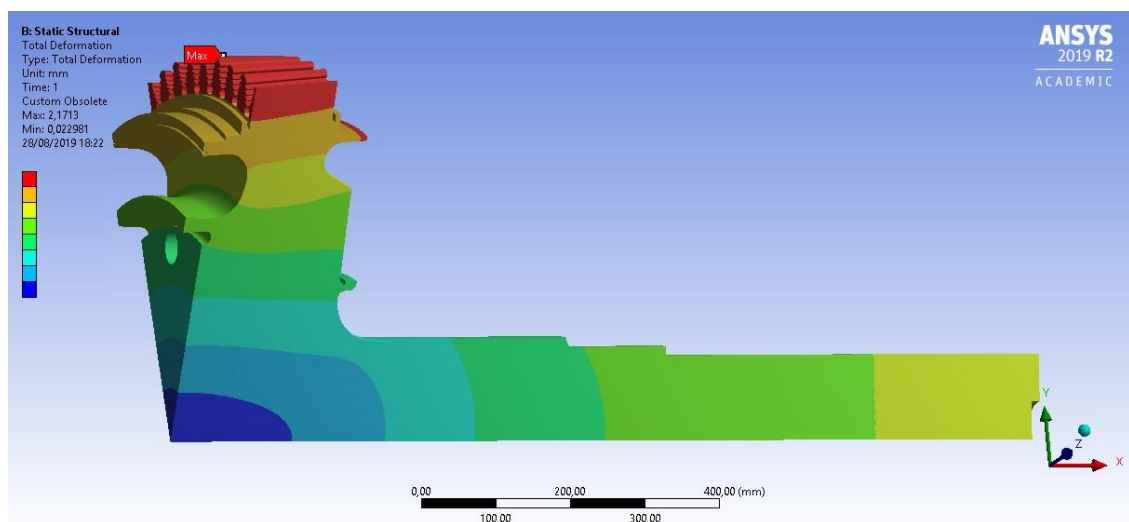
(c)

Figure 3.37: equivalent stress overall result view (a), zoom on the most stressed zone with whole values in MPa (b) and with only values higher than 800 MPa coloured (c).

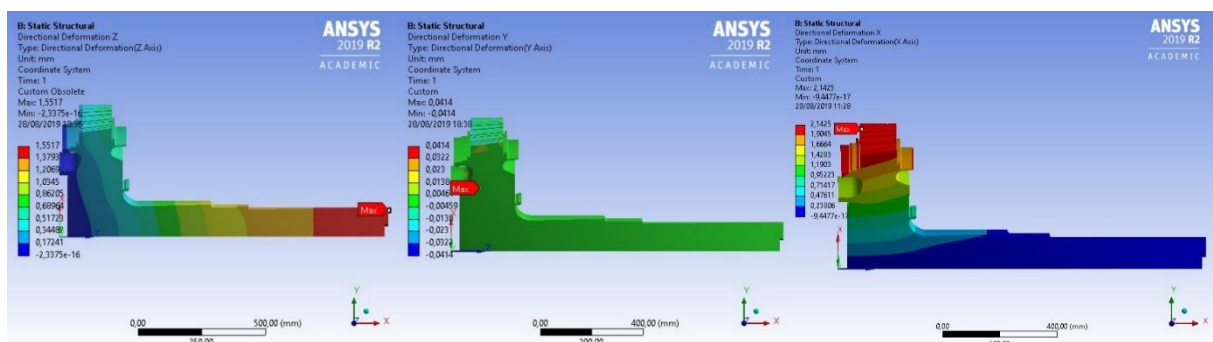
The last result analysed is the total deformation and its three different components: axial, circumferential and radial. The highest value in the result of the total deformation is equal to 2,2 mm when the machine is going to full speed. This is lower than the other two stages

(reduction of 11% respect the highest value of the first stage and 20% respect the one of the second stage). This peak value is located in the middle of the groove, on the top. In the *Figure 3.38* the overview about the total deformation is depicted: the most dangerous zone is the one of the grooves, as for the other stages. This is due to the rotational speed and to blade's equivalent loads applied in the active surfaces.

Here the total deformation reaches a higher value also in the final part of the body, where it is in contact with the bearing. This is due to the axial deformation (*Figure 3.38*) that behaves in his way also for the constraints that was chosen. The maximum value reached by the axial deformation is equal to 1,5 mm and it is discovered in the last part of the body, where it is in contact with the bearing. The most relevant component is still the radial one, that has a peak value very similar to the one of the total deformation (2,14 mm). As it happened for the other stages, the circumferential deformation has a negligible contribution: the highest value found is 0,05 mm.



(a)



(b)

(c)

(d)

Figure 3.38: total deformation (a) and deformation for (b) axial, (c) circumferential and (d) radial directions (different scales for the colours).

To conclude the study about the third rotating stage, the thermal load is removed from the previous simulation and only the effect of the structural load is studied. The three results, examined before for the combined load, are now compared to the ones coming from the structural load. The most marked effect of the temperature is seen on the total deformation: the one caused just by the structural load reaches a peak of 0,59 mm, it means that the thermal load increases the total deformation of approximately 240%. These two different results are compared in the *Figure 3.39* with the same colours' scale. The maximum principal stress is very similar in the two cases and the same happens for the equivalent stress, for which the difference between the highest value is less than 1 MPa and also the stress distributions are almost the same.

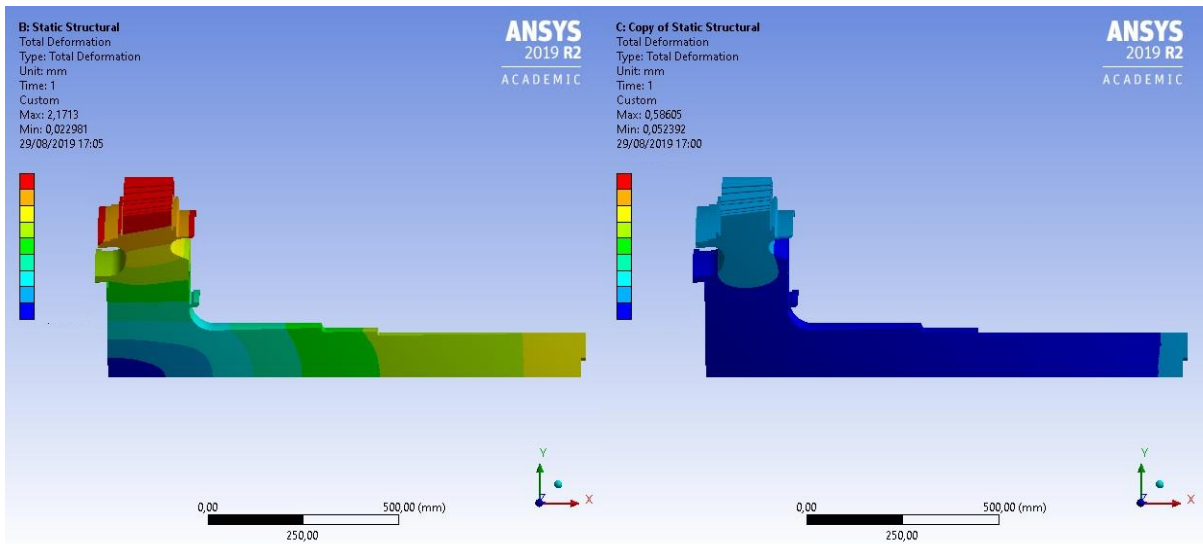


Figure 3.39: comparison of combined load (left) and only structural load (right) for the third stage.

3.7 Creep and cyclic life (LCF)

Maximum principal stress and equivalent stress are computed in order to estimate the life of the component by following an internal procedure recommended by the OEM (original engine manufacture) division of *Ethos Energy Group*. The maximum principal stress is used to evaluate the low cycle fatigue (LCF) of the points for which a dangerous equivalent stress is observed. The equivalent stress is also useful to understand if the component respects the minimum value of equivalent operating hours. All the disks seen before (one for each stage) are investigated since they are the parts that brake more easily. All the data about material is

necessary in this case, so the data about another customised structural steel (practical identically to the customised structural steel used for the disks and for which more material's information are available) give the limit for the life of each component.

Initially, it is important to identify which are the surfaces where the maximum principal stress and the equivalent stress are on average higher and where the peaks are located. These areas are the ones under examination. For each of them, four type of data are collected: maximum temperature (average one is used only for the grooves), average equivalent stress, peak of equivalent stress and the peak of maximum principal stress.

The first one investigation is done on the results for the primary (only structural analysis) and the secondary (thermal analysis) loads summed; theoretically, also the results of the primary load alone should be examined, but they are not since in the simulated cases they are always less dangerous than the combined case. The results for equivalent stress and maximum principal stress are examined to understand which zones are not safe and the equivalent stress of these zones are investigated too. For the first investigation, two values are selected for each unsafe surface: the average value of the equivalent stress and the highest temperature (to be safe) discovered. These values are plotted in a chart as function of temperature (X axis) and stress value (Y axis) and they are compared with the curve of “1.5 S_m” and “2 S_m”. “S_m” is a time independent allowable stress at temperature T, it is defined as:

$$S_m = \min\left(\frac{S_y}{2}; 0,4S_u\right)$$

Where:

- S_y is the minimum yield strength
- S_u is the minimum tensile strength

This stress is multiplied for 1.5 and for 2; in this way, two stress trends in function of the temperature are obtained. When a surface is analysed, the values of stress and temperature discovered define a point in the σ-T chart. If this point is below the “1.5 S_m” curve, it is safe. If this point is positioned between the “1.5 S_m” curve and “2 S_m” one, it needs to be verified for the LCF (by considering the maximum principal stress peak of the investigated surface). If the calculated point exceeds the “2 S_m” curve, it is not accepted and something must be modified on the examined part. Still following the *Ethos* internal document, in the same chart another curve to check the creep life of the component is plotted and it is called “1.25 S_t @200kh”:

$$S_t = \min\left(\frac{S_{CR}(avg)}{1.25}; S_{CR}(min); S_{CR}(Avg.) \text{ at } (T + 50^\circ F)\right)$$

Where:

- $S_{CR}(\text{avg})$ is the statistical average creep rupture strength
- $S_{CR}(\text{min})$ is the statistical minimum creep rupture strength
- 200kh are the equivalent operation hours for which the curve is sketched

If the point linked to the examined surface goes beyond this curve, the component is not able to reach 200.000 equivalent operating hours. Even if, the OEM division guarantees 96.000 equivalent hours for a turbine disk (the computation of equivalent hours is done differently for each company, they follow their internal design criteria).

Average equivalent stresses and peaks of equivalent stress of each dangerous surface are plotted in this chart as in *Figure 3.41*. The average equivalent stress are plotted to understand if an entire surface experience a permanent deformation (if this value is higher than $2S_m$) The calculated stress peaks are the result of an elastic stress analysis (*Ansys* compute the values by following only the Hooke's law, since it starts the computation of the equivalent stress from the deformation). But, since the material is not brittle, it has not a linear stress/strain relationship. Once the " $2 S_m$ " limit is overcome, a local plastic deformation (permanent) occurs that yields a redistribution of the overall load among the surrounding base material, with a consequent peak stress value reduction. The elastic-plastic behaviour is modelled with the Neuber's rule (the graphic representation is in *Figure 3.40*) that reduces the elastic peak stress evaluated for the Hooke's rule into an elastic-plastic peak one (where the red curve intercepts the black one) on the Ramberg-Osgood (R.&O.) curve.

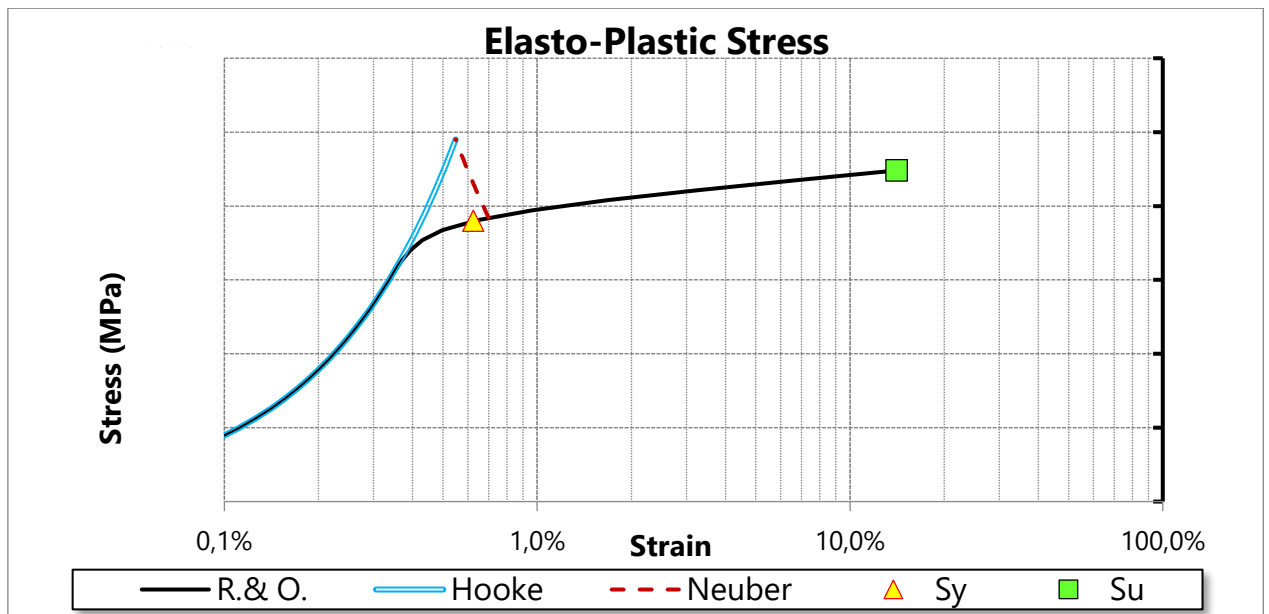


Figure 3.40: the graphic application of the Neuber's rule to pass from the value on the Hooke's domain to the R.&O.'s one.

The previous chart is function of the temperature that changes the curves' inclination.

This disagreement between the two laws starts before than the yield strength (S_y), so the stress values under this threshold have also to be analysed. Thereafter, the new peaks of equivalent stress (in R.&O.'s curve) are plotted into the σ -T chart, the same used for the average equivalent stresses, with the "1.5 S_m ", "2 S_m " and "1.25 S_t @200kh" curves. The points positioned here show if the requested equivalent operating hours are respected (creep life) and if the component is safe, unsafe or if some areas must be verified for LCF life.

The next step of the *Ethos energy* design criteria establishes that the dangerous areas for the equivalent stress investigation has to be furthermore assessed by an LCF analysis. This is based on the comparison between the calculated stress and the results of the fatigue tests performed with specimens of the base material. The LCF analysis technique adopted by the company is based on Smith-Watson-Topper stress (σ_{swt}) that can group and collect the results of tests performed at different cyclic stress ratio (R). In addition, σ_{swt} coincides with the maximum elastic stress reached in a load cycle starting from the zero (R=0). All the investigated parts experience a stress concentration due to irregular shapes. For this it is defined a fatigue notch factor (K_f), different from the stress concentration factor (K_t). It is possible to get the LCF result by reducing the peak of maximum principal stress with the ratio $\frac{K_f}{K_t}$ also called "notch sensitivity"), that is lower than 1. The exact value of this ratio depend on the number of LCF equivalent cycles that the un-notch specimen can bear with the peak value and the highest temperature in that area, as it is possible to see from the chart in *Figure 3.41*. Then, the reduced peak of maximum principal stress is used in the minimum LCF curve (Smith-Watson-Topper for the customised structural steel) plotted for the highest temperature of that part. Finally, the minimum number of equivalent cycles to the crack initiation int the disk (N) is computed and based on a service life (n) of the component (3200 equivalent cycles for a turbine disk), the Palmgren-Miner's linear damage $\left(\sum \frac{n}{N}\right)$ explain which part of the component is the most dangerous.

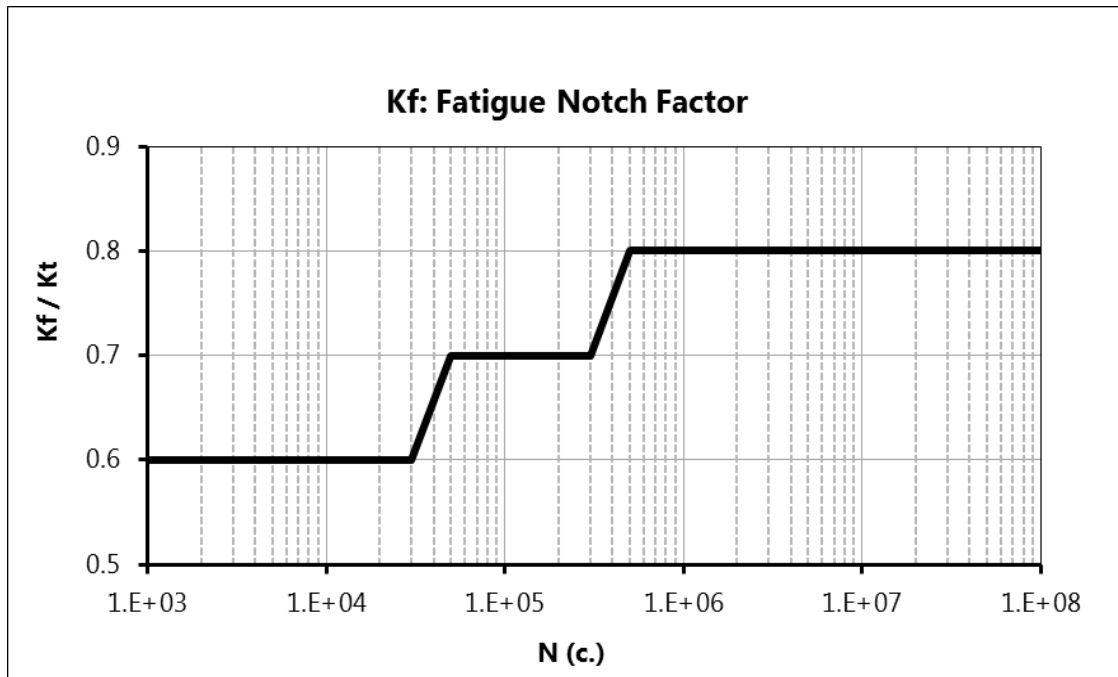


Figure 3.41: the plot used to compute the notch sensitivity for the notched geometry.

3.7.1 First stage analysis

Starting from the results of the thermo-structural load for equivalent stress and the maximum principal stress (Figures 3.13 and 3.15), the most dangerous areas are identified (Figure 3.42) and the data required for the life analysis are extrapolated and listed in Table 3.5. “Unions” are surface that connect two part of the body with a different thickness.

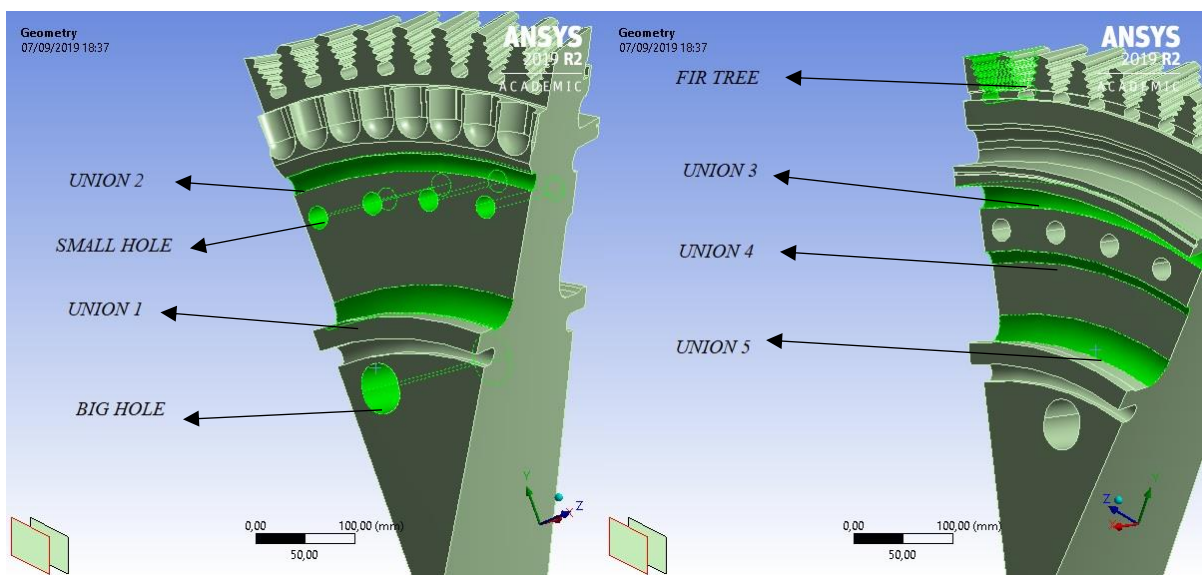


Figure 3.42: the analysed surfaces highlighted in the front face (left) and rear one (right).

zone	max temperature (°C)	equivalent stress average (MPa)	equivalent stress peak HOOKE (MPa)	maximum principal stress peak (MPa)
union 1	250	350	560	630
union 2	260	330	640	740
union 3	260	350	645	740
union 4	255	360	580	670
union 5	250	430	730	840
big hole	250	580	710	700
small hole	260	580	740	730
fir tree	270	220	670	690

Table 3.5

As first step, the equivalent stress average of each surface is plotted in the σ -T chart (Figure 3.43)

with “1.5 S_m ”, “2 S_m ” and “1.25 S_t @200kh” curves. All the points are under the 2 S_m curve, so no zone is not accepted. Holes are positioned in between 2 S_m and 1.5 S_m , it means that they need a check for the LCF life. Regarding the creep life, all the points are far from the limit line and no problems occur.

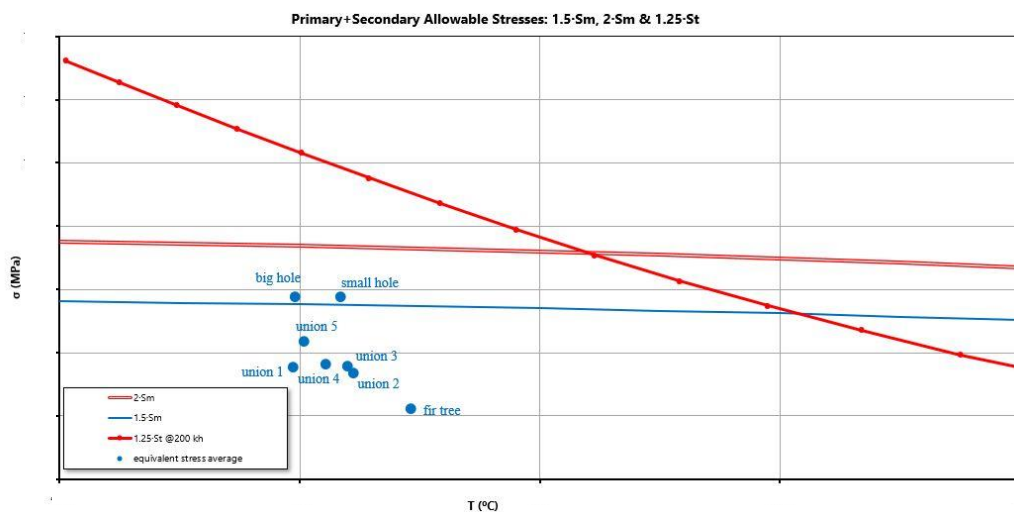


Figure 3.43: average equivalent stress of the first stage analysed for allowable stresses.

Now as established by the internal procedure, the peaks of equivalent stress found for each investigated surface need to be corrected to consider the real behaviour of the material (elastic-plastic) and this is done with the Neuber’s rule. Union 1, union 2 and union 4 peaks do not need correction, because they are still in the Ramberg-Osgood (R.&O.) curve. The computed new values are listed in the Figure 3.44, with the chart for the allowable stress, where peaks of

equivalent stress are plotted (the one for elastic behaviour coloured in blue and the elastic-plastic one coloured in green).

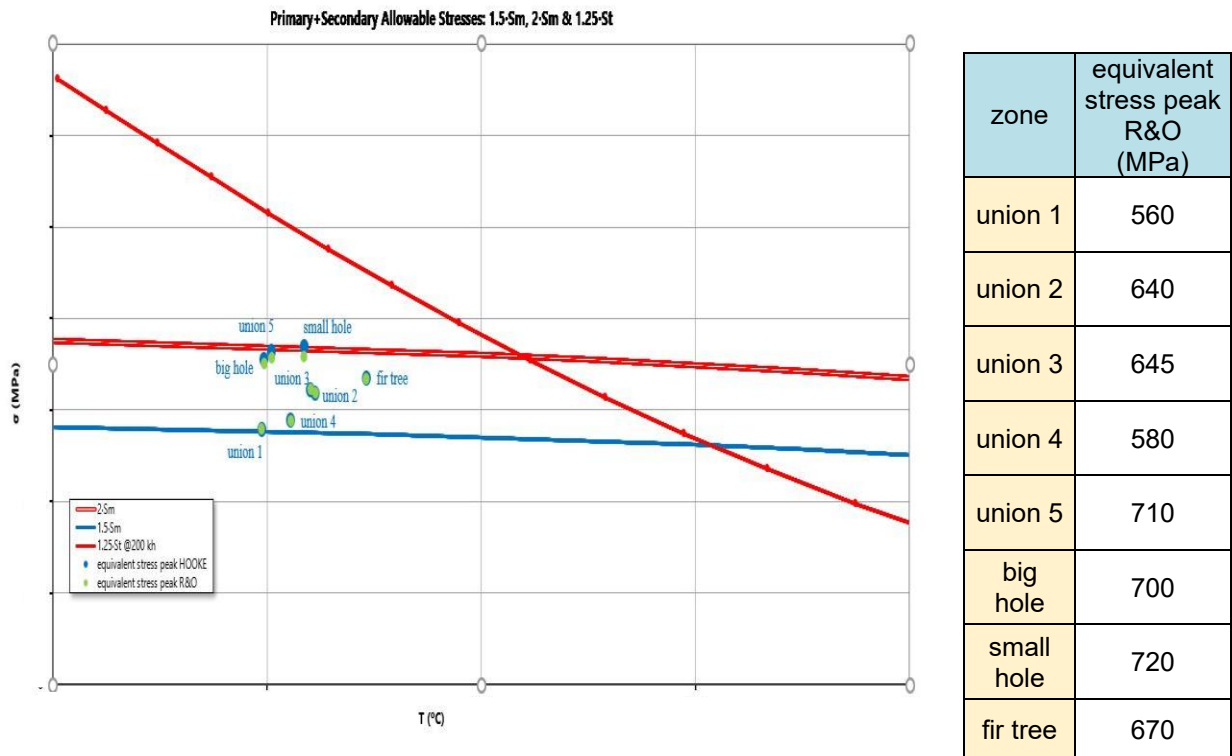


Figure 3.44: peaks of equivalent stress verification and values of peaks after correction.

From this chart is clear that all the surfaces need a further analysis to verify the cyclic life of the component, since they are all arranged between the two S_m lines.

About the creep life, it is important to report that the fir tree surface, it is very near the curve of the creep life for 200.000 equivalent hours. It could be a dangerous situation, but it is also important to say that *Ethos* ensures this component for 96.000 operating equivalent hours, so when this limit is reached, the component is replaced with a new one.

The last step is the low cycle fatigue analysis based on the peak of maximum principal stress detected for each investigated surface. The Smith-Watson-Topper minimum design curve is plotted for the maximum temperature of the analysed surface, except for the fir tree where the considered temperature is the average one, since the peak are not located where the temperature reaches the highest value. So, the number of allowable equivalent cycles is computed for a certain surface, but since the surface is not regular, the notch sensitivity $\left(\frac{K_f}{K_t}\right)$ is taken into account (it depends on the number of equivalent cycles computed before) and the peak's value is multiply for this factor. Finally, the minimum LCF equivalent cycles are computed for each surface with these reduced stresses (the notch sensitivity is considered also for the holes). The

numbers must be always higher than 3200 (the ones ensured by *Ethos Energy*) for an acceptable disk. In the last column of the *Table 3.6*, where all the data regarding LCF analysis are listed, there is the result of the Palmgren-Miner's linear damage and here the "union 5" reaches a 60% of its total life. This value is the highest value among the turbine's disks, it means that the disk of the first stage is the most prone to breakage.

Zones	Actual values			Reduced values	
	Temp (°C)	Peak Max Princ. Stress (Mpa)	Kf/Kt	Stress (Mpa)	$\Sigma(n/N)$
union 1	250	630	0,6	380	9%
union 2	260	740	0,6	445	29%
union 3	260	740	0,6	440	28%
union 4	255	670	0,6	400	14%
union 5	250	840	0,6	500	60%
big hole	250	700	0,6	420	18%
small hole	260	730	0,6	440	25%
fir tree	270	680	0,6	410	16%

Table 3.6

3.7.2 Second stage analysis

As it was done for the disk of the first stage, the results are used to identify the most loaded surfaces for maximum principal stress and equivalent one (*Figures 3.26 and 3.27*). Based on experience, it is known that the second stage is the most prone to rupture among the three turbine disks, so a particular attention is needed. The most critical areas are identified (*Figure 3.45*) and the data required for the component's life examination are extrapolated from the *Ansys* analysis and listed in *Table 3.7*.

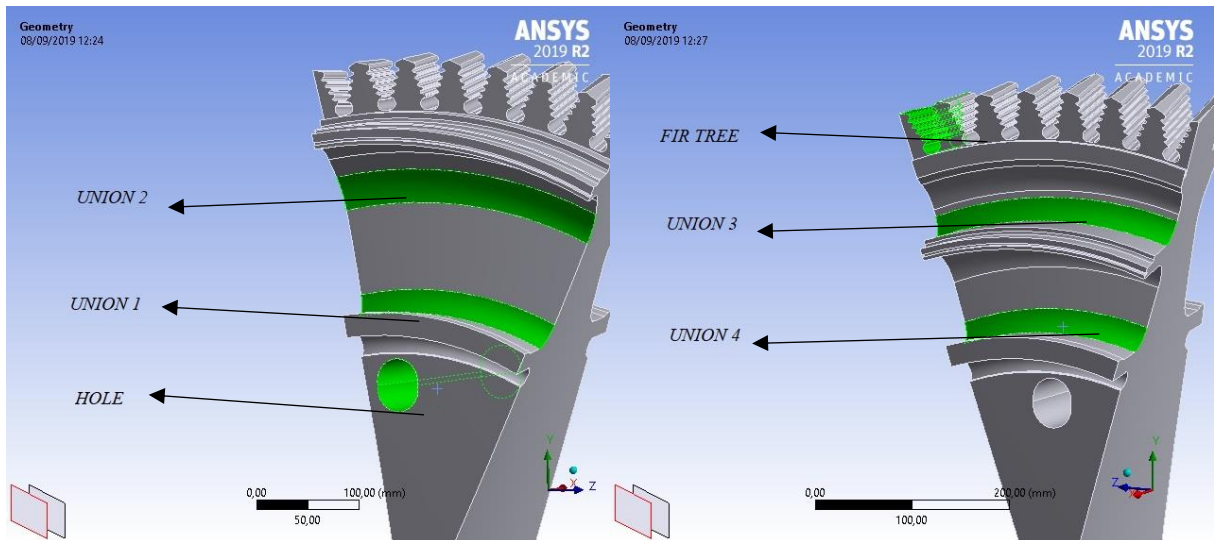


Figure 3.45: the analysed surfaces highlighted in the front face (left) and rear one (right).

zone	max temperature (°C)	equivalent stress average (MPa)	equivalent stress peak HOOKE (MPa)	maximum principal stress peak (MPa)
union 1	305	350	550	620
union 2	315	400	520	580
union 3	315	300	460	515
union 4	305	320	490	550
fir tree	335	260	715	710
hole	305	550	660	655

Table 3.7

In the table above, the data are not all coincident with ones seen on the simulation for what regard the fir tree: here, the maximum principal stress and equivalent one reach the highest peaks of the entire disk, but they are singularities and not diffused values. So, the design criterion explains for the fir tree in general that peaks made by only few and concentrated dots are not considered realistic because they are a consequence of the FEM model automatic meshing performed with very small tetrahedral finite elements (errors on sharp corners). Being them a few, their weight in the FEM model result accuracy is negligible, so that they can be neglected. The results selected as “peak” for maximum principal stress and equivalent stress

are an average of the values of the maximum loaded surface of the fir tree (the one in the middle for the maximum principal stress, and the lowest one for the equivalent stress).

The equivalent stress average of each surface is plotted in the σ -T chart (*Figure 3.46*). All the points are under the $2 S_m$ curve, so no zone is not accepted. Only the hole is positioned in between $2 S_m$ and $1.5 S_m$, it means that it needs a check for the LCF life.

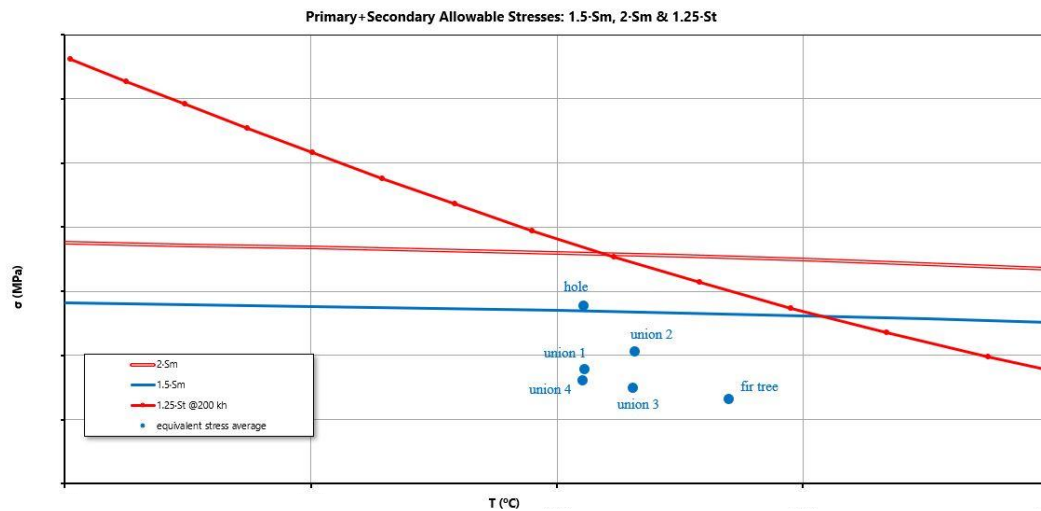


Figure 3.46: average equivalent stress of the second stage analysed for allowable stresses.

Neuber’s rule is applied on the peaks of equivalent stress, as explained before. The values for the four unions do not need it, since they are still plotted in the R.&O. curve. New values are calculated and index in the table of *Figure 3.47* together with the chart where peaks of equivalent stress are plotted (same colours of before).

This time only three areas exceed the $1.5 S_m$ curve (without exceed the $2 S_m$ one). The LCF analysis is needed for union 1, the hole and the fir tree. The latter points out an issue: as it possible to notice from the chart, the point representing the fir tree goes beyond the “ $1.25 S_t @200kh$ ” curve. It means that probably it may not achieve the 200 kh: as it was said in the chapter 3.5.2, the company knows this problem and for this reason the disk of the second stage is one of the components substituted after 96 kh (equivalent). To avoid this problem, the new configuration of the TG20 B7/8 has a dedicated cooling system for the second stage. It is interesting to notice that before the application of Neuber’s rule, the peak value of the fir tree exceeded also the $2 S_m$ curve.

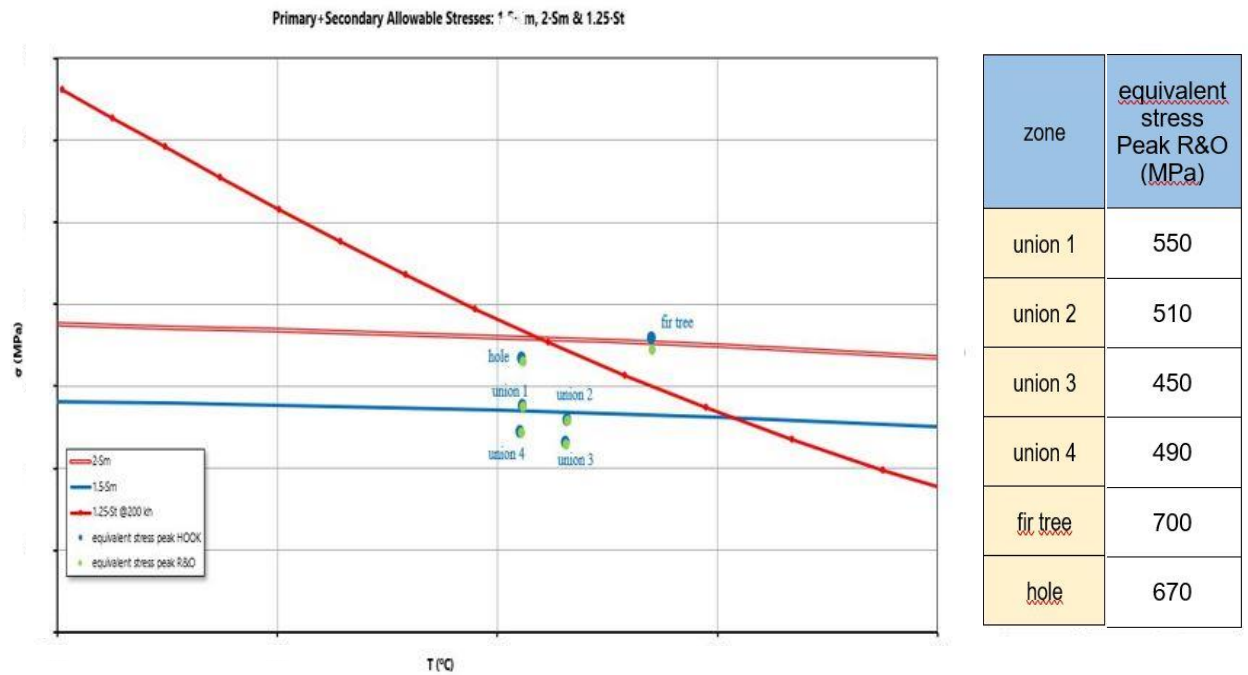


Figure 3.47: peaks of equivalent stress verification and values of peaks after correction (in MPa).

The last step of the design criteria is the inspection of the low cycle fatigue for the disk. As it was explained for the first stage's disk, the peaks of maximum principal stress are reduced for the notch sensitivity factor (the analysed surfaces have a sort of notch). So, the minimum LCF equivalent cycles are computed by using the reduced stresses. All the values used in this procedure are listed in the Table 3.7. All the stresses are not dangerous for the LCF, since they can survive more than 3200 equivalent cycles. The highest load (both thermal and structural) is the one of the fir tree, for which it is considered an average value as peak of the maximum principal stress (for the reasons explain before). Even if the highest value discovered (810 MPa) had been considered, the Palmgren-Miner's linear damage would have reached 66%. It means that the disk is safe from the LCF point of view.

	Actual values			Reducted values	
	Temp °C	Peak Max Princ Stress Mpa	Kf/Kt	Stress Mpa	$\Sigma(n/N)$
union 1	305	630	0,6	380	10%
fir tree	335	710	0,6	430	45%
hole	305	655	0,6	390	14%

Table 3.7

3.7.3 Third stage analysis

Finally, also the third stage is investigated for creep and LCF. The procedure is the same of two other stages: the input data are the equivalent and the maximum principal stresses. Considering these, the most dangerous areas are selected (*Figure 3.48*) and data are listed in the *Table 3.8*. In this case only two unions need to be investigated, so only the front face of the disk is shown, where these two are located.

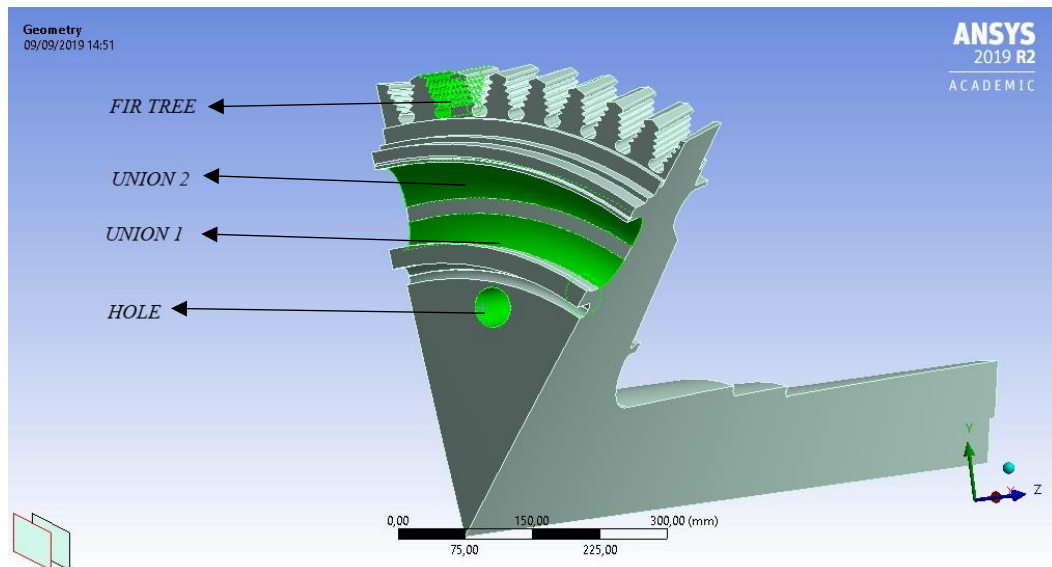


Figure 3.48: all the analysed surfaces highlighted in the front face of the third disk.

zona	temperatura max (°C)	equivalent stress average (MPa)	equivalent stress peak HOOKE (MPa)	maximum principal stress peak (MPa)
union 1	275	340	560	650
union 2	280	315	570	650
fir tree	290	300	670	710
hole	270	500	630	600

Table 3.8

As it happens for disk of the second stage, the value of the peaks for the fir tree listed in this table are different from the ones coming from the simulation (*Figures 3.36 and 3.37*). The highest values for the whole disk are found exactly in the fir tree, but the magnitude of these peaks is not considered reliable for the reason explained during the results discussion in the chapter 3.6.2. Therefore, the design criterion explains which type of peaks must be considered.

In this case they are few and the peaks are substituted with the average of the values of the maximum loaded surface of the fir tree for the maximum principal stress and for the equivalent one.

Now, the equivalent stress average of each surface is plotted in the σ -T chart (*Figure 3.49*). All the points are under the 1.5 S_m curve, so the surfaces are all safe by considering the average of the equivalent stress.

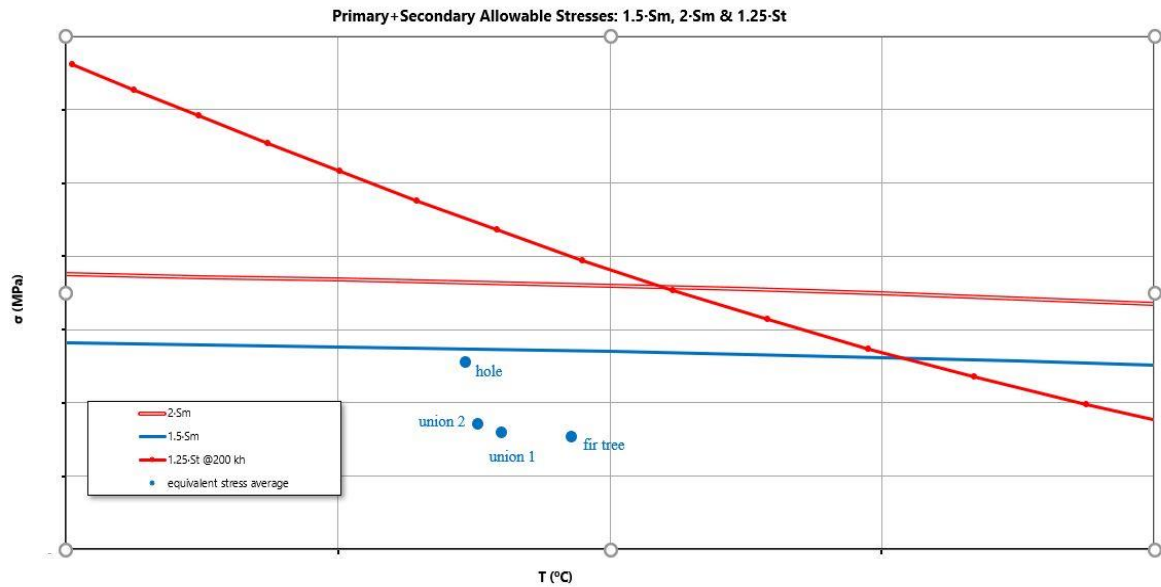


Figure 3.49: average equivalent stress of the third stage analysed for allowable stresses.

In this disk, the Neuber's rule is applied only to the fir tree, because all the other values do not need it, since they are still plotted in the R.&O. curve as it possible to see from the table in the *Figure 3.50*.

In this figure, all the peaks of equivalent stress are plotted. All these points need to be verified to LCF but they are not in dangerous regarding creep life.

The following step is the LCF analysis: the peaks of maximum principal stress are reduced by the notch sensitivity and then the number of equivalent cycles obtained are compared with the threshold value imposed by the internal design criterion (3200 equivalent cycles).

All the values used for this analysis are listed in the *Table 3.9*, where the final results for each surface is given as Palmgren-Miner's linear damage $\left(\sum \frac{n}{N}\right)$.

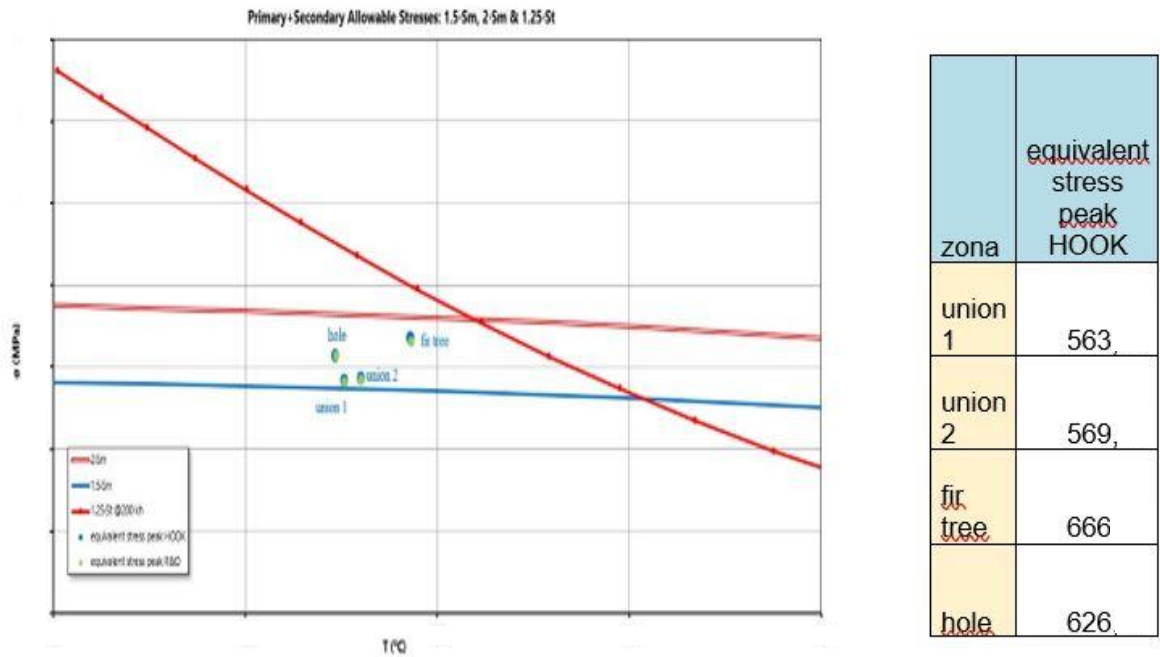


Figure 3.50: peaks of equivalent stress verification and values of peaks after correction (in MPa).

The fir tree is the most dangerous surface for the LCF, as for the creep life, but it is far from the threshold (only the 24% of the operating life is used after 3200 equivalent cycles). The third rotating stage is the safest among the three stages, regarding the low cycle fatigue life.

	Actual values			Reduced values	
	Temp °C	Peak Max Princ Stress Mpa	Kf/Kt	Stress Mpa	$\Sigma(n/N)$
union 1	275	650	0,6	390	11%
union 2	280	650	0,6	390	12%
fir tree	290	710	0,6	430	24%
hole	270	600	0,6	360	6%

Table 3.9

4 Case study: TG20 B7/8 UG3

4.1 The engine

The next step of this thesis work focuses on the upgrade of the machine TG20 B7/8 produced by *Ethos Energy Group*. Some modifications have to be done to improve the efficiency and the net power produced; the rotational speed of the whole engine is still equal to 4918 rpm. The company decided to modify only the turbine part and does not change the compressor at all. It is still made by 18 stages forced into the compressor shaft (compression ratio is 11,9). An adjustment regarding the NO_x reduction on combustor is planned too. The variations move from the idea of reducing the temperatures in the second rotating stage, since this one is just critical for creep and the turbine inlet temperature is increased (6%) to rise up the net produced power from 41MW to 44,2 MW. So, a dedicated cooling system is created for the second rotating system, where the blades are drilled to obtain the cooling channels that allows the passage of the air flows. Other modifications concern the reduction of the mass flow rate extrapolated from the compressor for the cooling system (this improvement allows to increase the efficiency of the machine), as the addition of a pin on the shank of the first stage's blade to reduce flow losses and the turbulence of the cooling channels of the same blades. The last one allows to increase the heat transfer coefficients of the cooling air that pass through the internal channels of the blade. It means that now it is possible to cool more than before with the same mass flow rate or to reduce this mass flow rate without losing capability to cool down. The internal cooling scheme of the blade is also changed, now inside the blade's root there is a chamber (root core) where the air is collected before to be sent through the channels cross radially the blade. All these variations lead to many changes in the cooling air mass flow rates: the total flow bleed from the compressor is reduced and each mass flow rate is changed to adapt to the new cooling scheme. It means that the scheme on software *PH4165* need to be modified with a new cooling matrix and then it will be run and new data will be used to compute the new heat transfer coefficients on the disks and blades.

Ansys is set as it was done for the standard version and all the details specified for that analysis kept unchanged.

4.2 TG20 B7/8 UG3: Turbine stage 1

The first stage is the most modified one: blades are changed internally and externally and disk is remodelled too. The blade's shape is changed to allow the integration of a pin (a sort of hollow cylinder) on its shank to reduce the amount of mass flow loss of 75%. It is arranged into a space dug into the blade's shank; here, thanks to the centrifugal force, the pin goes up and close the area between two shanks. In this way the loss of cooling air (it moves to the expansion chamber, but it is a fluid with low internal energy, turbine cannot use it to produce energy) is reduced and it means that less mass flow rate has to be taken from the compressor, so more mass flow will expand in turbine chamber and an higher power will be produced. For what regard the internal part of the blade, the cooling channels are modified and an entire thesis work is dedicated to them. In a nutshell, the channels in the standard version have smooth walls, instead in the UG3 version they show many ribs in the surfaces that increase turbulence of the cooling air and in this way the heat transfer coefficient of this fluid is increased (easier to cool down the blade) and the cooling mass flow rate required is less if it is considered the same turbine inlet temperature; if this temperature is risen, obviously the temperature of the blade will be higher and it should be cooled more to avoid the creep problem. The disk of the first stage is also adapted to the new cooling system of the second rotating stage: to admit the necessary air to the second stage 10 holes are drilled into the disk and they pass through it totally.

4.2.1 Thermal analysis

The first rotating stage is changed and a new study about it is necessary, especially the thermal one since the turbine inlet temperature is increased of 6%. The number of channels used for cooling system and number of blades (80) remain unchanged respect the standard case. So, the CAD model adopted for this examination is still a slice and it is one eightieth of the entire stage (*Figure 4.1*).

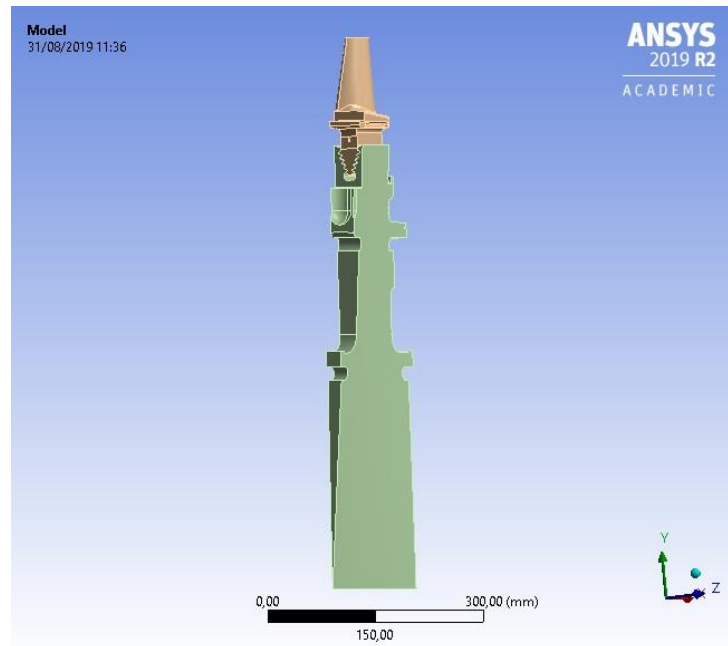


Figure 4.1: analysed slice of the first stage turbine, modified version.

Regarding the materials used to build the turbine, they are not change from one version to the other: the disk is made with a customised structural steel, *Ethos* alloy, whereas the blade is made by an Inconel alloy, an austenitic nickel-chromium-based superalloy. They could be critical, since the temperatures in the turbine are increased.

The active surfaces remain unchanged respect the thermal analysis for the standard version: “No separation” is the type of contact that represent the reality in the best way, since the surface are always in contact due to the centrifugal force. The mesh adopted has different dimension for different parts: the highest element size is equal to 6 mm for the disk, 2 mm for the blade and 2 mm also for the active surfaces. This choice is necessary for the details of the blade as the cooling channels, that need a high accuracy.

The cooling scheme is now modified by adding the holes through which the air goes to the second rotating stage. It is depicted in *Figure 4.2*, that is similar to the scheme of the standard machine (*Figure 3.9*) but now a branch is added in the bottom right of the picture to bring cool air to the second stage.

However, most of all many modifications are done by changing the mass flow rates and pressures of the cooling system (temperature of the fluid is still the same since it is extracted from the same compressor), since a reduction in the amount of cooling air is planned in the new model.

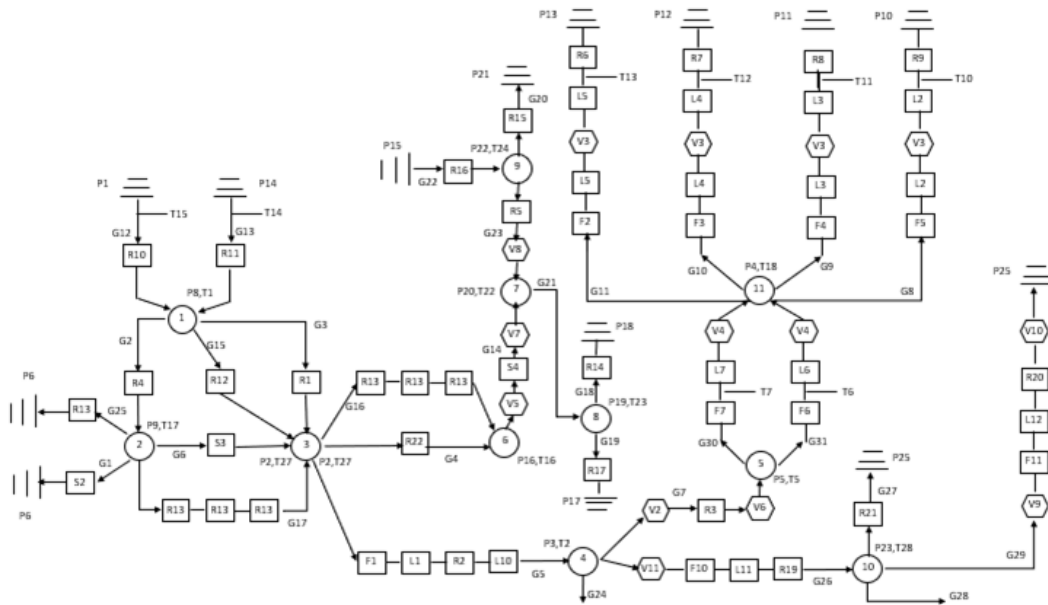


Figure 4.2: the new cooling scheme for the entire first stage of the turbine

These variations are seen from the result of the *PH 4165*, the software used to compute all the cooling's data. These results are used to compute the new heat transfer coefficients that affect disk's surfaces and some part of the blade (listed in *Table 4.1*), by using the DuPont formulation. The disk and the blade are divided into many surfaces, because the heat transfer coefficient changes area by area. This method compares the geometries and data of the TG20 B7/8 UG3 with the ones of TG50 C, for which the heat transfer coefficients are well-known. Thus, a good approximation of the heat transfer coefficients is obtained for the disk and the blade.

For the part of the blade in contact with hot air-gas mixture, data about this fluid are got from software *AxSTREAM*: speeds, inlet and outlet temperatures (static and total), pressures and density. All these data are taken for two section, one in the middle and one in the tip of the blade; the coefficient finally adopted is the average between the resultant coefficients computed for the two sections individually. Temperatures coming from this software are the ones given to the fluid that is in touch with the blade, so they define a parabolic thermal load. The different temperatures of the air-gas flow on the inlet and outlet surfaces (supposed as stagnation points) are the total ones, whereas the temperatures of the fluid on the pressure and suction surfaces (where fluid is moving) are the average between the static inlet temperatures and the outlet ones. Once the different temperature profiles are computed they are set in simulation, surface by surface. For what concern data about cooling system on the blade channels (they are 15 divided into 4 groups), they are taken from a dedicated thesis work about them: heat transfer coefficients and temperatures are computed by CFD analysis, by means the software *STAR*

CCM+. Since the ribs in the channel create an oscillating heat transfer coefficient, an average value is computed and it is assigned to each group (the firsts three are composed by three channels and the last one is composed by 6). So, for these surfaces only temperature varies along the height of the channels. The same type of information is selected for the root core of the blade: an average value for the heat transfer coefficient and a variable temperature between the inlet and the outlet of the region.

Region	Heat transfer coeff.	Max air temperature	Min air temperature
BLADE	$\frac{W}{m^2 \cdot K}$	°C	°C
Inlet surface	2620	1135	1020
Outlet surface	250	930	830
Pressure surface	770	940	830
Suction surface	808	940	830
Shank	170	340	340
Root core	630	230	270
Channel group 1	2754	285	410
Channel group 2	2628	329	627
Channel group 3	2673	295	641
Channel group 4	2636	310	651
DISK			
Root input surface	260	340	340
Root output surface	150	340	340
Inlet surface	175	210	210
Outlet surface upper	100	340	340
Outlet surface middle	30	230	230
Outlet surface lower	20	220	220
Grooves surface	360	230	230

Table 4.1

Theoretically, there is another convection that is not considered here: the new hole, used to bring air to the second stage, is passed through by cold air. This one influence the temperature trend, but since in this CAD model there are no holes, this thermal load will be taken into account during the thermal-structural analysis. In this turbine too, there are the seals that guaranteed the division between the environment with hot gases and the one with colder air in contact with the disk. In this way, disk maximum temperature is mainly function of the blade root temperature, considering that the gas ingestion is prevent.

The result is the temperature map of the entire stage when the machine is at full load. The examination of the results is divided to study each body individually: the disk (*Figure 4.3 a*)

has a peak value of temperature equal to 267,41 °C and it is found in the upper outlet part of the groove, whereas for the blade (*Figure 4.3 b*) the highest temperature detected is 815,57 °C and it is located in the inlet surface.

So, it is possible to see as the blade's temperature peak increase of 8,8% respect the standard case, due to the increasing turbine inlet temperature; whereas the highest temperature of the disk is decreased of 9,8% respect the initial case, due to the different cooling system of the stage. So, the new cooling scheme reduce the peak temperature in the disk and it limits the temperature increasing on the blade.

In the thermal-structural analysis the temperature scenario will be depicted in a more complete way, considering that also the cooling due to the “new” hole is taken into account.

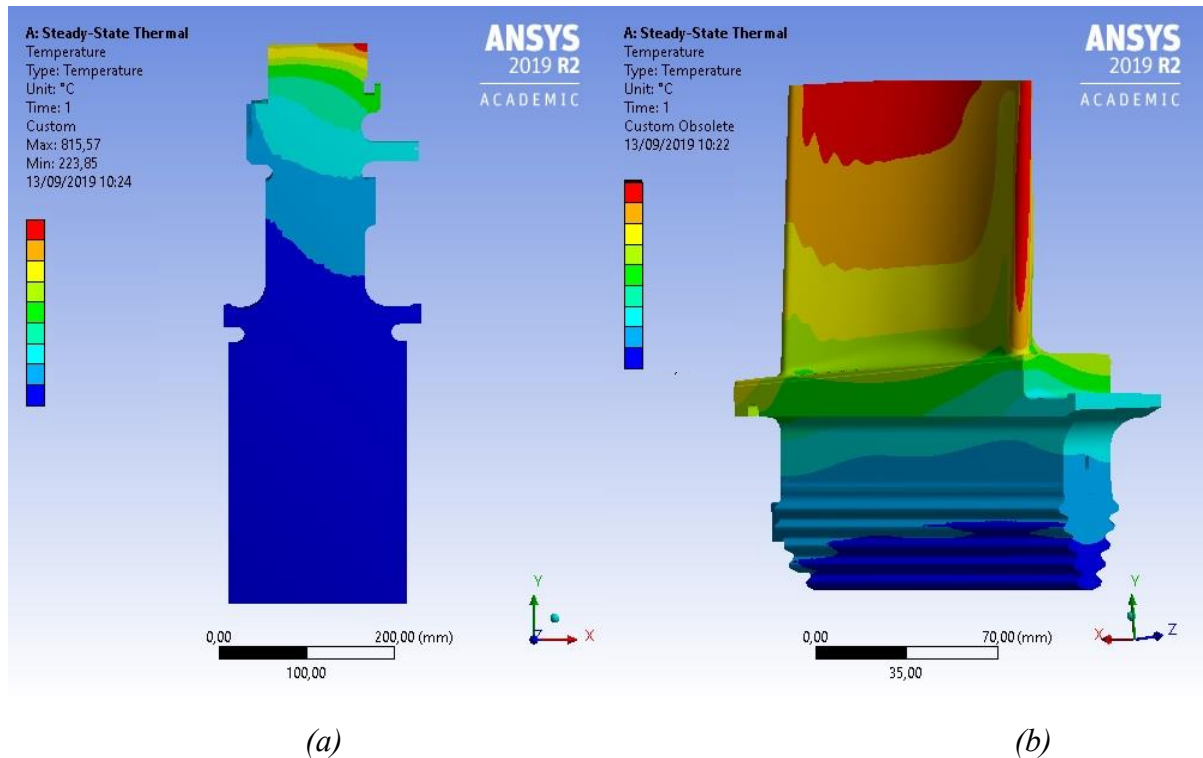


Figure 4.3: temperature scenarios for disk (a) and blade (b) of the second rotating stage (pay attention to the different scales).

4.2.2 Thermo-structural analysis

In this step, the results of the thermal analysis are combined to the structural one, in order to have an overview on the behaviour of the stage and to compute the values for the life computation. Initially, the CAD model is replaced with a new one (*Figure 4.4*) with 8 grooves, it is one tenth of the entire disk. This model is characterized by three type of holes that can be

seen only by increasing the slice dimensions: biggest one is for the tie rod that keeps together the three stages, the medium size one (highest positioned) is the one used to tighten bolts to fix the front ring for the cooling air direction and the smallest one (only one is present in the slice of *Figure 4.4*) is the new hole added to extend the cooling scheme to the second stage. Material, coordinate system and cyclic symmetry conditions are the same applied for the thermal analysis; connections are not described since only one body is present on the system.

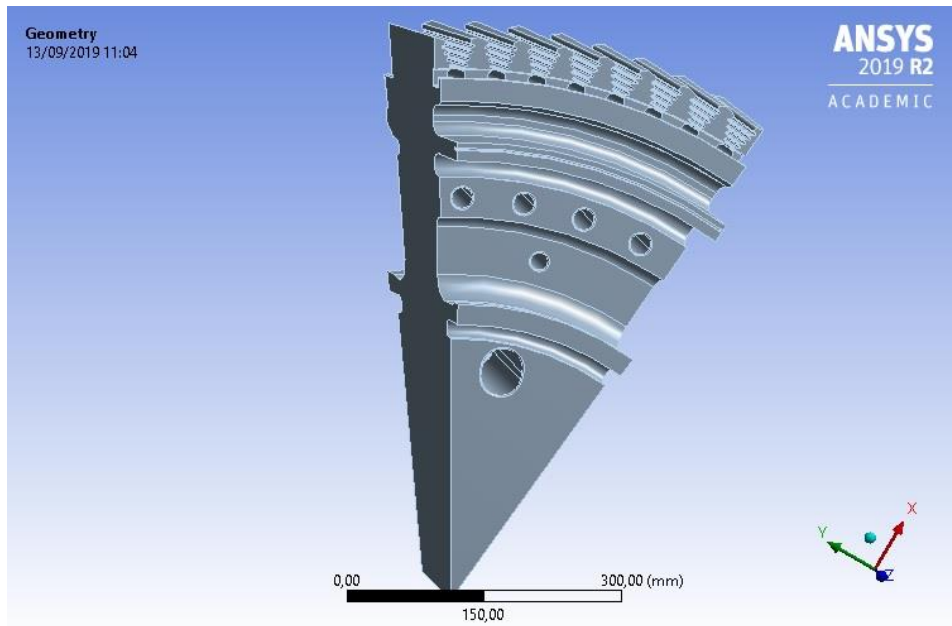


Figure 4.4: investigate slice for the thermo-structural analysis of the first rotating stage (UG3).

Regarding the mesh, the maximum dimension of the element is imposed equal to 4 mm for the whole structure and refined in the grooves (as it was done for the standard case) where the maximum dimension is 2 mm. This value of sizing is also adopted for the new hole adopted, but this setting was chosen later, as the analysis done with an element size of 4 mm was not accurate.

The first load applied is the thermal one and two type of condition are imposed. Temperatures measure on the active surface of the blade (from the thermal simulation) are imposed on the active surface of the disks (as Dirichlet boundary condition); these temperature trends are divided into 5 groups, as it was done in the previous analyses. The temperature goes from 240 °C to 270 °C.

The second type of thermal load is the convection on the disk, the same applied for the thermal analysis are applied and in addition the one for the new hole. The heat transfer coefficient for

this one is computed by Dittus-Boelter correlation for turbulent fluid in a tube (data are taken from PH4165):

$$h = \frac{k_w}{D_h} \cdot Nu$$

where:

- k_w is the thermal conductivity of the fluid (cooling air in this case)
- D_h is the hydraulic diameter of the tube (a hole in this case)
- Nu is the Nussel number

The final value computed is equal to $1240 \frac{W}{m^2 \cdot K}$ and it is function of many variables as dynamic viscosity, density and speed. The temperature of the air that passes through this hole is $190 \text{ }^\circ\text{C}$. This convection creates a temperature scenario (Figure 4.5) similar to the one seen for the thermal analysis, but with a colder surface near the hole for the air passage.

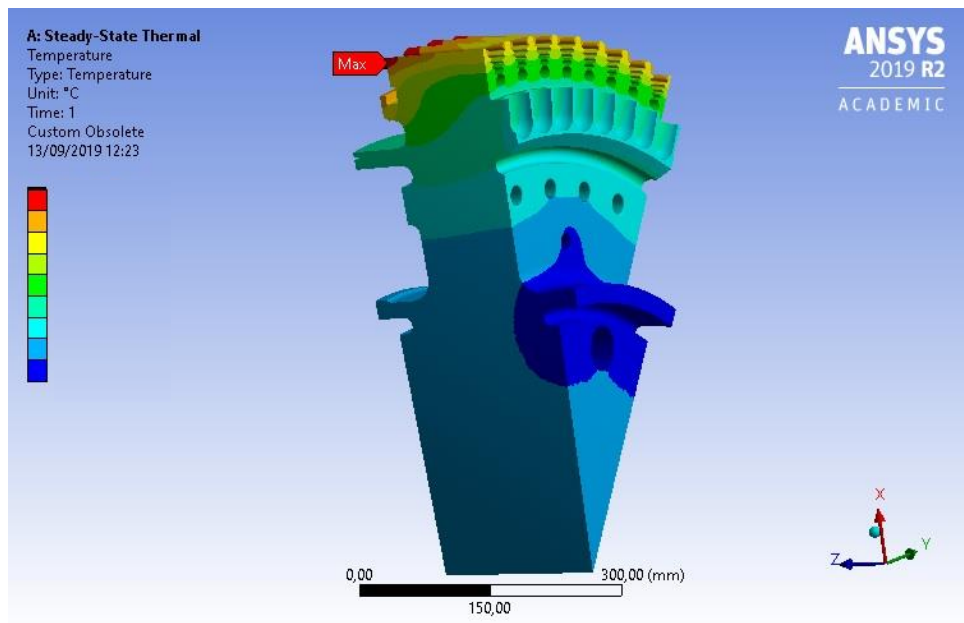


Figure 4.5: the resulting temperature scenario by including all the thermal loads.

The following step is the addition of the centrifugal loads: the one due to the blades and the one due to the weight of the disk.

The centrifugal force due to the blade is applied to the active surfaces of the groove and its magnitude depend on the rotating speed (5065 rpm, considering the overspeed), the position of the centre of gravity (almost the same of the standard case) and the weight of the blade, that is increased for the addition of the pin (heavier than the first stage). The final value of the force is 660 kN and it is directed along the radial direction of the disk. Also in this case, the best solution

for the condition of constraint is the same surface chosen in the other simulations (shown in *Figure 4.6*).

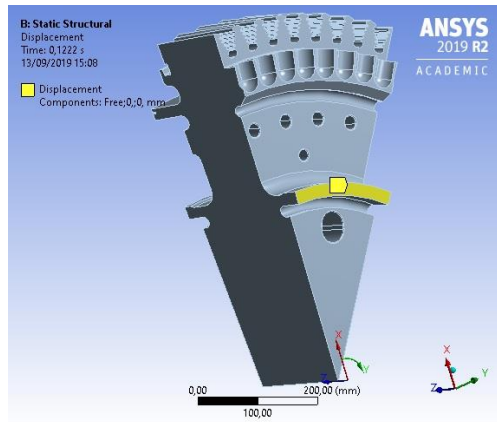


Figure 4.6: the constrain is imposed in the highlighted surface, in the front face of the disk.

This surface is constrained to have no displacements along the circumferential and the axial directions. Instead, the radial displacement of the selected surface is free.

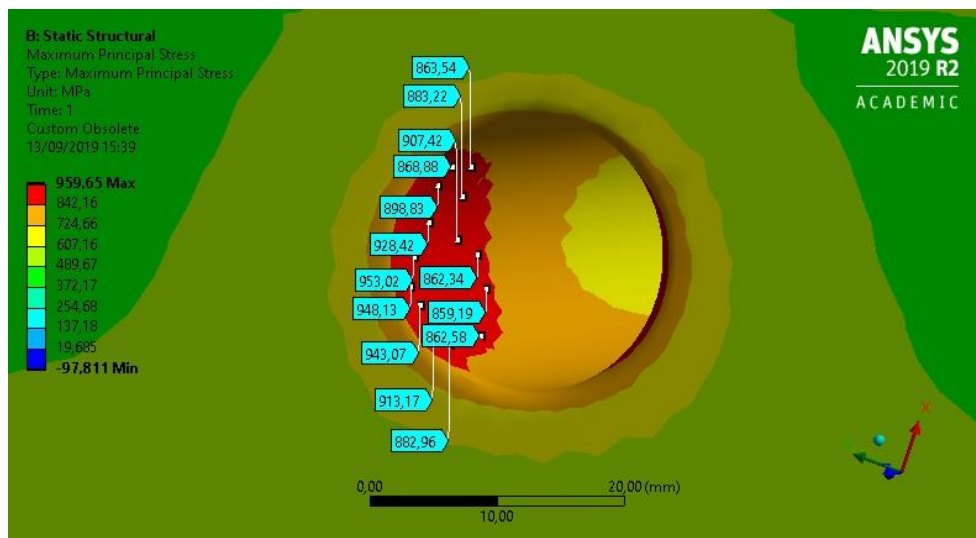


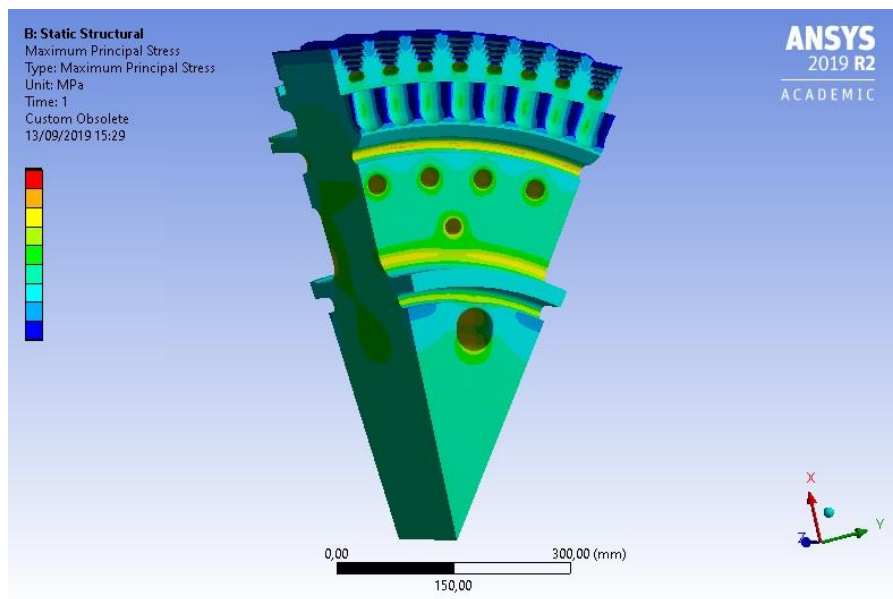
Figure 4.7: some measurements on the most loaded zone for maximum principal stress.

This displacement is choice because it produces a solution that has reasonable values and distribution of the stress.

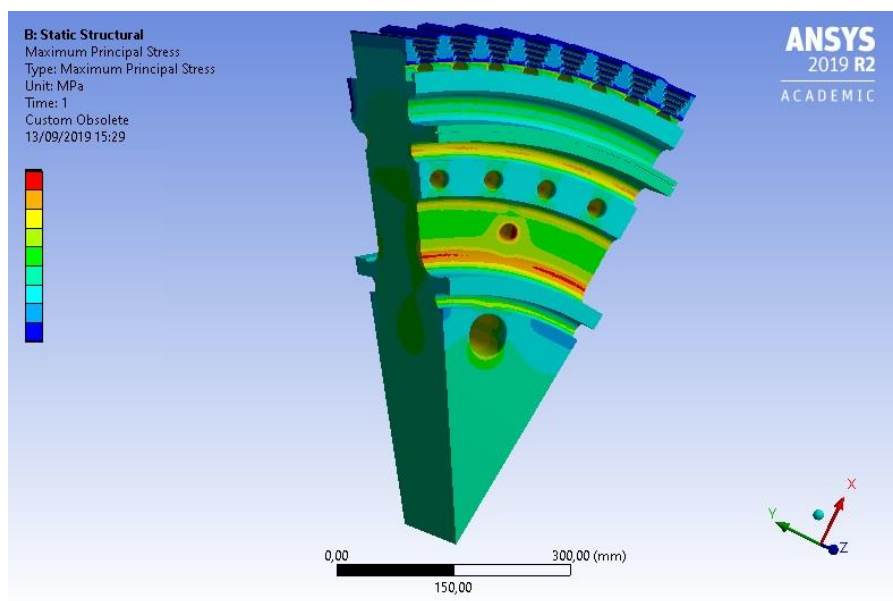
Once the results of the thermal analysis are loaded, the last step is the definition of the required solutions: maximum principal stress, equivalent stress and total deformation. The maximum principal stress reaches a peak of 959,65 MPa that is located near the outlet section of the new

hole for the transfer of the cooling air to the second stage (*Figure 4.7*). This high load is symmetric and it is distributed stress, not an isolated point.

Other surfaces experience a high load, as the lower union in the outlet face (caused by the shrinkage); it was the most loaded zone in the first stage of the standard engine and now there is a higher load than the standard case (856,36 MPa for the UG3 and 836,07 for the standard). The grooves are always dangerous cause the highest temperatures of the disk are located there. The overview for the slice is shown in *Figure 4.8*, where it is possible to notice that the outlet face is more loaded than the inlet one.



(a)



(b)

Figure 4.8: results of maximum principal stress for the inlet (a) and outlet (b) faces.

The maximum value of the equivalent stress is 951,1 MPa and this time again it is detected in the new hole and it is diffused and symmetric. The most loaded zones are the same seen for the maximum principal stress and them will be used to evaluate the component's life.

The results of this simulation are reported in the *Figure 4.9*, where it is shown the panorama of the equivalent stress and a zoom on the most dangerous zone.

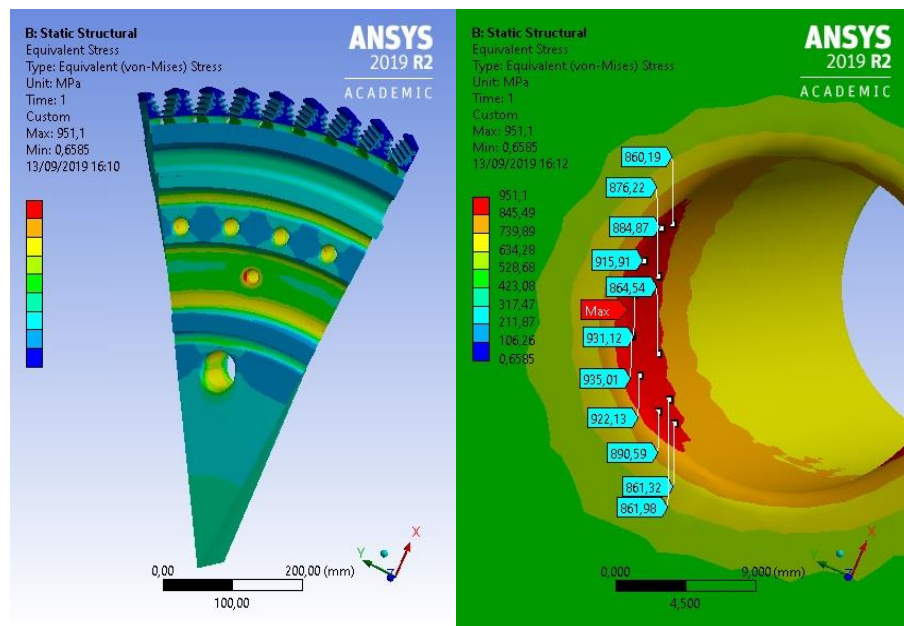
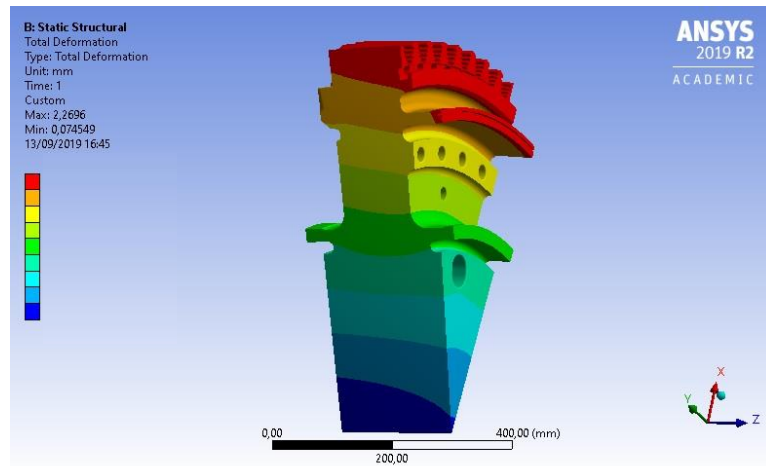


Figure 4.9: overall view of the equivalent stress result (left) and a zoom on the peak's zone (right).

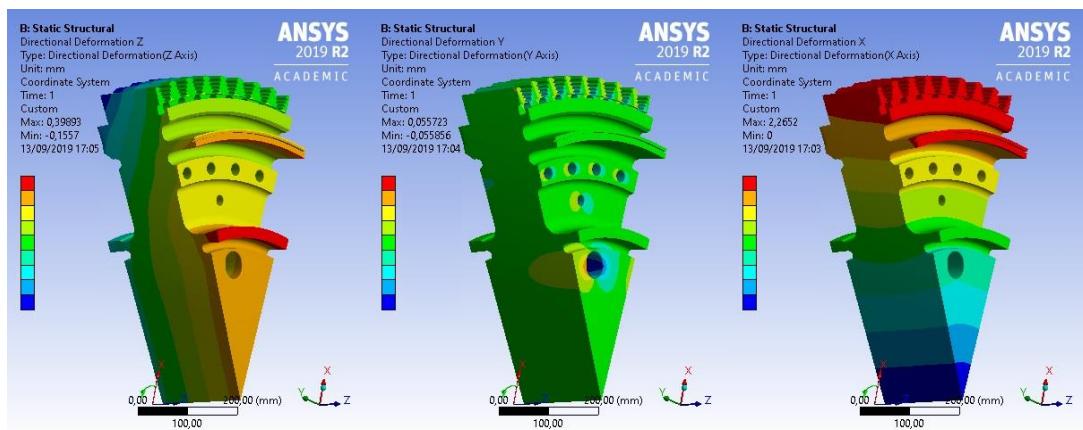
Now, the total deformation is examined: the highest value is 2,3 mm and it is located in the upper part of the groove (*Figure 4.10 a*). This reduction on the peak value (7% less than the standard engine) is due to the temperature that is decreased as well. From this figure it possible to notice as the outlet part of the disk is more deformed: this behaviour is linked to the fact that the most loaded areas are in the outlet face. The asymmetric configuration of the disk causes this asymmetric solution (this happened also for the first stage of the standard engine).

Each direction of the deformation is investigated separately: the axial deformation peak is equal to 0,39 mm and it is located in the outlet face. The circumferential one is equal to 0,1 mm and it is located in the bore for the tie rod. Finally, the radial deformation that is the most influent component has a peak equal to 2,3 mm that is obviously in the tip of the groove.

The life of this component will be inspected with these new values.



(a)



(b)

(c)

(d)

Figure 4.10: total deformation (a) and deformation for (b) axial, (c) circumferential and (d) radial direction (different scales for the colours).

As last step, the primary load is evaluated and compared to the combined one (primary and secondary summed) to estimate the influence of the temperature.

4.3 TG20 B7/8: Turbine stage 2

The second rotating stage is modified respect the standard case to allow the modifications that increase net produced power and efficiency. The blade is changed internally: now it has internal channels where the air pass through to cool down the blade. Obviously, since the turbine inlet temperature increased, also the temperature of the fluid near the blade increased; so, this new cooling scheme is fundamental for the life of the stage. To carry the cooling air for the blade, a new hole is drilled into the disk, to connect the inlet face of the disk with the root of the blade. This cooling air is also useful to reduce the temperature of the disk.

4.3.1 Thermal analysis

A new thermal analysis is needed for the second rotating stage, since external conditions and components are changed and a dedicated cooling system is added to. The blades are still 70, but now they are drilled to allow the passage of cooling air inside. So, the CAD model is one seventieth of the entire disk with a blade assembled on the groove (*Figure 4.11*). As the first stage, the disk is made of customised structural steel and the blade of Inconel alloy.

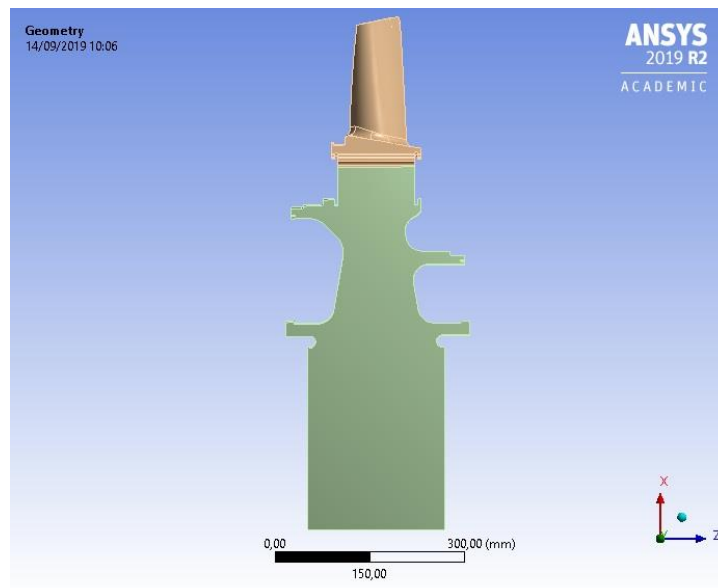


Figure 4.11: analysed slice of the second turbine stage (UG3).

As it was done for the other simulations, coordinate system and cyclic symmetry condition are set to ensure the correct study of the whole stage. The contacts between the 10 active surfaces of the disk and the corresponding surfaces on the blade root are defined as “No separation”, as for the other cases. The mesh maximum dimension is chosen equal to 6 mm for the disk and 2 mm for the blade; then also the active surfaces have a maximum dimension of 2 mm for the elements. The mesh in the new hole (included in the disk for the air passage) is also refined to 2 mm because the geometry is not simple.

In this new configuration, the cooling is provided also from the first rotating stage, not only by the second vane stage. The air is directed to the cooling channels inside the blade and to arrive there a new hole is drilled (the inclination is chosen as the one that minimize the stresses on the disk, by previous simulations, *Figure 4.12*) and it is shown through a section plane in the *Figure 4.12*. There are 70 holes, one for each groove.

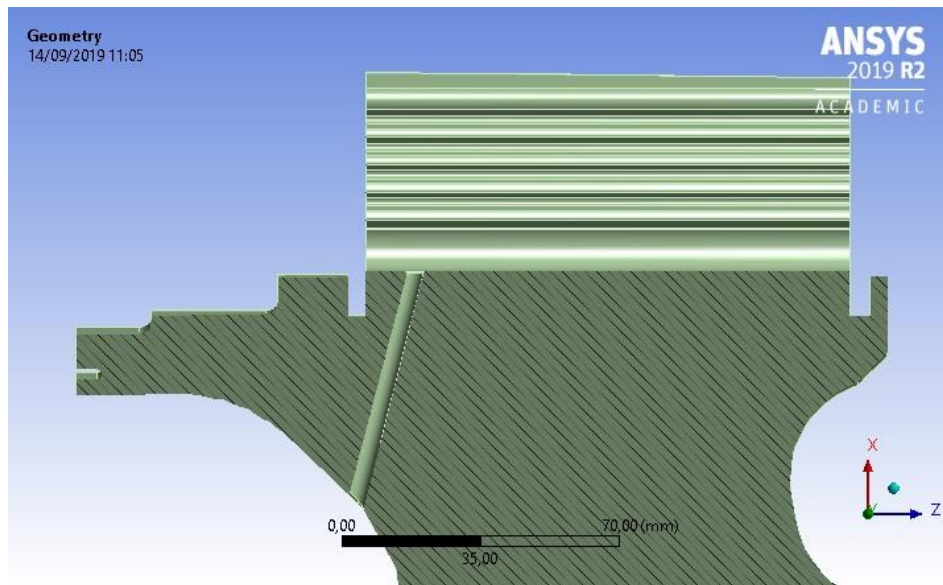


Figure 4.12: the hole that allows the air passage from the disk inlet face to the groove.

The heat transfer coefficient for the air in this channel is computed again through the Dittus-Boelter correlation for turbulent fluid in a tube (the same used in the first stage). The necessary data for this computation are taken from the *PH4165* computation for the new cooling matrix. Heat transfer coefficients need to be computed also for the new internal channels of the blade: the 13 channels of the blade are similar to rectilinear tube, therefore the Dittus-Boelter correlation can be adopted again and an average heat transfer coefficients for the entire channel is computed for the 4 groups in which the channels are divided. The way to compute them:

- Computation of the speed of the fluid in the channel from mass flow, density and section of the tube.
- Computation of Reynolds number through channel diameter, density, dynamic viscosity and speed.
- Computation of Nusselt number trough Reynolds and Prandtl numbers.
- Finally, the heat transfer coefficient is computed by using the Nusselt number, the tube diameter and the thermal conductivity.

For what regard the heat transfer coefficients on the external surfaces of the blade, they are estimated thanks to data about temperature and speed of the fluid obtained by *AxSTREAM*, that it was adapted to the new scheme of the TG20B7/8 UG3. For all the remaining areas, the heat transfer coefficients are still computed by DuPont formulation, by comparison with the TG50C. All the computed values are listed in the *Table 4.2*.

Region	Heat transfer coeff.	Max air temperature	Min air temperature
BLADE	$\frac{W}{m^2 \cdot K}$	°C	°C
Inlet surface	1650	920	820
Outlet surface	170	740	630
Pressure surface	480	750	650
Suction surface	540	750	650
Shank	50	340	340
Channel group 1	1420	560	340
Channel group 2	1440	530	330
Channel group 3	1455	500	320
Channel group 4	1210	420	310
DISK			
Inlet surface upper	60	230	230
Inlet surface lower	20	220	220
Outlet surface middle	50	240	240
Outlet surface lower	20	200	200
Grooves surface	70	230	230
Disc hole	3360	200	230

Table 4.2

Once all the thermal loads are imposed, the simulation is ran and the temperature result is examined (*Figure 4.13*): the highest temperature in the blade is equal to 769,32 °C and it is located in the inlet surface.

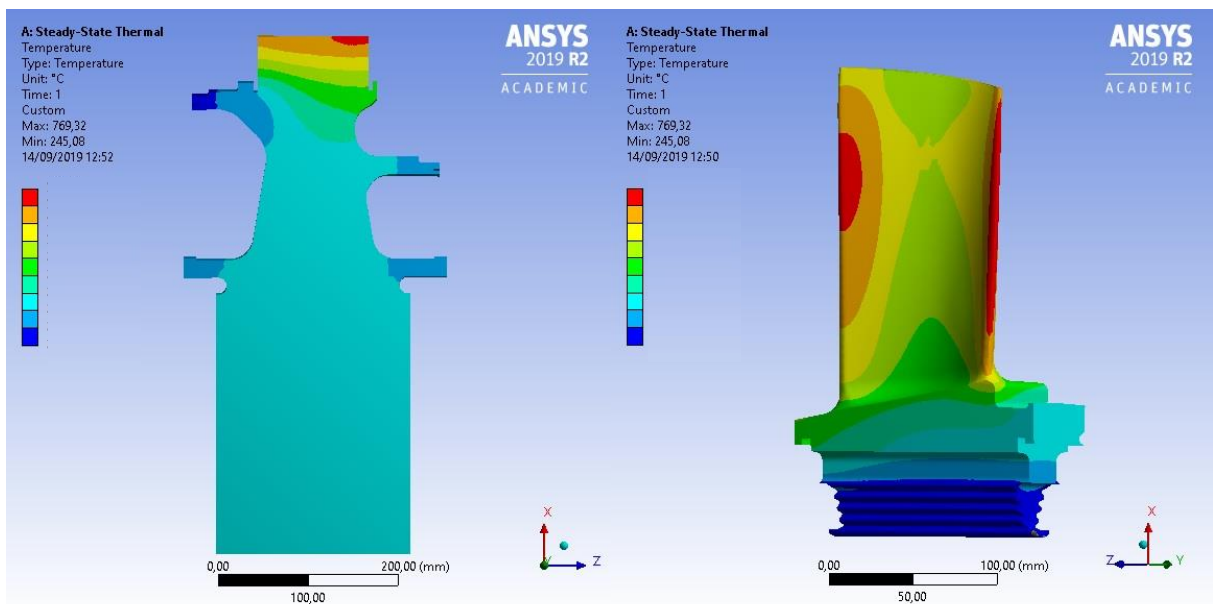


Figure 4.13: temperature scenarios for disk and blade of the second rotating stage (pay attention to the different scales).

While, the highest temperature discovered in the disk is 331,15 °C and it is detected in the upper outlet part of the groove.

Thanks to the new cooling system, the peak of temperature in the blade is increased by only 6 °C, even though the turbine inlet temperature is increased of 6%. It could be noticed how the outlet surface of the blade experience a high temperature: this is due to the absence of cooling channels in the last part of the blade. Another advantage is shown from the disk: the highest temperature is reduced by 32 °C. Since the disk has a short creep life, this reduction is very important for the life of the second rotating stage in the new engine.

4.3.2 Thermo-structural analysis

After that temperatures are computed, the following step is the combined analysis. The CAD model is changed with a larger one (*Figure 4.14*). This model has 7 grooves, it is one tenth of the entire disk, to have all the details of the real disk. This model is characterised by the hole for the tie rod and the holes for the adduction of the cooling air to the blade; therefore, in this model the curve clutch is not cut, but its presence is not influent in the analysis. Material, coordinate system and symmetry condition are the same of the thermal analysis.

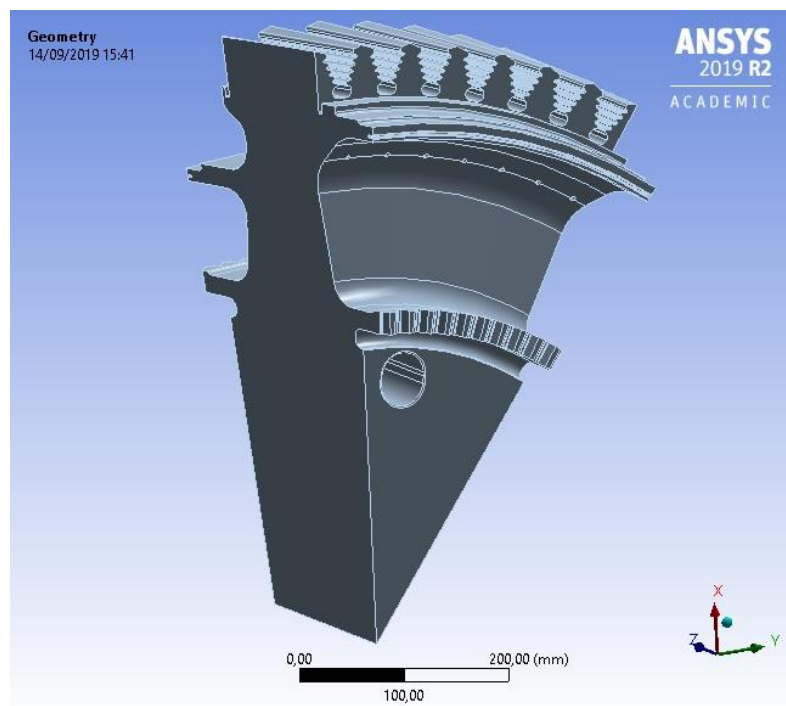


Figure 4.14: investigate slice for the thermo-structural analysis of the second rotating stage (UG3).

Regarding the mesh, it has a largest element size equal to 4 mm for the whole structure, but some parts are refined with an element size of 2 mm because a higher accuracy is needed: the grooves and the new holes.

Two types of thermal loads are applied: the temperatures and convections. Temperature of the active surfaces of the blade root computed before are divided into 5 groups and they are applied to the active surfaces of the disk. The temperature goes from 330 °C (In the highest active surface) to 290 °C (in the lowest one). The convections are the ones computed for the disk in the thermal analysis and are applied in the inlet and outlet surfaces.

The following step is the addition of the centrifugal loads: the one due to the blades and the one due to the weight of the disk.

The centrifugal force due to the weight of the blade is considered by set a rotational speed of the disk equal to 5065 rpm (nominal speed + 3%). The centrifugal force of the blade is divided among the active surfaces of the disk. In this case, the force magnitude is decreased respect the standard case, since the weight of the blade is also reduced. The value of the force is 830 kN (-1,5% respect the one of the standard case).

The last condition is the constrain: this time the position is still the same, but it is applied in a different way for the curve clutch on the model (*Figure 4.15*). The oblique surfaces of the teeth are constrained for the circumferential and axial displacement, whereas the radial displacement is free.

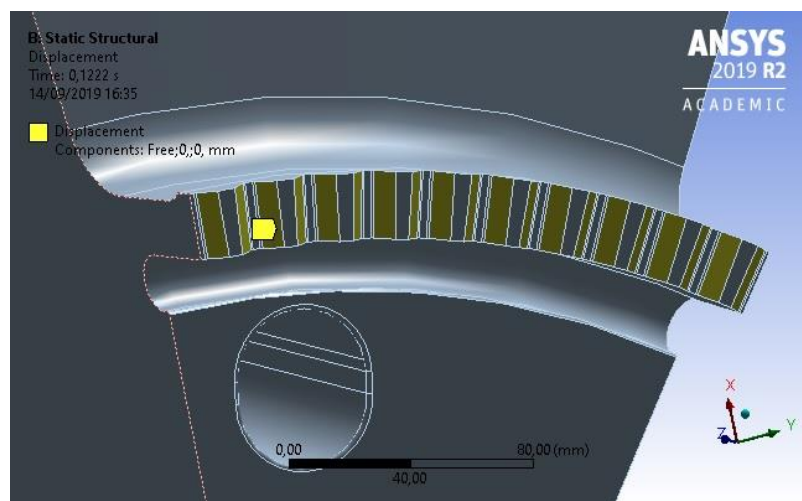


Figure 4.15: the constrain is highlighted in the inlet surface of the second stage disk.

Then, the results of the simulation can be investigated. The first result is the maximum principal stress, that reaches a peak of 1120 MPa, but it is clearly an error due to the mesh, indeed it is discovered in a single node in the curve clutch (*Figure 4.16*). The value considered is 896,77

MPa and it is detected in the new hole. It is not a distributed peak but a singular node, so also this value cannot be used for the computation of the component's life (an average of the most loaded zone will be adopted as final value).

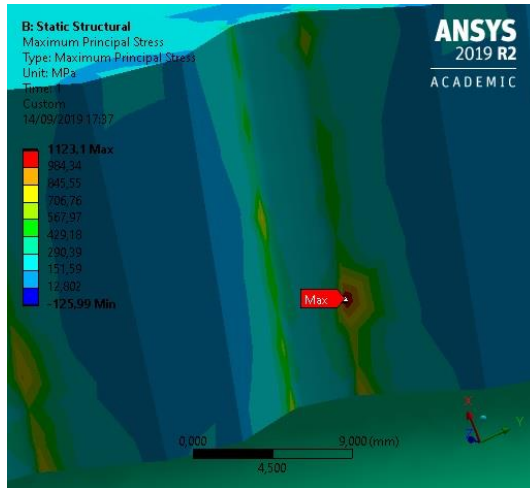
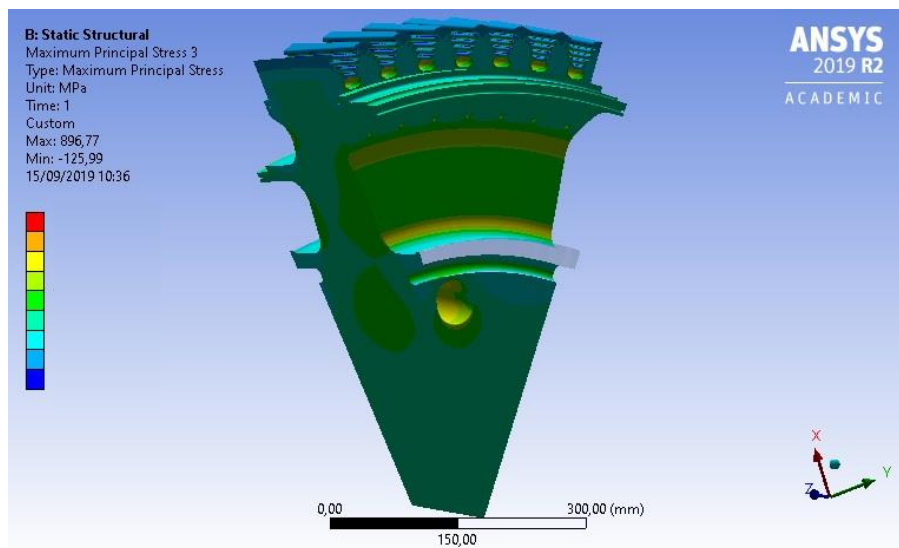


Figure 4.16: the resultant peak for maximum principal stress is an error of the software.

Other surfaces are also highly loaded and they will be investigated for the creep and LCF life. The result for the entire slice is depicted in the Figure 4.17, from which is possible to realize that the most critical areas are the same of the standard's second rotating stage (except for the small holes added only in the newest one).



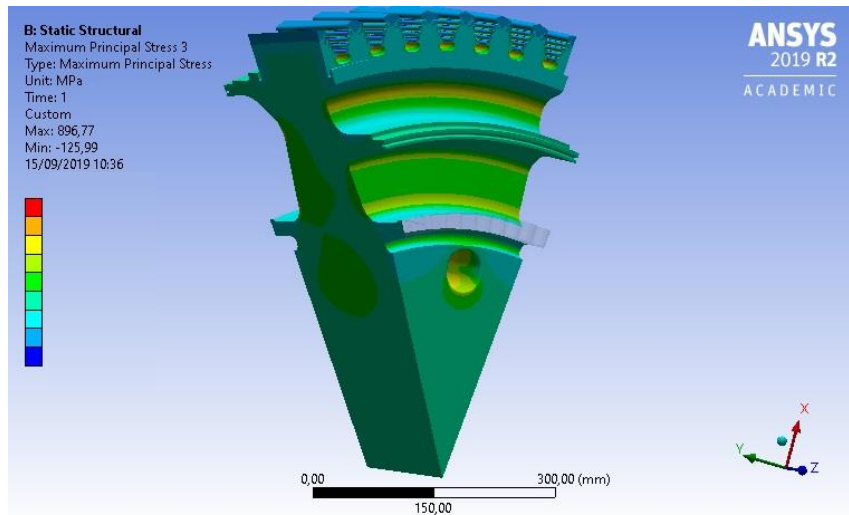


Figure 4.17: maximum principal stress for the inlet (first) and outlet (second) faces of second stage.

The equivalent stress gives a reasonable result: the peak is reached in the fir tree, in the same area where it was detected for the standard configuration of the second stage. The magnitude is 830,42 MPa, but the high stress is not diffused here, exactly how it happened for the standard case. In the Figure 4.18 the overall result and the detail on the most loaded zone are shown.

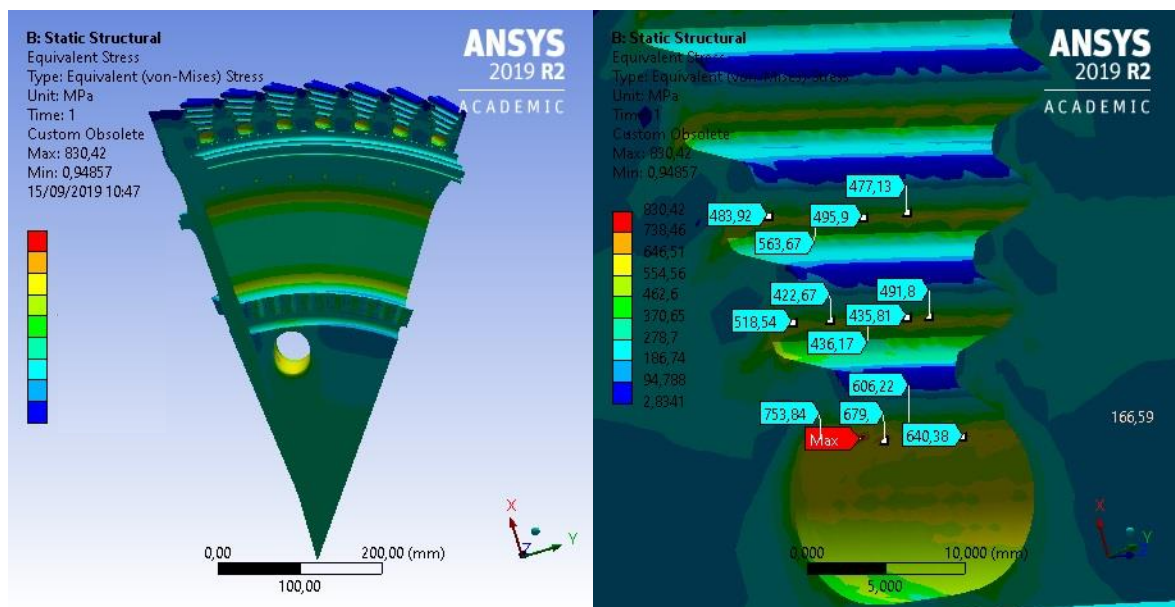
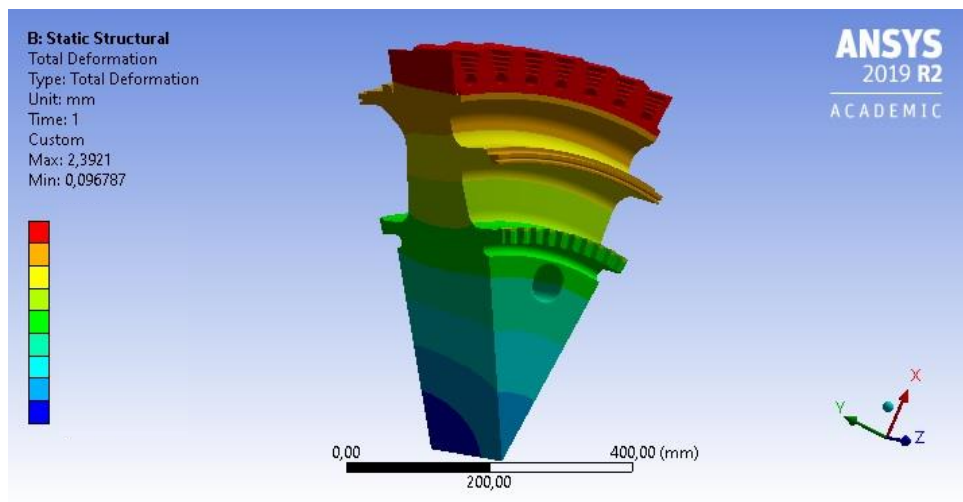


Figure 4.18: equivalent stress overall result view and zoom on the most stressed zone (MPa).

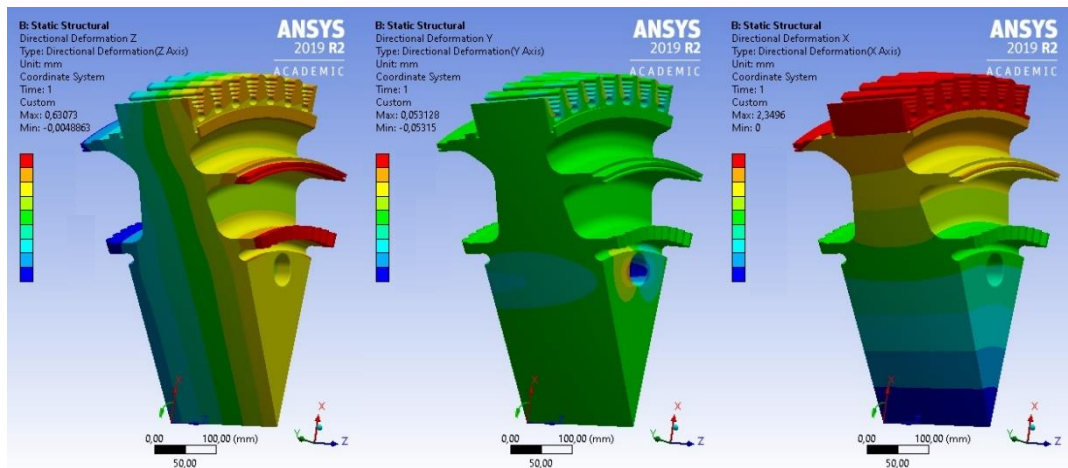
The last result analysed is the total deformation, that reaches a peak of 2,39 mm. It is detected in the upper part of the groove, near the outlet face. This value is 12% smaller than the

corresponding peak for the second rotating stage of the standard engine. This is due to the lower temperature reached by the new version of the disk. This result (*Figure 4.19*) is more symmetric than the one obtained for the first stage and this is due to a more symmetric structure of the second stage disk respect the first one.

The three components of the displacement are shown independently to understand their contribution: the axial displacement experiences a highest value of 0,6 mm in the outlet face; the circumferential one reaches the peak in the hole for the tie rod with 0,05 mm.



(a)



(b)

(c)

(d)

Figure 4.19: total deformation (a) and deformation for (b) axial, (c) circumferential and (d) radial direction (different scales for the colours).

The maximum radial displacement, the most influent, is 2,35 mm and it is discovered in the tip of the groove. All the displacements are lower than the ones of the standard second stage, this is due to the lower temperatures that affect the body under investigation.

4.4 TG20 B7/8: Turbine stage 3

This stage is unchanged from the geometrical point of view. The modifications about it regard the cooling flux and the temperatures of the fluid that affects the blade. Since no cooling system is added in this stage, an increase on the general temperatures is expected, due to the increasing turbine inlet temperature.

4.4.1 Thermal analysis

Since the geometry is unchanged respect the third rotating stage of standard engine, the CAD model used for the thermal simulation is the same used in the chapter 3.6.1 and reported in the *Figure 4.20*. It is one sixty-fifth of the whole stage, since here the blades are 65.

Material, coordinate system, cyclic symmetry and contact are still the same used for the analysis of the same stage in the standard engine, since the change in the fluxes does not change these conditions.

The mesh dimension adopted for this simulation is the same used for the other thermal analyses: the maximum dimension of the elements is 6 mm for the disk and 2 mm for the blade and for the active surfaces.

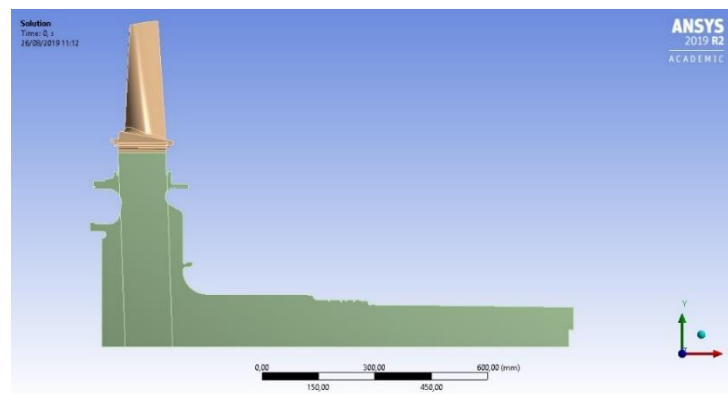


Figure 4.20: CAD model slice of the third rotating stage.

Heat transfer coefficients for the third stage of the standard engine were computed by comparison with the second stage, since no information were allowable. In this case the second rotating stage is different from the third one, since it has a cooling system, that is not present in the third one. So, the heat transfer coefficients for the fluxes in contact with the disk are not computed again, but the ones of the standard simulation are used again. This could be done because the air in contact with the disk is changed ineffectively for what regard the heat transfer coefficients. Contrariwise, the coefficients are computed for the hot mixture that is in contact

with the blade, since its temperature is risen. The DuPont formulation and *AxSTREAM* are used to compute the resultant coefficients. The software is also useful for collecting the temperatures of the hot mixture in the inlet and outlet blade's surfaces. The temperature of the bearing is still imposed equal to 80°C, since it is in contact with the extended part of the disk. All the coefficients are computed for the third stage and listed in the *Table 4.3*.

Region	Heat transfer coeff.	Max air temperature	Min air temperature
BLADE	$\frac{W}{m^2 \cdot K}$	°C	°C
Inlet surface	1170	740	630
Outlet surface	150	560	440
Pressure surface	370	570	450
Suction surface	400	570	450
Shank surface	40	290	240
Inlet/Outlet root	80	290	240
DISK			
Inlet surface upper	30	240	240
Inlet surface lower	20	200	200
Outlet surface upper	50	290	290
Outlet surface lower	20	200	200
Grooves surface	80	290	240

Table 4.3

The results of the two bodies that compose the investigated system are examined separately (*Figure 4.21*).

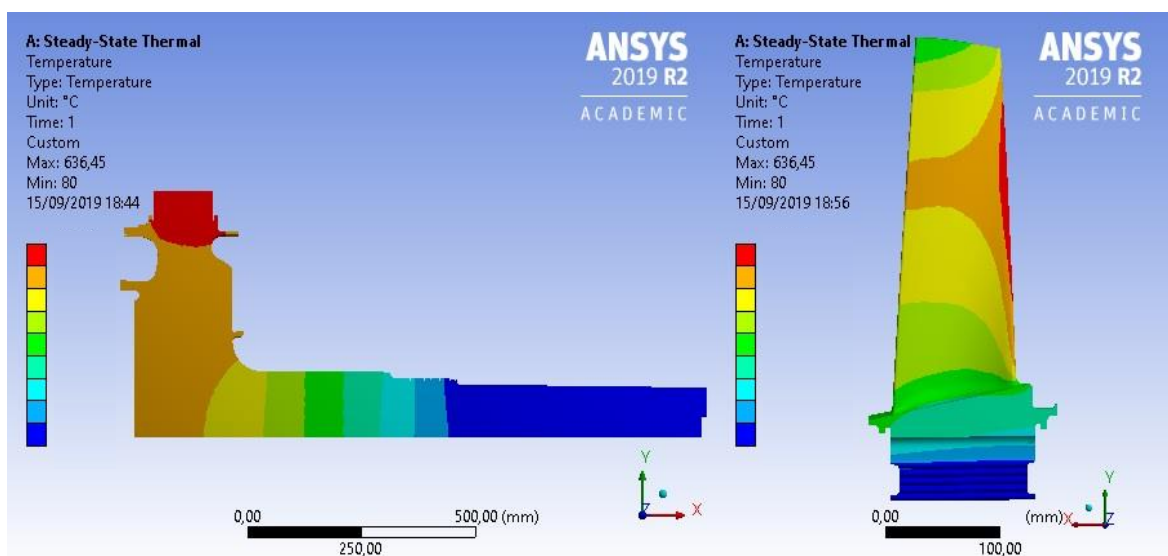


Figure 4.21: temperature panorama for disk and blade of the third rotating stage (different scale).

The maximum temperature discovered in the blade is 636,46 °C and it is located in the inlet surface. The value in the standard case was 575,95 °C, so the temperature is higher for the UG3 stage, as it is expected.

The same situation occurs for the disk, where the peak of temperature is 315,52 °C and it is discovered in the groove. The highest value found in the standard engine for the disk was 300,35 °C.

The temperatures along the active surfaces of the blade's root are taken to be imposed on the thermo-structural analysis of the disk.

4.4.2 Thermo-structural analysis

The investigation about the combined loads on the disk starts from the substitution of the CAD model: a model that include all the details of the real body is needed. Since the geometry of this stage is unchanged, the model is the same used in the thermo-structural analysis of the standard version (chapter 3.6.2). The real body has 65 grooves, but to obtain a slice of the disk that observes the symmetric conditions, in the model for the simulation, the number of the grooves is reduced to 64 and a slice that is one eighth of the entire disk is used for the simulation (*Figure 4.22*).

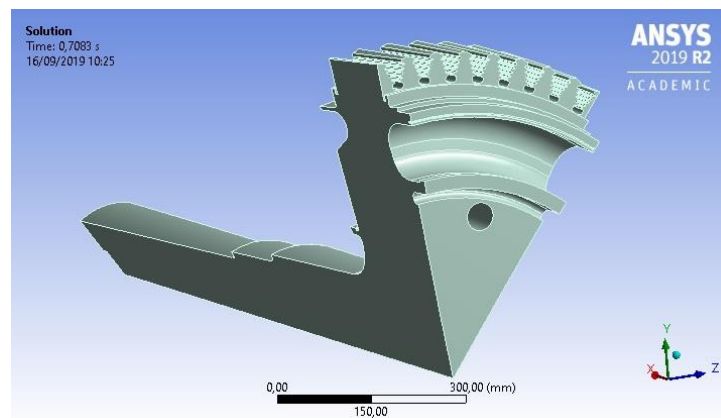


Figure 4.22: disk slice of the third rotating stage, one eighth of the entire disk.

Setting data requested by *Ansys* are the same of the other studies: materials, coordinate systems, symmetry regions and the connections (that are not present for one body examination).

The maximum element size for the mesh is 4 mm and as in the other simulations, this size is refined for the groove part, where the maximum element size is 2 mm.

To impose the thermal load, the convection on the disk are imposed surface by surface for the inlet and outlet faces. Furthermore, to consider the temperature of the blade that strongly influence the one of the disk (for the thermal conduction), many temperature values of the blade's active surfaces are stored from the thermal analysis and they are imposed as temperatures of the active surfaces of the disk in this study. These data are collected along the axial direction of the blade's root and they range from 290 °C to 315 °C. The bearing's temperature is also imposed equal to 80°C, as it was done for the thermal analysis.

The centrifugal (or primary) loads affect the structure of the body under investigation. The first centrifugal force on the disk is the one due to its own weight and it is set by impose the rotational speed of the body (nominal value +3%). The other centrifugal force is the one due to the weight of the blades. Since they are not changed from the standard configuration, the magnitude of the centrifugal load on the active surfaces of each groove is the same of before (1010 kN). Obviously, it is radially directed. This load of the blade is the highest among the three stages. The constraint imposed to avoid the rigid body motion is equal to the one applied for the standard case (*Figure 3.35*); it is used to avoid the circumferential and axial displacement of the surface. The first simulation result analysed is the maximum principal stress; it is shown in the *Figure 4.23*: the highest value is equal to 923,33 MPa and it is located in the active surface in the middle of the groove. This value is not diffused but it is punctual. So, for the life analyses this peak value is not used. As it happened for the first two stages, the shrinkage of the disk and the hole for the tie rod are high stresses zones, due to stress concentration.

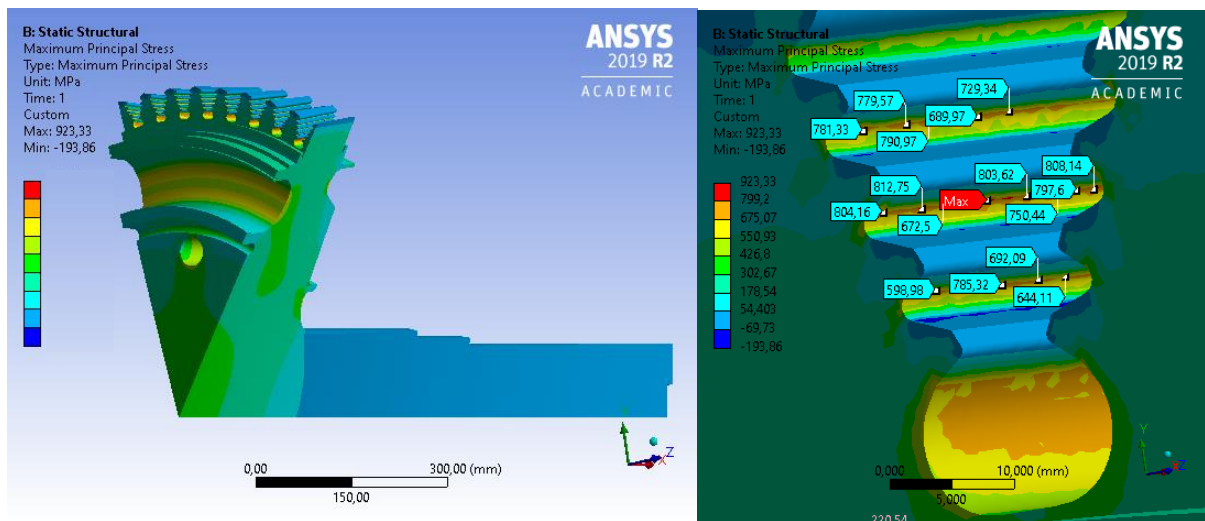


Figure 4.23: maximum principal stress overall result view (left) and zoom on the groove result (right) of the third stage.

The second result investigated is the equivalent stress (*Figure 4.24*): the highest value is equal to 909,6 MPa and it is discovered in the groove but this high value is not scattered but it is punctual as the maximum principal peak stress (these two results are linked, so it is expected). Therefore, during the computation of the component's life, it is needed to pay specific attention to data processing.

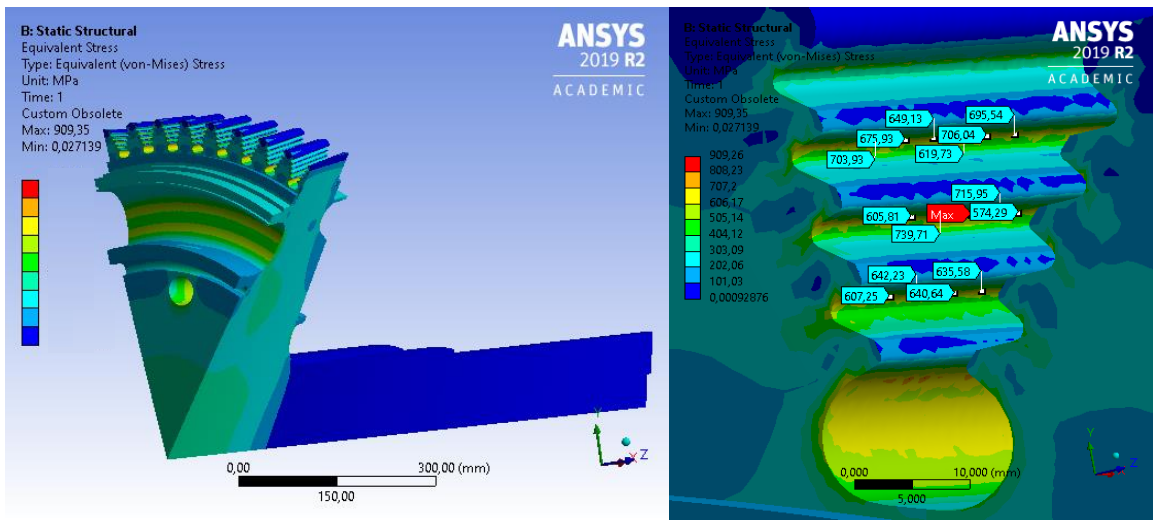
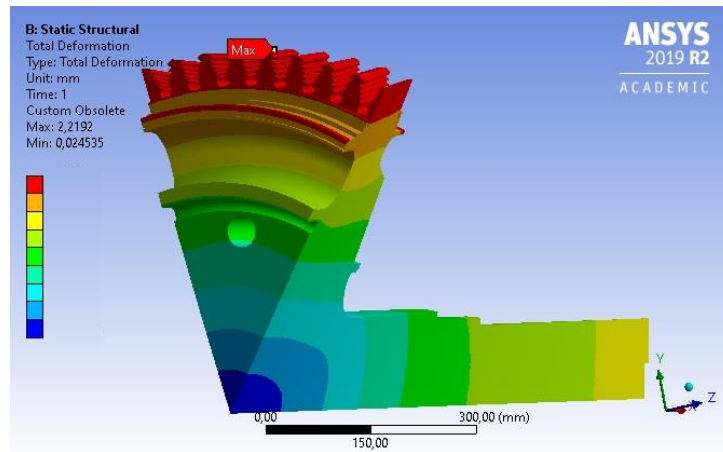


Figure 4.24: equivalent stress overall result view (left) and zoom on the most stressed zone (right).

The last result analysed is the total deformation and its three different components: axial, circumferential and radial. The highest value of total deformation is 2,25 mm and locate in the tip of the groove (*Figure 4.25*). Respect the same result of the standard engine, the peak value is increased by 2%, due to the increasing temperature in the disk. The axial deformation here is higher than the other stages, because the disk is very long for the extension on the outlet face. It reaches a peak of 1,6 mm, located in the last part of the prolongation, where the disk in contact with the bearing. The peak of radial deformation is the most relevant one, 2,2 mm. Instead the circumferential one is similar to the one of the other simulations, and it reaches a peak of 0,05 mm.



(a)



(b)

(c)

(d)

Figure 4.25: total deformation (a) and deformation for (b) axial, (c) circumferential and (d) radial directions (different scales for the colours).

4.5 Creep and cyclic life (LCF)

The last step of this thesis work is focused on the investigation of the upgraded components, to understand if they reach the targets fixed by *Ethos Energy*: 96.000 equivalent hours and 3.200 equivalent starter cycles. The material used for the disks is always the same customised structural steel, so the material data used for the analysis of the standard engine are adopted also for the UG3 version (data are about another structural steel, very similar to the material actually used).

4.5.1 First stage analysis

As it was done for the standard engine, the first step of this investigation is to identify the critical areas (*Figure 4.26*) and extrapolate from them the data necessary for the life estimation (maximum principal stress, equivalent stress and temperatures). These values are listed in the *Table 4.4*; the areas are the same analysed in the first rotating stage of the standard engine, but now the new hole is added.

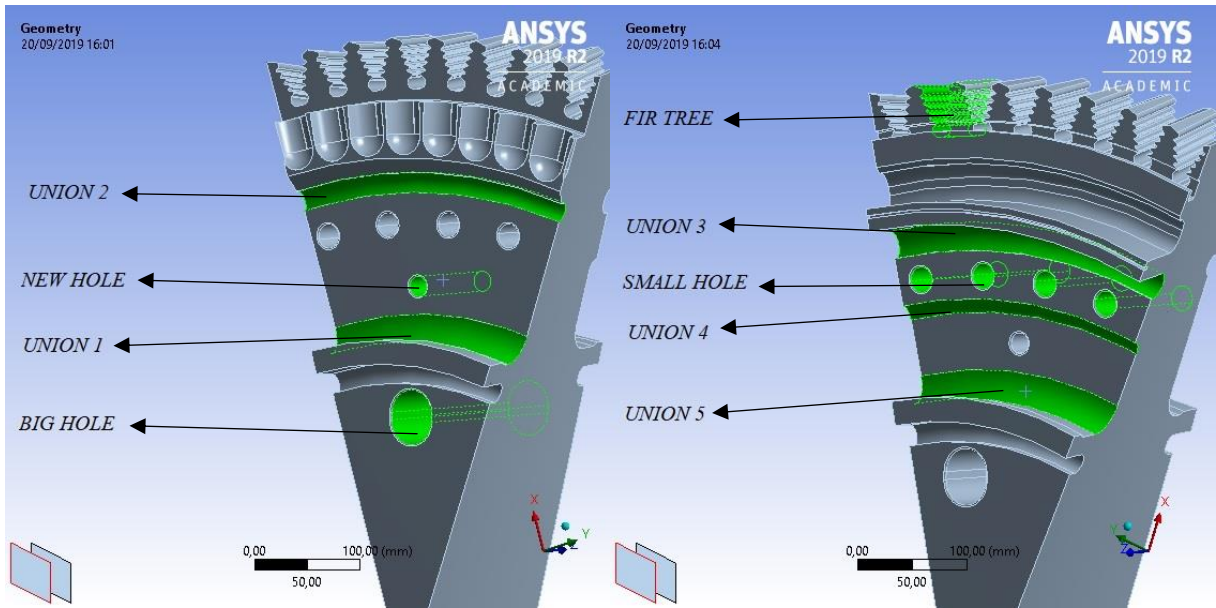


Figure 4.26: the analysed surfaces highlighted in the front face (left) and rear one (right).

zone	temperatura max (°C)	equivalent stress average (MPa)	equivalent stress peak HOOKE (MPa)	maximum principal stress peak (MPa)
union 1	225	370	565	640
union 2	235	350	660	760
union 3	240	385	660	760
union 4	230	390	620	700
union 5	230	460	745	860
big hole	225	590	720	705
new hole	230	710	950	960
small hole	230	600	760	750
fir tree	250	230	710	720

Table 4.4

By following the internal design criteria of *Ethos Energy Group*, initially the averages of the equivalent stresses computed for each zone are plotted into the chart of *Figure 4.27*. these stresses are represented by points: if they are below the “2Sm” curve, the investigated body will pass the first examination, as in this case.

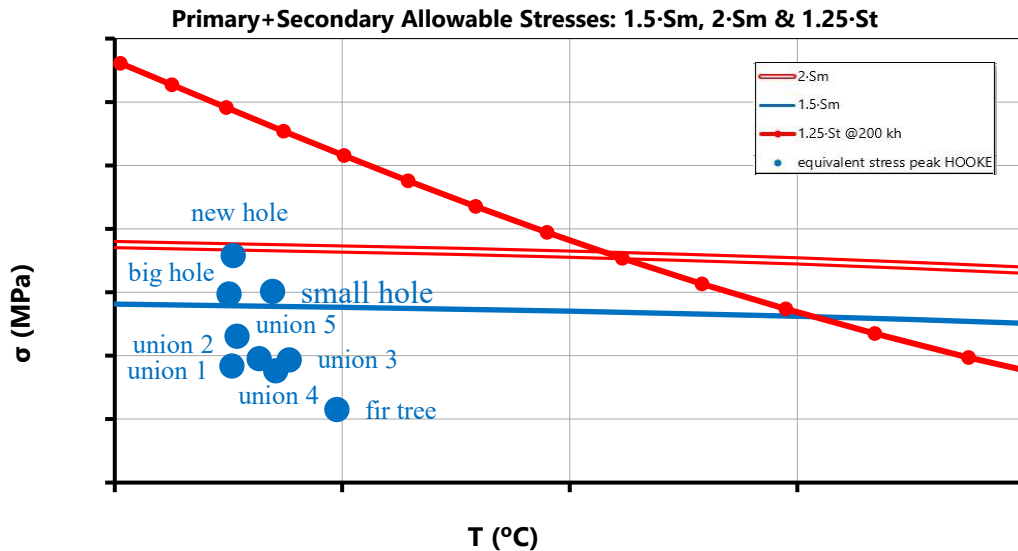


Figure 4.27: average equivalent stress of the first stage analysed for allowable stresses.

Since the points are situated in “cold” surfaces, as it is expected the limit for the creep life is very far from the analysed points. The points below the “1.5 Sm” curve do not need a control for the LCF, but a study about the peaks of equivalent stress are necessary before.

Now as it was done during the examination of the standard component, Neuber’s rule is adopted to correct the peaks of equivalent stress coming from the *Ansys* results that do not consider the elastic-plastic behaviour of the real material. The highest values of equivalent stress found for “union 5”, “big hole”, “new hole”, “small hole” and “fir tree” are adjusted and they are reported in the Ramberg and Osgood curve. The final values considered are reported in the *Figure 4.28*. All the values plotted in this chart (for the analysis, the attention is focused on the green points, that represent the R&O values) are above the “1.5Sm”, so all the areas must be verified for the LCF life. But this does not happen, since the point representing the new hole is above the “2Sm” curve. It means that the component is not accepted and it must be modified.

So, the new holes added to allow the passage of the cooling air for the second stage are a critical detail, since here the stresses reach very high values in a diffused surface (it is shown in *Figure 4.7*).

So, the disk analysis is stopped with the evaluation of highest values of the equivalent stress. Though if the LCF analysis had been done, the value of maximum principal stress of “new hole” would not allow the disk reaches the 3200 equivalent cycles (it achieve almost 2400 equivalent cycles, so also for the LCF analysis, the element is refused).

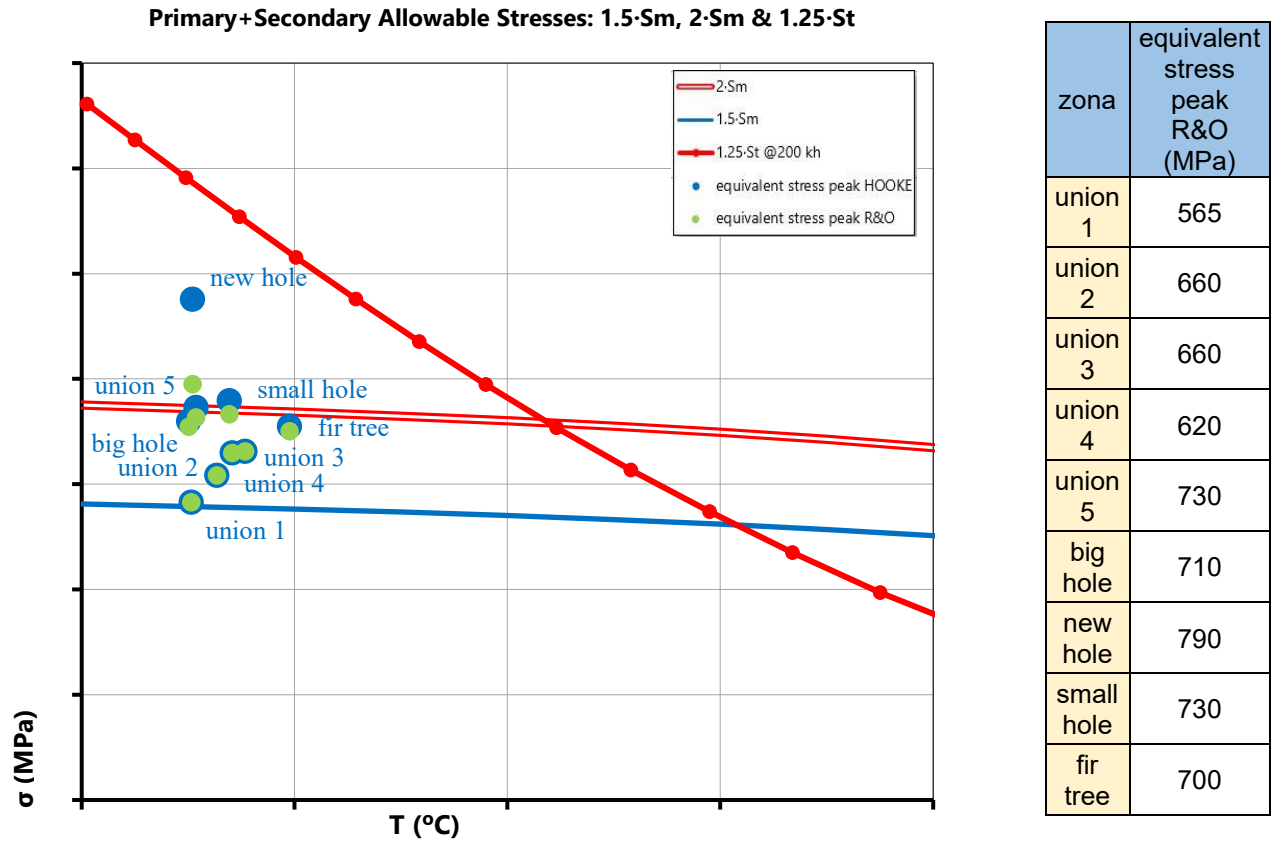


Figure 4.28: peaks of equivalent stress plotted in allowable chart and values of peaks after correction (corresponding to the green points)

4.5.2 Second stage analysis

Since the second rotating stage of the standard engine showed a problem regarding the creep life of the disk connected with the high temperatures reached in the fir tree. So, a dedicated cooling system is added to this stage to solve this problem. Although the turbine inlet temperature is increased (+6%), the highest temperature discovered in the disk is lower than the standard case.

The most loaded surfaces are identified with the scenario of maximum principal stress and the one of the equivalent stress (*Figures 4.17 and 4.18*). The critical areas are the same of before with the addition of the “small hole” surface, the one for the adduction of the cooling air to the blade channels. All the analysed areas are depicted in the *Figure 4.29* and the data required for the component’s life examination are extrapolated from the *Ansys* analysis and listed in *Table 4.5*.

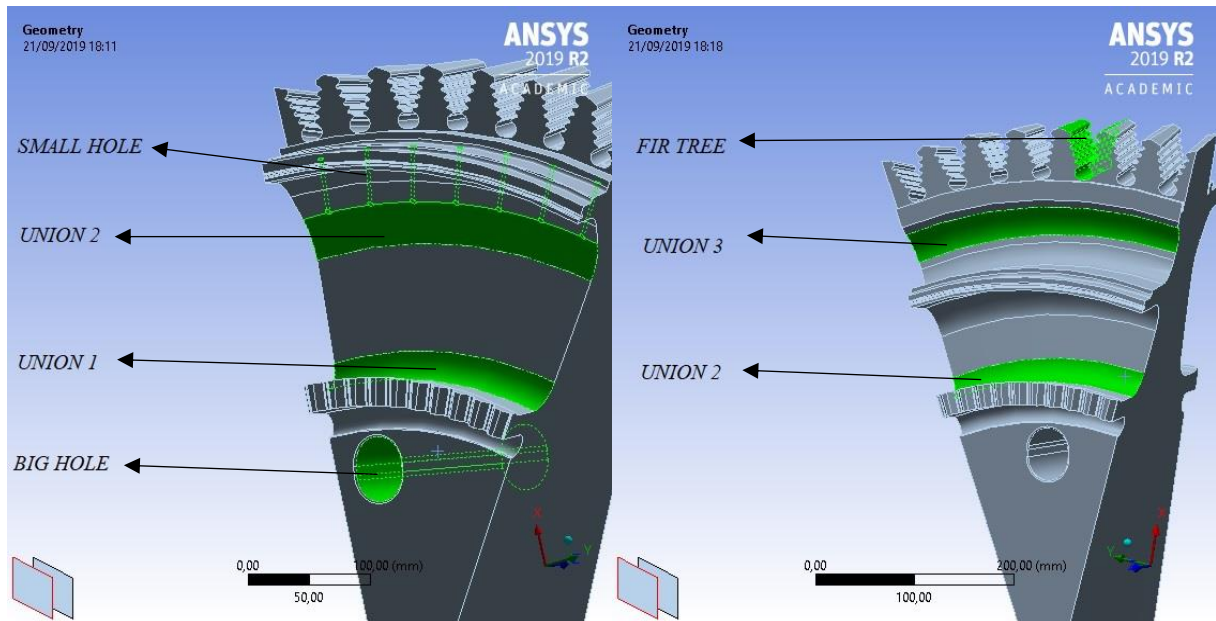


Figure 4.29: the analysed surfaces highlighted in the front face (left) and rear one (right).

zona	temperatura max	equivalent stress average	equivalent stress peak HOOK	maximum principal stress peak
union 1	270	340	530	600
union 2	270	405	510	560
union 3	290	340	510	580
union 4	270	320	490	560
fir tree	310	260	700	730
big hole	270	560	660	650
small hole	270	345	695	740

Table 4.5

As it was done in other cases, not all the peaks value correspond to the ones shown from the figures: if the discovered peak is a singularity and the stress is not diffused (FEM errors), the result selected as “peak” for maximum principal stress and equivalent stress is an average of the values of the maximum loaded surface (this procedure is explained by the *Ethos* internal design criterion).

The first analysis is the one of the equivalent stress averages for each zone: These values are plotted in the σ -T chart (Figure 4.30). All the points are under the $2 S_m$ curve, so no zone is

not accepted. Only the big hole is positioned in between $2 S_m$ and $1.5 S_m$, it means that it needs a check for the LCF life.

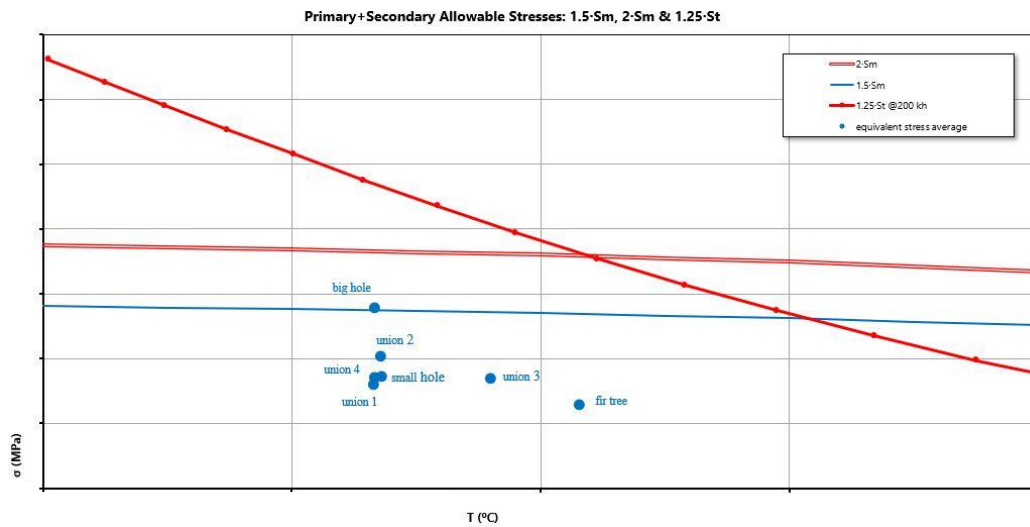


Figure 4.30: average equivalent stress of the second stage analysed for allowable stresses.

The second step is the analysis of the equivalent stress peaks, but the reduction of the highest peaks is needed (Neuber's rule) to evaluate correctly them. The four unions do not need correction. The final values considered are reported in the Figure 4.31, together with the chart where peaks of equivalent stress are plotted (green points for the R&O values).



Figure 4.31: peaks of equivalent stress plotted and peak values reported in R&O curve.

From this chart is possible to see how the fir tree now is below the “1.25 St@200kh”, so also this peak respect the threshold imposed by the company. This means that a remarkable improvement is obtained for the disk of the second stage, that was critical in the standard case. From the last plot, it is known that “fir tree”, “big hole” and “small hole” are the area for which an LCF investigation is needed.

The last step of the internal design criteria is the examination of these three areas to verify that they can exceed 3200 equivalent starting cycles. The minimum LCF equivalent cycles are computed by using the reduced value of stresses (by notch sensitivity factor). All the values used in this procedure are listed in the *Table 4.6*. The component is safe, since all the analysed areas exceed 3200 equivalent cycles. The life of the second disk of UG3 model is longer than the standard one (45% was for the standard the percentage of life used in 3200 equivalent cycles, against the 31% in this case).

	Actual values			Reducted values	
	Temp °C	Peak Max Princ Stress Mpa	Kf/Kt	Stress Mpa	$\Sigma(n/N)$
Fir tree	310	730	0,6	445	31%
Big hole	270	650	0,6	390	11%
Small hole	270	740	0,6	440	27%

Table 4.6

4.5.3 Third stage analysis

The disk of the last stage is the only one for which the peak of temperature is increased respect the standard case: the temperature of the fluid around the blade is increased and the cooling scheme has not been modified. So, the disk is analysed to understand what is changed in terms of life. The critical surfaces are the same of the standard engine and they are highlighted in the *Figure 4.32*. There are no critical union on the outlet face of the disk. The data selected for each surface (maximum temperature, maximum principal stress, equivalent stress) are listed in the *Table 4.7*.

As it happens for disk of the second stage, the value of the peaks for the fir tree listed in this table are different from the ones coming from the simulation (*Figures 4.23 and 4.24*). The design criterion explains which type of peaks must be considered.

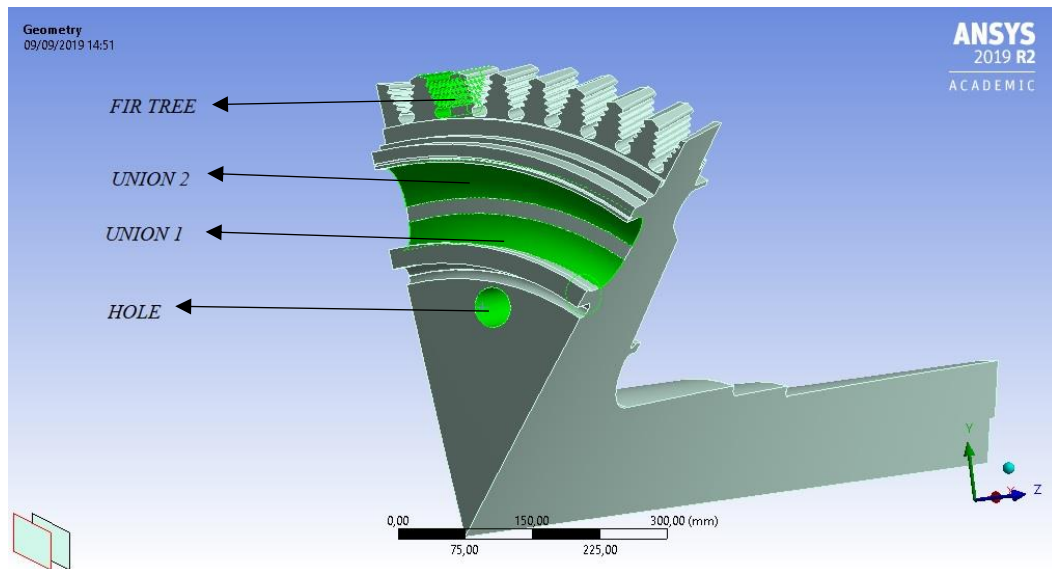


Figure 4.32: investigated surfaces to compute disk's life in the third stage of UG3.

zona	temperatura max (°C)	equivalent stress average (MPa)	equivalent stress peak HOOKE (MPa)	maximum principal stress peak (MPa)
union 1	280	340	560	650
union 2	290	315	600	650
fir tree	280	510	630	605
hole	300	300	685	740

Table 4.7

The equivalent stress averages of each surface are plotted into the chart σ -T, as first analysis. These data are plotted in the Figure 4.33, where it is possible to notice that all the points are below the “1.5Sm” curve, as it happened in the standard case; but now all the points are further to the right, due to the higher temperatures reached in these areas. The second step of the investigation is the examination of the equivalent stress peaks, after that they are adjusted by Neuber’s rule (the corrected values are reported in the Figure 4.34) to have these stresses in the R&O curve. Only the value of the fir tree needs a correction, but all points are in between the “1.5Sm” and “2Sm” curves, it means that all the zones must be verified for the LCF life. This chart is similar to the one of the third stage of the standard engine, but this time the points are closer to the curve for the creep life. Obviously, this is attributed to the increasing temperatures.

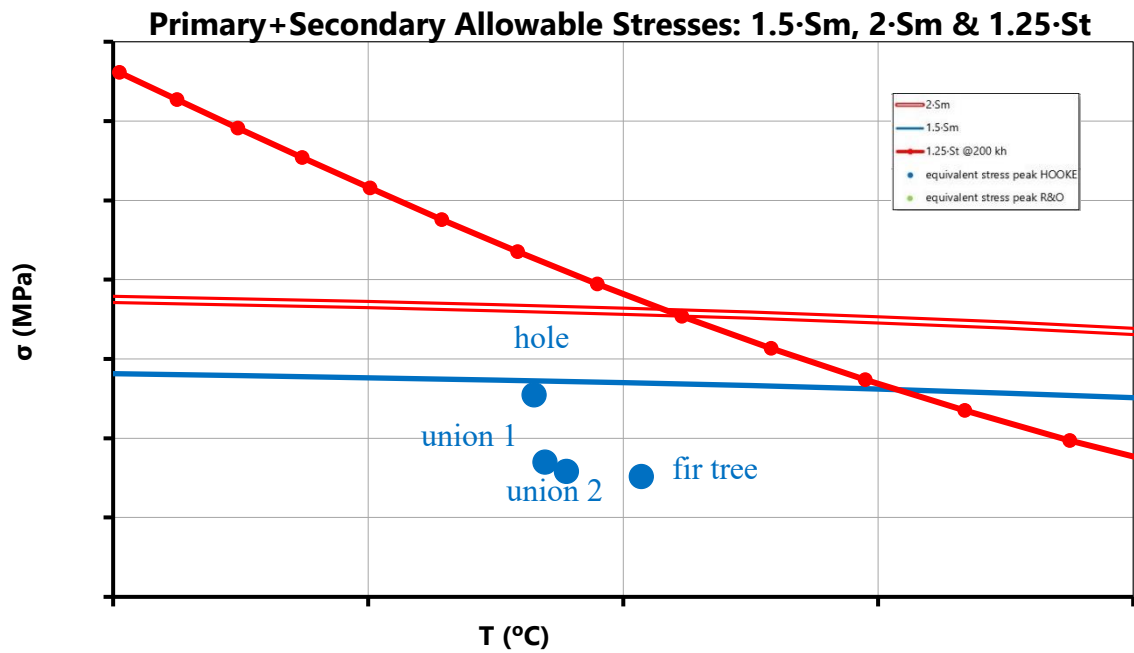


Figure 4.33: averages of equivalent stress plotted into the Allowable stress chart.

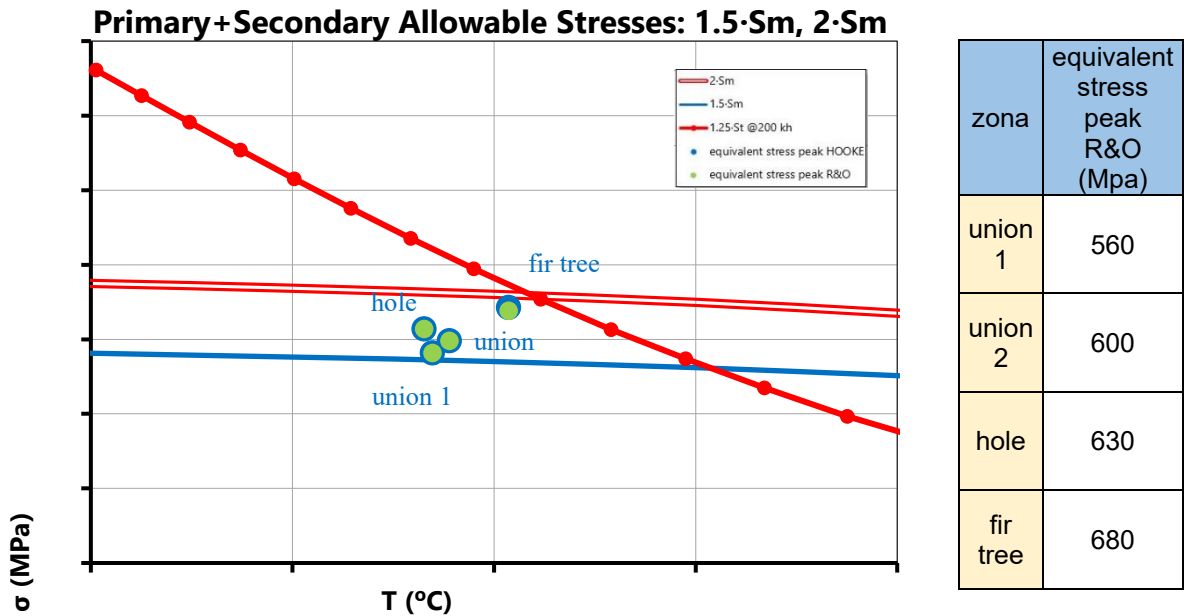


Figure 4.34: equivalent stress peaks plotted to evaluate the creep life and acceptability.

The last step is the LCF analysis (Table 4.8): the peaks of maximum principal stress for each critical area are reduced by the notch sensitivity factor and then the number of equivalent cycles obtained are compared with the threshold value (3200 equivalent cycles), to obtain the Palmgren-Miner's linear damage (if all the values are lower than 100%, the disk is acceptable). The fir tree is the most dangerous area as it happened in the standard engine. This time, the

amount of consumed life is 33%, higher than before (24%), due to an increase on temperature and peak value. This value of life is also higher than the one of the second stage, so the third rotating stage now is more critical than the second one, regarding the LCF life. Anyway, the disk of the third stage is safe and it can work safely.

	Actual values			Reducted values	
	Temp °C	Peak Max Princ Stress Mpa	Kf/Kt	Stress Mpa	$\Sigma(n/N)$
union 1	280	650	0,6	390	11%
union 2	290	650	0,6	390	12%
hole	280	605	0,6	360	7%
fir tree	300	740	0,6	445	33%

Table 4.8

4.6 First stage disk examination

The investigation about the disks' life highlighted a problem regarding the first disk, as it was discussed in the chapter 4.5.1. Since this disk is not acceptable, the disk's geometry is modified as first approach to the problem. The position and shape of the "new hole" (the one in which are located the critical stresses) are modified to find a new configuration that decrease the stresses on the hole. Three of the new disk's slice investigated are reported in *Figure 4.35*.

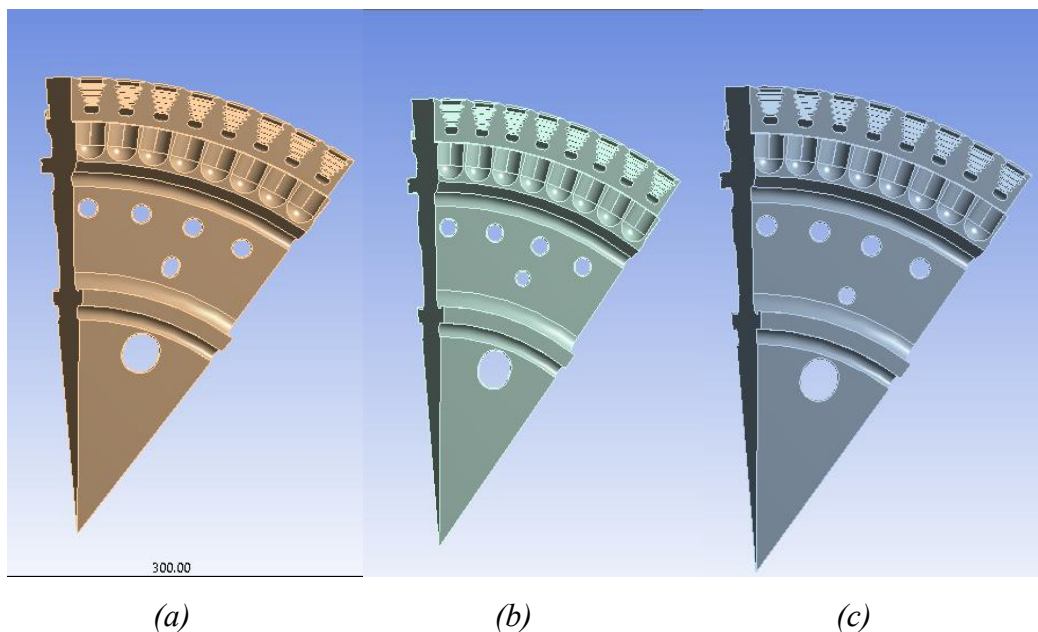


Figure 4.35: model with modified hole (a), with a higher hole (b) and with the lower one (c).

The only modification that decreases the peaks of equivalent stress and maximum principal stress is the (c) of the *Figure 4.35*. This one has the “new hole” closer to the centre of the disk.

5 Conclusions

This thesis work evaluates all the modifications applied to the TG20 B7/8 to understand the feasibility of them. The increased turbine inlet temperature is a dangerous modification (+6%), but it is compensated by an improved cooling system of the entire turbine. These variations lead to many variations on the highest temperatures discovered on the blades and on the disks. In the *Figure 4.36*, the peaks temperature on the blades for the two investigated engines are compared and the variations are reported in percentage for each comparison: all the blades of the UG3 engine are hotter than the standard one, despite the new cooling system added.

Regarding the disks, the firsts two decrease their maximum temperatures, thanks to the cooling system that affect the blades 'root and some areas of the disks. The comparisons between the two engines are reported in the *Figure 4.37*, where it is possible to notice that only the third disk (the only one without modifications) is increased its peak temperature.

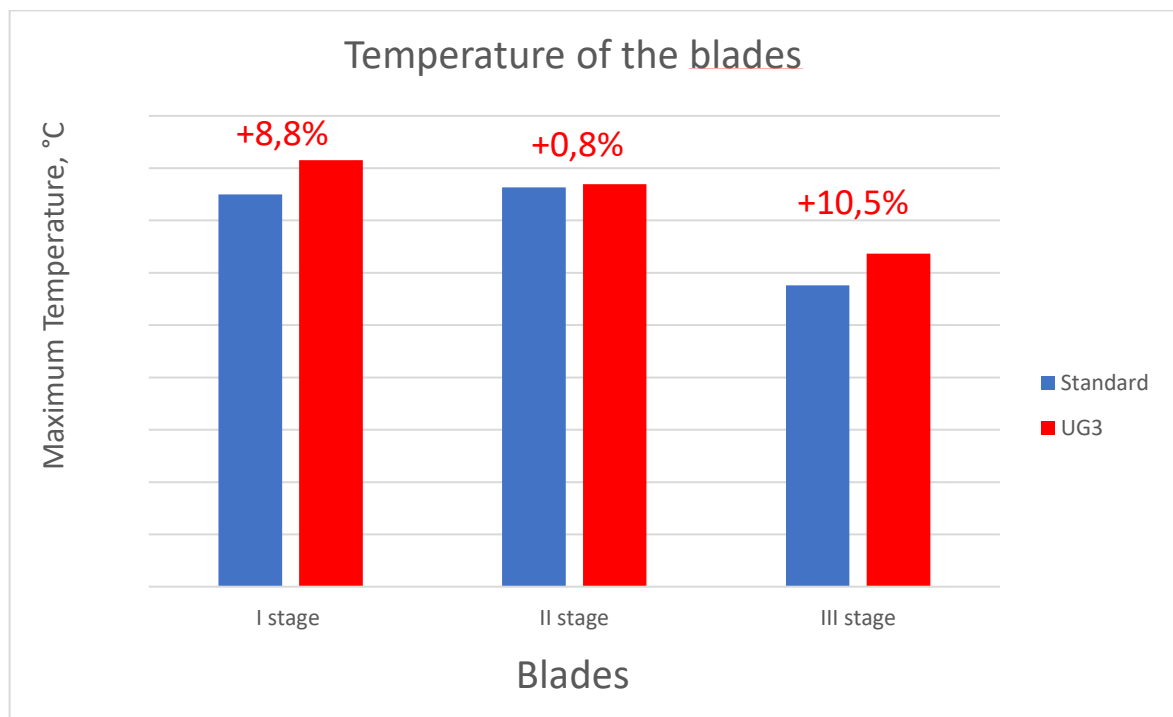


Figure 4.36: comparison of blades peaks temperature for each turbine stage.

The life of the second disk has improved and it is no longer at risk of creep brake, despite the maximum temperature in the blade is increased. In the third disk, the temperatures are increased both on the blade and in the disk, but the disk analysis does not highlight any problems.

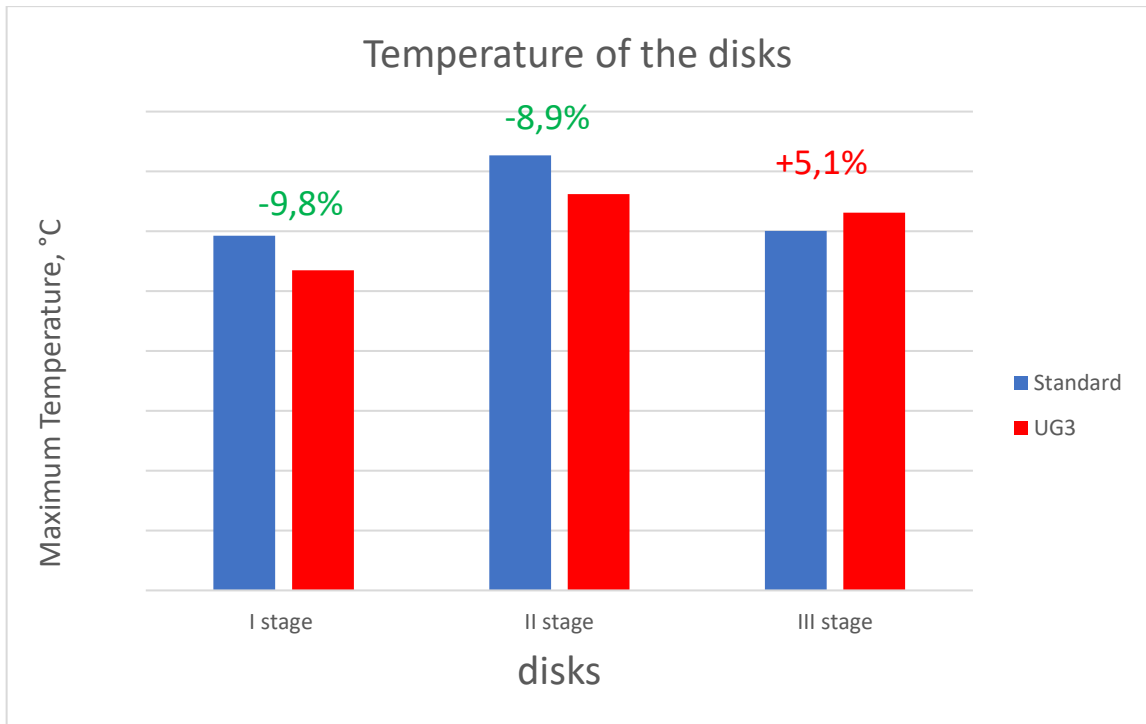


Figure 4. 37: comparison of disks peaks temperature for each turbine stage.

The first stage is the most critical one, since the modifications to the disk cause the early breakage of the body under investigation. Despite the temperatures are decreased, the maximum principal stress and the equivalent one reach very dangerous level in the new hole for the adduction of the cooling air to the second stage. It is important to specify that these analyses do not take into account the frontal ring in contact with the disk of the first stage: the company will have to analyse the total configuration (the stress scenario could change) and then they will optimise the hole for the passage of the air and then they will have to verify that the disk meets the condition imposed by the internal design criterion.

References

1 International Energy Agency

World Energy Outlook 2018 (<https://www.iea.org/weo2018/>)

2 The Global Journal of Energy Equipment

Gas Turbine Forecast (<https://www.turbomachinerymag.com>)

3 A. Beccari

Macchine – Clut, 1993

4 Autodesk

Finite Element Analysis Software (FEA Software)

(<https://www.autodesk.com/solutions/finite-element-analysis>)

5 Simscale

FEA, Finite Element Analysis

(<https://www.simscale.com/docs/content/simwiki/fea/whatisfea.html>)

6 Ansys

Meshing Solution

(<https://www.ansys.com/-/media/ansys/corporate/resourcelibrary/brochure/ansys-meshing-brochure.pdf>)

7 X. Wang, E. Bibeau, G.F. Naterer

Experimental correlation of forced convection heat transfer from a NACA airfoil – ScienceDirect, accepted 23 November 2006

8 F. Cardile

CFD Analysis of the Cooling Flow in a Heavy Industrial Gas Turbine Blade – February 2019

9 G. Petrucci

Lezioni di costruzioni di macchine

10 Ansys

ANSYS Mechanical APDL Theory Reference, November 2013

11 J. Han, S. Dutta, S. Ekkad

Gas Turbine Heat Transfer and Cooling Technology, CRC Press

12 N.Rosafio

Analysis of cooling solutions in a gas turbine blade by means of CHT CFD, October 2019

13 S.D'Imperio

Steady-state turbogas plant performance optimisation through mean-line and stream-line analysis of turbine and compressor, October 2019

14 Ethos Energy Group

Engineering Note 018-17, internal design criterion

Acknowledgement

Vorrei dedicare questo spazio a tutte quelle persone che hanno contribuito a questo lavoro di tesi, ai 2 anni passati al Politecnico e più in generale alla mia vita.

Al Prof. Baratta e alla Prof. Misul per il tempo e l'aiuto dedicatomi lungo tutto il periodo di tesi. Vorrei ringraziare Daniela anche per aver reso più semplice il mio inizio al Politecnico.

A Marco, Luca, Massimo, Emanuele, Giovanni e tutte quelle persone che hanno reso semplice e piacevole ogni giorno passato in Ethos. Una menzione speciale è d'obbligo per Francesco e Pierluigi, per la pazienza con cui mi hanno sopportato.

Ai miei genitori, Francesco e Fulvia, perché ogni traguardo raggiunto, ogni possibilità che ho avuto, ogni singola esperienza della mia vita, è senza alcun dubbio merito loro, che sono i pilastri della mia crescita.

A mio fratello Matteo, per la capacità di strapparmi sempre un sorriso in ogni situazione e per la sua costante presenza.

A mia nonna, agli zii e le zie e ai cugini che hanno sempre reso ogni mio rientro a casa una festa.

A Carlotta, persona fondamentale nella mia vita, che nonostante la distanza ho sempre sentito al mio fianco. A lei sicuramente va il merito di avermi sempre spronato a dare il meglio.

Ai Frames, amici fraterni, che sento vicino ogni singolo giorno e che mi stanno dimostrando che in realtà "i veri amici sono quelli del liceo".

A tutto il gruppo Fanta, per le risate quotidiane e per farmi sempre sentire come se non me ne fossi mai andato da Palermo.

A tutti i Palermitani di Torino, perché siamo arrivati da colleghi e siamo diventati una famiglia (di gente strana) e sicuramente questi 2 anni non sarebbero stati così belli e semplici senza di voi.

A Rich, che è stato un cugino più che un coinquilino e mi tocca ammettere che è stato fonte di tante risate che mi hanno aiutato nelle giornate peggiori.